TECHNISCHE UNIVERSITÄT
BERGAKADEMIE FREIBERG
The University of Resources. Since 1765.

Grain Refinement in Hypoeutectic Al-Si Alloy Driven by Electric Currents

To the Faculty of Materials Science and Materials Technology

of the Technische Universität Bergakademie Freiberg

approved

THESIS

to attain the academic degree of

Doktor-Ingenieur

(Dr.-Ing.)

submitted

by M. Eng. Yunhu Zhang

born on the 17.03.1987 in Gansu P.R.China

Reviewers: Prof. Dr.-Ing. Gotthard Wolf

Prof. Dr.-Ing. Franz Josef Feikus

Date of the award: 19.02.2016

Versicherung

Hiermit versichere ich, dass ich die vorliegende Arbeit ohne unzulässige Hilfe Dritter und ohne Benutzung anderer als der angegebenen Hilfsmittel angefertigt habe; die aus fremden Quellen direkt oder indirekt übernommenen Gedanken sind als solche kenntlich gemacht.

Bei der Auswahl und Auswertung des Materials sowie bei der Herstellung des Manuskripts habe ich Unterstützungsleistungen von folgenden Personen erhalten:

Dirk Räbiger, Sven Franke, Bernd Willers (Experiment);

Dr. Vladimir Galindo (Simulation);

Dr. Sven Eckert (Writing)

Weitere Personen waren an der Abfassung der vorliegenden Arbeit nicht beteiligt. Die Hilfe eines Promotionsberaters habe ich nicht in Anspruch genommen.Weitere Personen haben von mir keine geldwerten Leistungen für Arbeiten erhalten, die nicht als solche kenntlich gemacht worden sind. Die Arbeit wurde bisher weder im Inland noch im Ausland in gleicher oder ähnlicher Form einer anderen Prüfungsbehörde vorgelegt.

M. Eng. Yunhu Zhang

Declaration

I hereby declare that I completed this work without any improper help from a third party and without using any aids other than those cited. All ideas derived directly or indirectly from other sources are identified as such.

In the selection and use of materials and in the writing of the manuscript I received support from the following persons:

Dirk Räbiger, Sven Franke, Bernd Willers (Experiment);

Dr. Vladimir Galindo (Simulation);

Dr. Sven Eckert (Writing)

Persons other than those mentioned above did not contribute to the writing of this thesis. I did not seek the help of a professional doctorate-consultant. Only those persons identified as having done so received financial payment from me for any work done for me. This thesis has not previously been published in the same or a similar form in Germany or abroad.

M. Eng. Yunhu Zhang

Acknowledgements

This work was conducted in the Magnetohydrodynamic department at the Helmholtz-Zentrum Dresden-Rossendorf. It would have been impossible to finish this dissertation without the help of my colleagues.

I deeply appreciate that Dr. Sven Eckert and Dr. Gunter Gerbeth provided the opportunity to study in this famous and excellent group. In particular, I am eternally grateful to my PhD supervisor Dr. Sven Eckert for his everlasting support in academic guidance and even concerning my private matters. His foresight, immense knowledge in MHD and solidification really impress me and I have benefitted tremendously. He always gives me his fruitful, helpful and constructive advice for my research in time. Also, he carefully revises my scientific writings with great patience. I would like to sincerely thank Dr. Dirk Räbiger and Bernd Willers. They always give me kindly technical support and are open to beneficial discussions for my research. I would like to be especially thankful to Dr. Xincheng Miao, with whom I share the same office. I have learned a lot from him to understand the flow problems. Equally, I would like to express my sincere appreciation to Sven Franke, Dr. Vladimir Galindo, Steffen Borchardt, Bombis Doris, Aida Roch, Dr. Dominique Buchenau, and other colleagues in our department for their help with my research.

I would like to sincerely thank Professor Gotthard Wolf for being my supervisor and offering me the valuable opportunity to graduate at the famous university Technische Universität Bergakademie Freiberg.

I would like to take this opportunity to express my gratitude to my former supervisor at the Shanghai University, Professor Changjiang Song and Professor Qijie Zhai, who supported me to apply for the scholarship at the China Scholarship Council (CSC). I am also very grateful to the China Scholarship Council for funding the scholarship under the grant 2011689010. The research work was financially supported by the German Helmholtz Association in form of the Helmholtz-Alliance “LIMTECH”.

I would also like to thank my other colleagues at the HZDR and friends in Germany.

Finally, a great acknowledgment is given to my girlfriend and family for their understanding and support.

Abstract

The present thesis investigates the grain refinement in solidifying Al-7wt%Si hypoeutectic alloy driven by electric currents. The grain size reduction in alloys generated by electric currents during the solidification has been intensively investigated. However, since various effects of electric currents have the potential to generate the finer equiaxed grains, it is still argued which effect plays the key role in the grain refinement process. In addition, the knowledge about the grain refinement mechanism under the application of electric currents remains fragmentary and inconsistent. Hence, the research objectives of the present thesis focus on the role of electric current effects and the grain refinement mechanism under the application of electric currents.

Chapter 1 presents an introduction with respect to the subject of grain refinement in alloys driven by electric current during the solidification process in particular, including the research objectives; the research motivation; a brief review about the research history; a short introduction on the electric currents effects and a review relevant to the research status of grain refinement mechanism.

Chapter 2 gives a description of research methods. This chapter shows the employed experiment materials, experimental setup, experimental procedure, the analysis methods of solidified samples, and numerical method, respectively.

Chapter 3 focuses on the role of electric current effects in the grain refinement process. A series of solidification experiments are performed under various values of effective electric currents for both, electric current pulse and direct current. The corresponding temperature measurements and flow measurements are carried out with the increase of effective electric current intensity. Meanwhile, numerical simulations are conducted to present the details of the flow structure and the distribution of electric current density and electromagnetic force. Finally, the role of electric current effects is discussed to find the key effect in the grain refinement driven by electric currents.

Chapter 4 investigates the grain refinement mechanism driven by electric currents. This chapter mainly focuses on the origin of finer equiaxed grain for grain refinement under the application of electric current on account of the importance of the origin for understanding the grain refinement mechanism. A series of solidification experiments are carried out in Al-7wt%Si alloy and in high

purity aluminum. The main origin of equiaxed grain for grain refinement is concluded based on the experiment results.

Chapter 5 presents three further investigations based on the achieved knowledge in chapter 3 and 4 about the role of electric current effects and the grain refinement mechanism. According to the insight into the key electric current effect for the grain refinement shown in chapter 3, this chapter presents a potential approach to promote the grain refinement. In addition, the solute distribution under the influence of electric current is examined based on the knowledge about the electric current effects. Moreover, the grain refinement mechanism under application of travelling magnetic field is investigated by performing a series of solidification experiments to compare with the experiments about the grain refinement mechanism driven by electric currents shown in chapter 4.

Chapter 6 summarizes the main conclusions from the presented work.

Contents

List of figures

List of tables

1.Introduction

This chapter presents the research objectives, the research motivation, the research history, the electric currents effects and the research status of grain refinement mechanism, respectively. The alloys with finer grain size possess higher comprehensive mechanical properties and are of high commercial attraction to the production of high-performance structural alloys. In this thesis, the grain refinement in solidifying alloys driven by electric currents will be investigated.

In order to give an introduction about this subject, the research history is reviewed firstly. Then, the following section gives briefly some fundamentals of electric currents effects and a literature review on the role of electric currents effects in the grain refinement process. Finally, the reviewed literature presents the research status of the grain refinement mechanism. The classical nucleation theory and the grain refinement mechanism in the ingots or casting without the application of electric currents are also given as a base for well understanding the grain refinement mechanism driven by electric currents. The reviewed literature shows that the knowledge about the role of electric current effects and the grain refinement mechanism driven by electric currents remains fragmentary and inconsistent. Hence, these two points will be investigated in the present thesis.

1.1 Research objectives

This thesis is devoted to understanding the grain refinement of alloys driven by electric currents during the solidification process. In order to approach this aim, we will concern the role of various electric currents effects in the grain refinement firstly. Since there are various effects having the potential to generate the grain size reduction, a series of experiments and systematic numerical simulations will be performed to find which effect plays the dominant role in the grain refinement of alloys. The grain refinement mechanism under the application of electric current will be investigated. On account of the fact that the grain refinement formation mainly depends on origins of the finer equiaxed grains, the possible origins of the equiaxed grains will be investigated based on a series of solidification experiments.

1.2 Research motivation

High-performance structural alloys are urgently required in the daily life of human beings, particularly in the automobile and aircraft industries. The application of high-performance structural alloys can reduce the weight of vehicles as well as the consumption of energy. In addition, the safety and stability of vehicles can be guaranteed or even promoted. Hence, the development of high-performance structural alloys is of high commercial importance and there has been paid much attention to it in the academic and industrial world, especially to the development of high-performance iron, titanium, magnesium and aluminum alloys [1-4].

The tensile strength of alloys can be dramatically enhanced by reducing the grain size in alloys. The famous Hall-Petch formula shows the relationship between the grain size and the yield strength, which is [5, 6]:

$$\sigma_y = \sigma_0 + \frac{k_y}{\sqrt{d}} \tag{1.1}$$

where σ_y is the yield strength, σ_0 is a constant representing the starting stress for dislocation movement (friction stress), k_y is the strengthening coefficient reflecting the relative hardening contribution of grain boundaries (a constant specific to each material), and d is the average grain diameter.

Moreover, it has been recognized for many years that the tensile strength of alloys can be promoted by approaches of solid-solution strengthening, precipitation strengthening, secondary phase strengthening or strain hardening. These approaches have been applied to obtain the high-performance structural alloys [7-9]. However, most of the approaches generate an undesired influence on the plasticity of alloys. Only the grain refinement, grain size reduction, can guarantee or even improve the plasticity of alloys [7]. According to the deformation theory [10], the higher numbers of grains allow the higher deformation as well as the enhanced plasticity.

Aluminum and its alloys have the characteristic properties of high strength over weight ratio, good formability, good corrosion resistance, and easy recycling. Hence, aluminum and its alloys are widely used to replace heavier materials to achieve the weight reduction demand in the industries, in particular for the automotive and aerospace industries [2, 11, 12]. Figure 1.1 shows the world production of aluminum from 2000 to 2014 [13]. It can be observed that the demand of

aluminum has gradually increased within the recent fifteen years. In 2014, the production was as high as 53,127,000 tons.

As one of the most important Al alloys, Al-Si alloys have been intensively investigated. Such kind of alloys do not only present the characteristic properties owned by all Al alloys, but also possess other attractive properties owing to the addition of silicon, such as high fatigue strength, good wear resistance, low thermal expansion, good castability and machinability, and so on [14]. Hence, the present thesis will focus on the grain refinement in Al-Si alloys.

Achieving finer grain size methods has been intensively investigated from the last century on. The most famous method is the plastic deformation technique, which has shown the capability of producing ultrafine grain sizes in the sub-micrometer or nanometer range, such as the equal-channel angular pressing [15] and the high-pressure torsion [16]. However, it is well known that almost all alloys experience a solidification process in the initial preparing stage (before the plastic deformation procedure). It has been found that the solidification process plays a key role in the final structure formation of alloys. Moreover, since the following processing procedures may be avoided by controlling the structure during the solidification process, it can be regarded as an energy saving approach. Hence, triggering the grain refinement during the solidification process is of high commercial importance.

Generally, two typical macrostructures can be obtained in the solidified alloys, columnar and equiaxed grains. A large number of equiaxed grains can be produced during the grain refinement process. Numerous techniques have been developed to obtain finer equiaxed grains in alloys during the solidification process, such as the technique of adding grain refiner [17-25], ultrasonic vibration [26-32], mechanical stirring [33-38], and electromagnetic fields [39-101]. The most intensively investigated technique is the addition of grain refiner in alloys. The remarkable grain refinement is achieved because of the really higher effective nucleation numbers obtained by the addition of the nucleating agents. Some kinds of grain refiners have been applied in the industry, especially for the production of aluminum alloys and magnesium alloys. But, there are some limitations for this technique. The most significant disadvantage is that the employed grain refiners without good dispersion lead to the non-uniform grain size. Moreover, the special grain refiner should be developed for each kind of alloys, and the operation process is complex. Only 1-3% of the added particles can be activated as the nuclei, and the impurity of the grain refiner

would sometimes change the designing properties of alloys [24].

Ultrasonic vibration treatment is another attractive way to cause the grain refinement [26-32]. Two effects induced by the ultrasonic vibration, the cavitation and melt agitation, are considered to cause the reduction in grain size. However, several disadvantages are found in this technique. Since the highest intensity of cavitation is near the surface of the immersed ultrasonic vibrator, the refined region is confined surrounding the ultrasonic vibrator and leading to the inhomogeneous macrostructure in samples, especially in the large scale ingots. Moreover, the oscillating vibrator is rapidly dissolved in the high temperature molten alloys.

It has been recognized for many years that the grain refinement in alloys can be initiated through the agitation induced by mechanical stirring [33-38]. However, it is unfortunate that the solid impeller immersed into the melt cannot be stirred for a long time because of the rapid dissolution and the creep deformation. In addition, the construction of the mechanical stirrer decides that the effective stirring in the whole melt region is achieved with difficulty.

The application of electromagnetic fields in the solidifying alloys is always attractive for the industries. The grain refinement induced by electromagnetic fields has been intensively investigated since last century. Various kinds of electromagnetic fields have been developed to meet the grain refinement, such as electromagnetic stirring (EMS) [39-44], electromagnetic vibration (EMV) [45-50], pulsed magnetic field (PMF) [51-59], and electric currents [60-101]. Magnetic fields, including the EMS, EMV and PMF, have two main advantages: contactless influence on liquid metal and easy handling, immediate control by applying different parameters. Similarly, as another typical electromagnetic field, electric currents are used to cause the reduction in grain size of alloys. However, although the interest in the grain refinement induced by applied electric currents in alloys during the solidification process has dramatically increased for the last ten years, the knowledge about the grain refinement under the impact of electric currents is still fragmentary and inconsistent [60-101]. Hence, the present thesis is devoted to investigating the grain refinement in Al-Si alloys driven by electric currents.

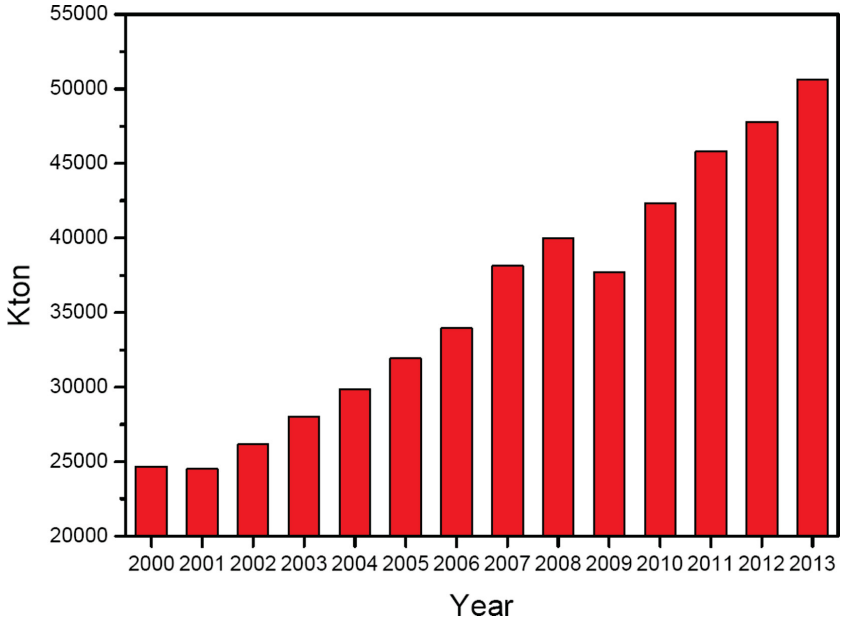

Figure 1.1: World aluminum production from 2000 to 2014 [13].

1.3 Research history

This section will give a simple introduction about the research history of grain refinement in solidifying alloys under the application of electric currents. In 1974, Vashchenko et al. [60] firstly applied direct current (DC, 4-5 mA/cm^2) through two electrodes in cast iron, which was solidified in a sand mold. One electrode was the mold frame, and the other directly connected with the cast iron. The size reduction of the graphite and the primary phases were observed in the as-solidified cast iron. In 1985, an Indian scholar, Misra [61], performed solidification experiments in a PbSbSn alloy in glass tubes of 5mm diameter and 100mm length. A DC of 30-40 mA/cm^2 was applied through electrodes on both ends of the tube during the solidification process of the alloy cooling at a vertical resistance furnace. It was found that the second phase was refined and uniformly distributed. Subsequently, Misra [63] studied a near eutectic PbSbSn alloy during the solidification process under the influence of electric current. It was observed that the eutectic structure was extremely refined. However, some researchers argued the experimental results in the PbSbSn alloy observed by Misra. They regarded that the electric current had no effect on the grain size. For example, Smith [64] repeated the solidification experiment under a DC of 50mA/cm^2 and 1 A/cm^2 with the same experiment conditions. The similar structure was obtained in both samples with and without electric current.

The following research not only confirmed the grain refinement induced by electric currents, but

also attempted to understand the grain refinement process. Nakada et al. [65] conducted electric current pulse (ECP) by discharging a capacitor bank with extremely high voltage (~10^3V) in a cylindrical Sn-Pb alloy sample during the solidification process through two parallel copper electrodes immersed through the surface into the melt. It was found that the solidified structure was driven from dendritic to globular with distinct reduction in grain size. Then, Li [66] performed ECP in a near-eutectic SnPd alloy during the solidification process. The similar result was found, the dendrite was modified to globular under the application of ECP. In 1995, Barnak et al. [67] applied a high density ECP (~10^3 A/cm^2) in two kinds of commercial near-eutectic SnPd alloys, which was solidified in a U-shaped Pyrex glass tube. Experimental results presented an increased undercooling and an order of magnitude reduction in the eutectic colony size under the impact of ECP. The reason for the reduction of grain size was discussed. The electromagnetic force can be generated by the interaction between the electric current and the self-induced magnetic field. Nakada et al. [65] proposed that the grain refinement was caused by the strong electromagnetic force breaking the dendrite. Barnak et al. [67] thought that the influence of electric current on the free energy and interfacial energy between the liquid and solid phase would induce the grain refinement. Subsequently, Qin et al. [68-71] considered the impact of electric current on the free energy theoretically, and concluded that the grain refinement was under the influence of electric current due to the reduction in the nucleation energy barrier.

The grain refinement of alloys driven by electric currents has been systematically and intensively investigated in the recent fifteen years, especially by Chinese scholars. Numerous metals and alloys were employed as the investigated materials, including zinc [73, 80], magnesium [77, 85], aluminum [74-76, 78, 79, 81-83, 86-88, 93, 96, 97, 99-101] and ferrum based metals or alloys [84, 89, 92, 94, 98]. Gao et al. treated a zinc alloy (ZA27) with ECP during the solidification process. It was found that finer grains were formed [73]. The similar macrostructure was obtained by Xu et al. applying ECP in the ZA27 alloy [80]. Yang et al. [77, 85] performed solidification experiments of magnesium alloy (AZ91D) under the impact of ECP. Experimental results presented a transition of structure from large dendritic grains to small nondendritic grains driven by ECP. The most frequently investigated materials were the aluminum metals and alloys, in particular the commercially pure aluminum (99.7wt.%Al) and Al-Si alloys. Cui et al. [79, 83] found the macrostructure of the commercially pure aluminum can be modified from coarse

columnar grains to finer equiaxed grains. Subsequently, the apparent grain refinement in the commercially pure aluminum was obtained by Zhai et al. [82, 86, 87, 96] and Zhao et al. [93] applying ECP during the solidification process of ingots. A series of solidification experiments were carried out to modify the structure of Al-Si alloys by ECP [74-76, 78, 81, 88, 99]. It was found that ECP not only had the capability to decrease the size of the primary aluminum in the hypoeutectic Al-Si alloy [74-76, 81, 88], but also gave rise to the finer eutectic silicon or/and primary silicon phase in the Al-Si alloys [76, 78, 81, 88, 99]. In addition, the grain refinement in various ferrous alloys also has been investigated [84, 89, 92, 94, 98]. Zhang et al. [84] applied the high energy of ECP in the austenite-ferrite two phases FeCrNi alloy during the solidification process. The size of austenitic phase was reduced from 120μm to 0.6μm, and the ferrite phase was refined in the nanometer range. Ma et al. [89] reported that fine equiaxed grains were produced in the Fe1C1.5Cr bearing steel under the treatment of ECP. He et al. [92] observed that the area percentage of equiaxed grains can also be promoted in silicon steel under the treatment of ECP. Cao et al. [94] performed the solidification experiment of the SUS430 ferritic stainless steel under the influence of ECP, and found that the number of equiaxed grains were significantly increased. Chen et al. [98] conducted ECP in the solidifying hypereutectic high chromium cast iron to modify the structure from large grains to finer equiaxed grains.

Various electric current waveforms were employed in the solidifying alloys (see figure 1.2). Cui et al. and Xu et al. [76, 79] used DC (see figure 1.2a) to modify the structure of commercial pure aluminum. The alternating current (AC, see figure 1.2b) was also applied to control the structure of alloys [76]. ECP generated by discharging a capacitor bank was adopted in most of the researches. The frequently employed waveform for ECP was a damping waveform (see figure 1.2c) [73-75, 81, 82, 86, 87, 92-94, 96]. Moreover, Xu et al. [80] applied a rectangle waveform pulsed current (see figure 1.2d) in the ZA27 alloy. In addition, a series of researches were carried out to investigate the influence of electric current intensity and frequency on the grain size. Yang et al. [77, 85] found that the grain size was gradually decreased by the growing of the electric current intensity. Zhao et al. [93] reported that the equiaxed grains were gradually refined by increasing current intensity firstly, and then were coarsened when the current intensity was over a critical value. Ma et al. [89] investigated the effect of current intensity and frequency on the solidified structure in Fe1C1.5Cr bearing steel. The area percentage of equiaxed grains was

expanded by increasing both, the current intensity and frequency. Cui et al. [83] compared the effect of intensity and frequency of ECP on the macrostructure. It was proposed that the frequency was the more important factor. Cao et al. [94] observed the influence of current intensity and frequency on the grain refinement in a ferritic stainless steel and proposed that the current intensity played the most important role. The applying time of electric current in the solidifying alloys was considered to study the impact on the grain refinement. Yang et al. [77] presented that the longer applying time can result in finer grain size in the magnesium alloy. But, the largest reduction in grain size occurred in the initial period of the applying time. Liao et al. [82] found that the dramatic grain refinement in pure aluminum occurred during the nucleation period.

The influence of electrodes configuration on the grain refinement was investigated in alloys under the treatment of ECP. Most of the researches performed the solidification of alloys under the configuration of upward-downward electrodes [77, 80-82, 85, 93]. A pair of parallel electrodes immersed through free surface into the melt were also employed [74, 76, 86, 88, 92, 94, 96]. Li et al. compared the grain refinement of pure aluminum between configurations of upward-downward electrodes and parallel electrodes under the same inputting energy of ECP, and found the refiner macrostructure formed under the configuration of parallel electrodes [86]. Ma et al. carried out a systematic research on the effect of the electrodes position on the grain refinement of pure aluminum. It was found that the highest proportion of fine equiaxed grain area was obtained under the configuration of electrodes located at the upper and lower lateral wall of the mould [87].

The mechanical properties of alloys treated by electric currents were examined. Gao et al. and He et al. [73, 75] reported the enhancement of the tensile strength and elongation in zinc and A356 alloy treated by ECP. Ding et al. [88] found that not only the tensile strength and elongation were increased in Al-Si alloys treated by ECP, but the micro hardness (HV) was also enhanced.

Many explanations have been developed to discuss the grain refinement formation process under the application of electric currents during this research period, such as the heterogeneous nucleation [73, 76, 77, 85, 93], dendrite fragmentation [73-75, 77, 81, 85, 96] and crystal rain mechanisms [82, 86, 100]. The details of these grain refinement mechanisms driven by electric currents will be introduced in the section 1.5.3.

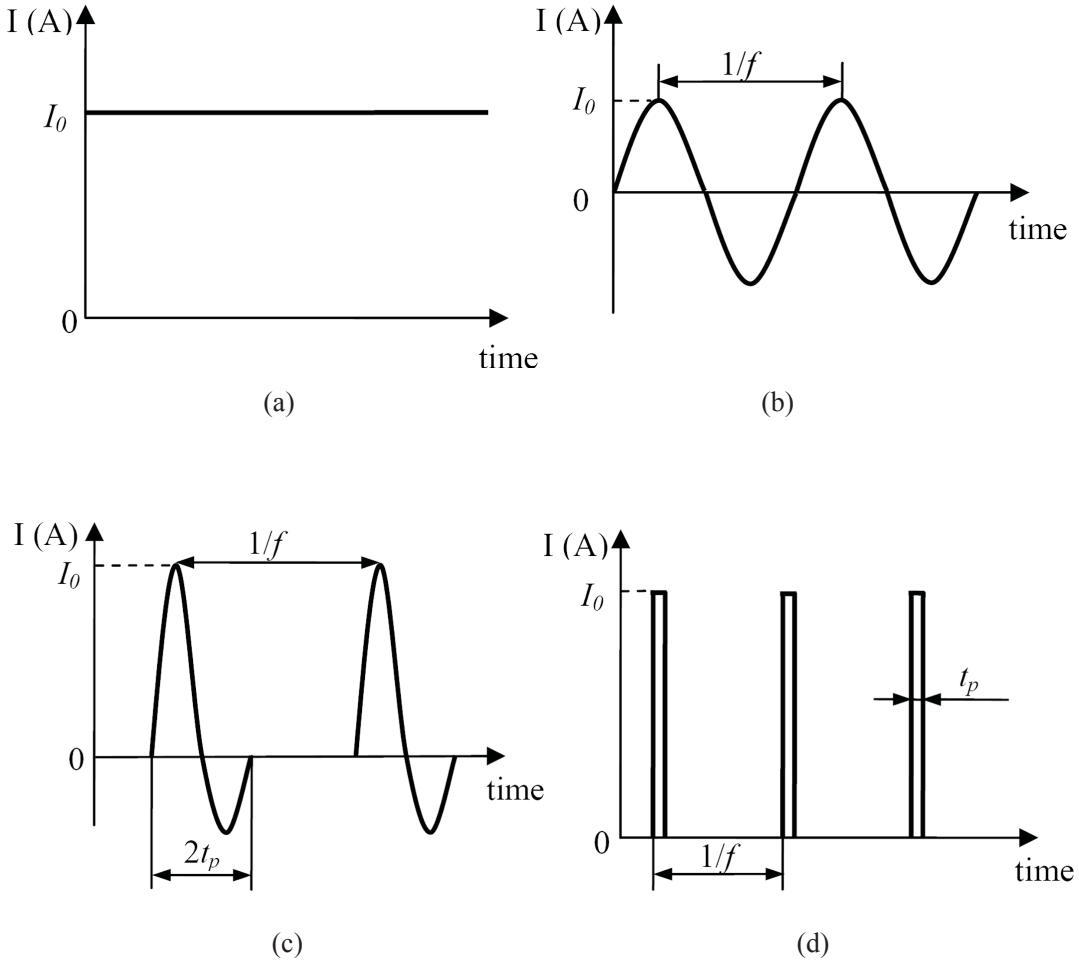

Figure 1.2: Schematic view of the waveform for electric currents: (a) direct current, (b) alternating current, (c) pulsed current with damping waveform, (d) pulsed current with rectangle waveform. I_0: current amplitude, f: frequency and t_p: pulse length.

1.4 Electric currents effects

To find which effects of electric currents drive the grain refinement of alloys is always the first step to understand the grain refinement mechanism. Many effects generated by electric currents have been known, such as the Joule heating, electromagnetic force, forced flow caused by electromagnetic force and skin effect of AC or ECP [37-50]. This section presents brief fundamentals of these effects firstly. Then, a literature review is performed to show the research status with respect to the role of each electric current effect on the grain refinement.

1.4.1 Some fundamentals

Joule heating

Joule heating, also termed as ohmic heating or resistive heating, is a released heat when an electric current flows through a conductor. The amount of Joule heating density (per unit volume) Q can be written as:

$$Q = \int_0^t \mathbf{J}^2 / \sigma dt \tag{1.2}$$

where t is the time, $\mathbf{J}$ is the electrical current density, and σ is the electrical conductivity.

The change in temperature ΔT induced by Joule heating can be calculated by:

$$\Delta T = Q / C \tag{1.3}$$

where C is the specific heat capacity per unit volume.

Force effects

The electromagnetic force per unit volume $\mathbf{F}$ in a conducting substance resulting from the interaction between the electric current and the self-induced magnetic field and can be calculated by the following equation:

$$\mathbf{F} = \mathbf{J} \times \mathbf{B} \tag{1.4}$$

where $\mathbf{B}$ is the magnetic field.

Skin effect

When an electric current with no-constant current intensity, such as alternating electric current (AC) or pulsed electric current (ECP) is conducted in a cylindrical conductor, the current value is highest at the lateral surface and decreases exponentially along the radial direction. Such kind of electric current that concentrates at the “skin” of the conductor is termed as skin effect, which is due to opposing eddy currents generated by the self-induced magnetic field of AC or ECP. The current density $\mathbf{J}$ is described as follows:

$$\mathbf{J} = \mathbf{J}_S \exp(-d / \delta) \tag{1.5}$$

where $\mathbf{J_S}$ is the current density value at the conductor surface, d is the depth from the surface and δ is the skin depth, which is defined as the depth below the surface where the current density has fallen to 1/e (about 0.37) of $\mathbf{J_S}$. It indicates that the electric current mainly distributes in the skin depth, especially for the electric current with high frequency. The skin depth δ can be approximately well calculated as:

$$\delta = (\sigma \pi \mu_r \mu_0 f)^{-1/2} \tag{1.6}$$

where μ_r is the relative magnetic permeability of the conductor and f is the frequency of the electric current.

Magnetohydrodynamics

The transient state of the incompressible flow in a differential form is described by continuity equation:

$$\nabla \cdot \mathbf{U} = 0 \tag{1.7}$$

and momentum equation:

$$\rho(\frac{\partial \mathbf{U}}{\partial t} + (\mathbf{U} \cdot \nabla)\mathbf{U}) = -\nabla p + \mu \nabla^2 \mathbf{U} + \mathbf{F} \tag{1.8}$$

where $\mathbf{U}$, ρ, μ, and p represent the velocity, the density, the molecular dynamic viscosity and the pressure, namely. It is evident from equation 1.8 that the electromagnetic force $\mathbf{F}$ in the melt acts as the cause of the melt flow when an electric current is conducted in a remelted alloy.

The evolution equation for the magnetic field, $\mathbf{B}$, can be written as:

$$\frac{\partial \mathbf{B}}{\partial t} + (\mathbf{U} \cdot \nabla)\mathbf{B} = (\mathbf{B} \cdot \nabla)\mathbf{U} + \frac{1}{\sigma \mu_0} \nabla^2 \mathbf{B} \tag{1.9}$$

where σ is the electrical conductivity, μ_0 is the permeability of vacuum.

The electric current density, $\mathbf{J}$, stated by Ohm's law, is defined as:

$$\mathbf{J} = \sigma(\mathbf{E} + \mathbf{U} \times \mathbf{B}) \tag{1.10}$$

where $\mathbf{E}$ is the electric field.

1.4.2 Role of electric currents effects in grain refinement

Revealing the role of electric currents effects in grain refinement is of high importance because it is the prerequisite to investigate the grain refinement mechanism. The role of electric currents effects has been investigated. Yin et al. [96] indicated that Joule heating played the key role in the grain refinement formation. However, the electromagnetic force generated by electric current was supposed as the key effect by other scholars. Nakada et al. [65] firstly suggested that the grain refinement was generated due to the electromagnetic force. Subsequently, many researches proposed that the electromagnetic force caused the reduction of the grain size [74, 75, 81, 82, 86]. The role of the skin effect was also discussed. Liao et al. [82] proposed that the skin effect was a benefit for the grain refinement, but, it was not the key effect for the grain refinement. Some scholars also suggested that the grain refinement was controlled by the effects all together. Gao et al., Yang et al. and Zhao et al. [73, 77, 85, 93] proposed that the grain refinement was the result of combined action coupling with the electromagnetic force and Joule heating.

Moreover, it has been recognized for many years that the fluid flow can be generated by electric currents [102]. Nikrityuk et al. [103] conducted a numerical study concerning the formation of an electro-vortex flow under a configuration of two planar electrodes at the bottom and the top of a cylindrical mould (see figure 1.3a). Since the diameter of cylindrical electrodes is less than that of the cylindrical mould, the electric current intensity, as well as electromagnetic force adjacent to the planar surface of electrodes, is higher than that of bulk melt. This kind of electromagnetic force concentration induces a force flow with a vortex ring flow pattern (see figure 1.3b). The forced flow generated by electric current has a potential to be the key effect on account of the fact that the grain refinement can be caused by the forced flow [40, 41]. However, little attention has been paid to the role of the forced flow in grain refinement driven by electric currents.

As mentioned previously, it is evident that there is not a widely accepted knowledge about the role of the electric currents effects played in the grain refinement of alloys. This thesis will examine which effect plays the key role in the grain refinement formation of alloys under the application of electric currents.

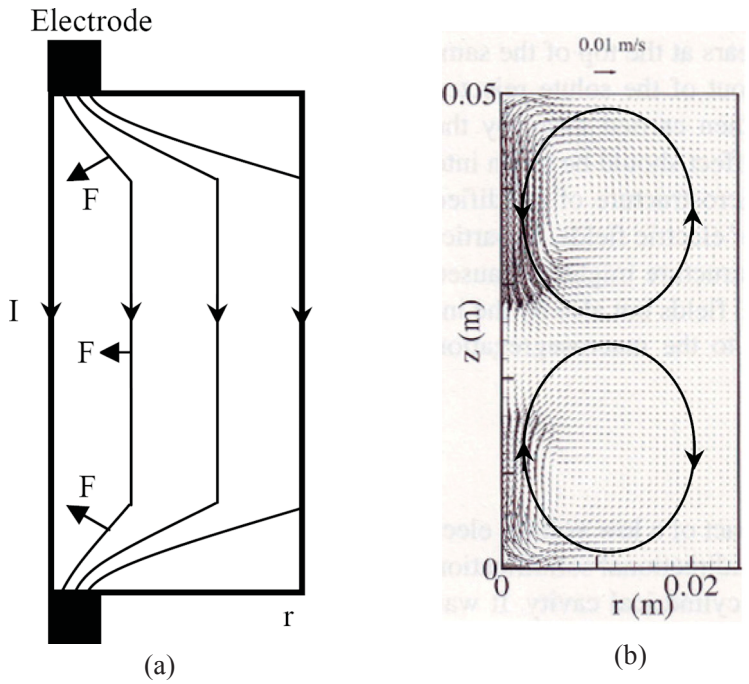

Figure 1.3: (a) schematic view of the distribution of electric current (I) and electromagnetic force (F) in a cylindrical liquid metal (r: radius), (b) contour plot of the fluid flow (numerical simulation results [103]).

1.5 Grain refinement mechanism

In order to well present the state of the art of the grain refinement mechanism driven by electric current, the classical nucleation theory is introduced firstly as a fundamental. Then, five explanations for the equiaxed grain formation in mould-solidified ingots without external energy fields are presented, because some of the grain refinement mechanisms under the application of electric currents are evolved from them. Subsequently, the research status with respect to the mechanism of the grain size driven by electric currents are reviewed and discussed. Finally, a brief introduction of the grain refinement mechanism under the application of magnetic fields is performed to use for reference.

1.5.1 Nucleation theory

Nucleation theories have been developed about one century since the classical nucleation theories were established in 1920s and 1930s [104-109]. Recently, a monograph has been published by Kelton and Greer [110] to present a comprehensive review of the nucleation process in

condensed systems. Here the classical nucleation theory is briefly introduced.

Free energy changes

The nucleation process is driven by the free energy changes during the liquid-solid phase transition. The volumetric free energy of solid is less than the liquid when the temperature is less than the melting point. Hence, the volumetric free energy change plays a "driving force" role in the solidification process. However, the nucleation occurs only when the melt is undercooled. For some critical conditions, the undercooling reaches as high as ~10^2K [104]. This is due to the appearance of interfacial free energy, which is regarded as a "resistant force" for the nucleation process. The volumetric free energy change ΔG_v during the solidification process is described as [104]:

$$\Delta G_v = \Delta g_v \cdot V = \int_{T_m}^{T_n} \Delta S_v dT \cdot V \approx -\Delta S_v \Delta T_n V \tag{1.11}$$

where Δg_v is the volumetric free energy change per unit volume, V is the volume, T_n is the nucleating temperature, T_m is the melting temperature, ΔS_v is the entropy change per unit volume and ΔT_n is the undercooling, defining as $\Delta T_n = T_m - T_n \geq 0$.

The nucleation of solid phase requires the formation of liquid/solid interface. The interfacial free energy change ΔG_i for a nucleus of area A is defined as [104]:

$$\Delta G_i = \alpha A \tag{1.12}$$

where α is the liquid/solid interface energy.

Homogeneous and heterogeneous nucleation

The homogenous nucleation considers that the formation of nuclei is strictly driven by thermal fluctuations in a homogeneous system, ignoring the influence of any extrinsic surface, such as the surface of dispersed particles inside the melt, the wall of crucible, or the oxide layer. A spherical form is assumed for the nucleus owing to the minimum A/V ratio during the homogeneous nucleation process (see figure 1.4a). The total free energy change ΔG for the formation of a spherical nucleus of radius R is derived by summing the volumetric free energy change and the interfacial free energy change:

$$\Delta G = \Delta G_v + \Delta G_i = \frac{4\pi}{3} R^3 \Delta g_v + 4\pi R^2 \alpha \tag{1.13}$$

Figure 1.5 plots the ordinary relationship among the ΔG, ΔG_v and ΔG_i when the melt is undercooled, according to the Equation 1.13. The evolution of ΔG shows a maximum value, which indicates the formation of a nucleus must overcome an energy barrier at the critical radius R^*. The energy barrier is also regarded as the activation energy, given by:

$$\frac{d\Delta G}{dR} = 4\pi R^{*2} \Delta g_v + 8\pi R^* \alpha = 0 \tag{1.14}$$

Solving Equation 1.14 gives:

$$R^* = \frac{-2\alpha}{\Delta g_v} = \frac{2\alpha}{\Delta S_v \Delta T_n^*} \tag{1.15}$$

Substituting Equation 1.15 into Equation 1.13 gives the energy barrier ΔG^* at the critical radius R^*:

$$\Delta G^* = \Delta G_v^* + \Delta G_i^* = -\frac{32\pi\alpha^3}{3\Delta g_v{}^2} + \frac{48\pi\alpha^3}{3\Delta g_v{}^2} = \frac{16\pi\alpha^3}{3\Delta g_v{}^2} = \frac{16\pi\alpha^3}{3(\Delta S_v \Delta T_n^*)^2} \tag{1.16}$$

Equation 1.16 shows that the "driving force", volumetric free energy change $\Delta G_v{}^*$ at the critical radius is two third of the "resistant force", interfacial free energy change $\Delta G_i{}^*$ at the critical radius. The remaining one third is the energy barrier ΔG^*. There is always a spectrum of thermal fluctuations in the melt at any finite temperature. In the melt, the random thermal fluctuations create tiny solid regions (embryos) instantaneously. The greater embryos occur with high probability when the temperature of melt is decreased. But, these embryos are unstable before the undercooling of melt arrives at $\Delta T_n{}^*$. Once the $\Delta T_n{}^*$ is achieved, the embryos, whose radius is ≥ R^*, overcome the energy barrier ΔG^* and grow continuously.

An alternative understanding of the nucleation process focuses on the curvature of embryos in atomic dimensions. A large pressure difference is generated between the solid (embryos) and melt phases owing to the curvature. The size of the solid phase is inversely proportional to the curvature and to the pressure difference. According to the thermodynamic theory, the pressure difference changes the free energy to reduce the equilibrium temperature of the solid phase dramatically (Gibbs–Thomson effect). It means that the embryos with the smaller radius have the lower melting point. The amount of the melting point change $\Delta T_n{}^*$ for a sphere can be calculated as [111]:

$$\Delta T_n^* = \Gamma K = \frac{2\Gamma}{R^*} \tag{1.17}$$

and R^* is:

$$R^* = \frac{2\Gamma}{\Delta T_n^*} \tag{1.18}$$

Where Γ is Gibbs–Thomson coefficient, K is the curvature, which is equal to $2/R^*$ for the sphere. R^* is the critical radius of sphere. It suggests that the sphere with a radius $\geq R^*$ is stable and grows continuously. The Γ is given as:

$$\Gamma = \frac{\alpha}{\Delta S_v} \tag{1.19}$$

Substituting Equation 1.19 into Equation 1.18 gives:

$$R^* = \frac{2\alpha}{\Delta S_v \Delta T_n^*} \tag{1.20}$$

As for the heterogeneous nucleation, the nucleation energy barrier ΔG^* is decreased if the nuclei were in contact with a solid substrate, such as the dispersed particles inside the melt, the wall of crucible, or the oxide layer. This is because the nucleus-melt interface of the nucleus is partly replaced by the nucleus-solid substrate interface to lower the energy. The nucleation energy barrier ΔG^* is calculated as [111]:

$$\Delta G^* = \frac{16\pi\alpha^3 f(\theta)}{3(\Delta S_v \Delta T_n^*)^2} \tag{1.21}$$

$$f(\theta) = \frac{(2+\cos\theta)(1-\cos\theta)^2}{4} \tag{1.22}$$

where θ is the wetting angle between the nucleus (spherical cap) and the solid substrate in the presence of melt, as shown in figure 1.4b.

If there is no wetting (θ=180^o), $f(\theta)$=1, the nucleation is homogeneous. The nucleation energy barrier ΔG^* for the heterogeneous nucleation is gradually reduced while the θ changes from 180^o to 0^o. θ=0^o means the complete wetting as well as no nucleation barrier. Moreover, it should be mentioned that the critical radius R^* for the heterogeneous nucleation is the same as for the homogeneous nucleation.

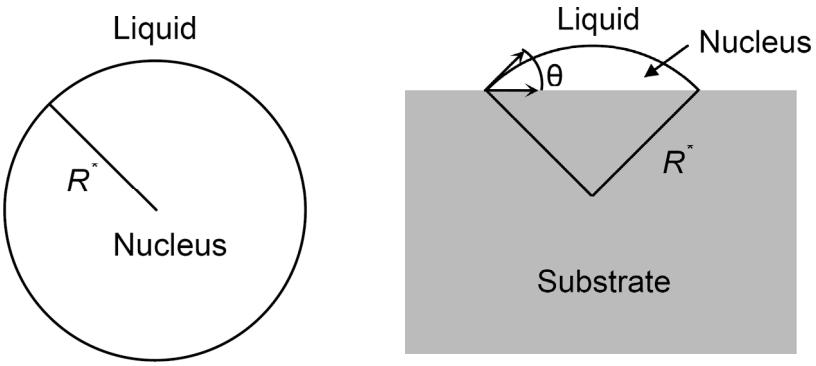

(a) (b)

Figure 1.4: Model of (a) homogenous nucleation, (b) heterogeneous nucleation [111].

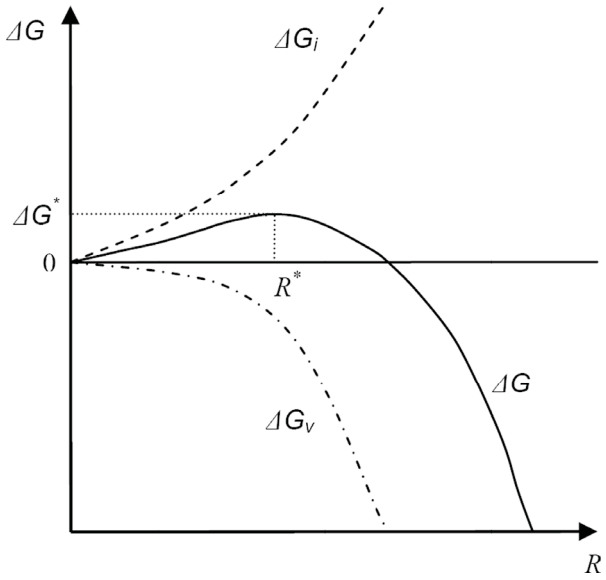

Figure 1.5: Schematic view of the relationship between the total free energy change ΔG and radius R [111].

Nucleation rate

The nucleation rate I is defined as the number of formed nuclei per unit volume and unit time. It can be calculated by [111]:

$$I = I_0 \exp(-\frac{\Delta G^* + \Delta G_d}{k_b T}) \tag{1.23}$$

where I_0 is a pre-exponential factor, ΔG_d is the diffusion activation energy for the transfer of atoms from melt to the solid/liquid interface, and k_b is the Boltzmann's constant. The value of I mainly depends on the change of the nucleation energy barrier ΔG^* and diffusion energy barrier ΔG_d. Generally, the ΔG_d is ignored during the solidification process of castings, because the

atoms can be transferred to the solid/liquid interface sufficiently. According to the Equation 1.21, the ΔG^* varies as $f(\theta)/(\Delta T_n^*)^2$. It means the nucleation rate I can be promoted largely when the nuclei have a good wetting on the substrates and the undercooling of the melt is increased.

1.5.2 Equiaxed grain formation without the application of external fields

Various solidified structures can be obtained by means of different solidification methods, such as the mould solidification, directional solidification, and so on. Here the equiaxed grain formation in the mould-solidified ingots is considered. Generally, three typical zones of solidification structures can be observed in mould-solidified ingots or castings, as shown in figure 1.6. Firstly, an outer equiaxed zone (chilling zone) with tiny grains is formed at or close to the mould wall, because numerous nucleation events are initiated due to the cold mould. Then, a positive temperature gradient is created from the wall to the core along the heat flow. Therewith, the columnar crystals with the most favorable orientations grow along the temperature gradient, forming the columnar zone. After a certain stage of columnar crystals growth, a columnar to equiaxed transition (CET) is observed. The growth of columnar crystals is inhibited by many independently growing equiaxed crystals. Consequently, an inner equiaxed zone, generally with coarser equiaxed grains than in the outer equiaxed zone, is obtained. Five major explanations have been developed to understand the formation of equiaxed grains.

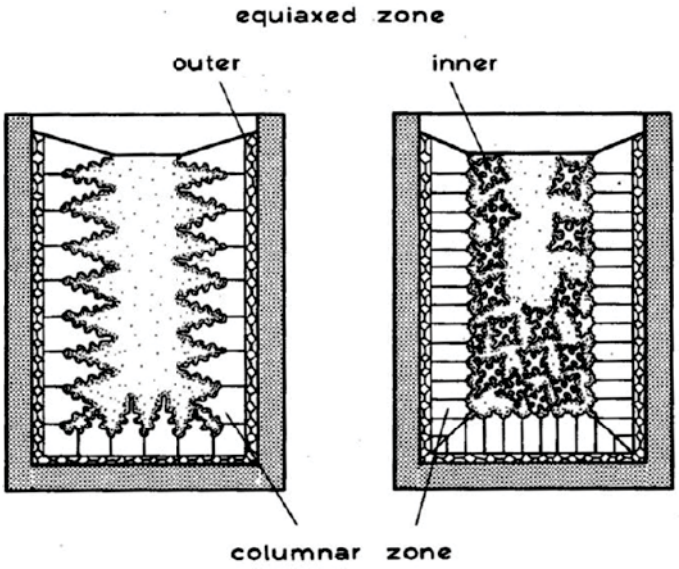

Figure 1.6: Typical solidified structures formation in an ingot [111].

Constitutional undercooling

Winegard and Chalmers [112] developed the constitutional undercooling theory to explain the formation of inner equiaxed zones in alloy ingots. The columnar crystals grow inwards after the tiny grains formed in the chill zone. There is an enriched solute layer at the columnar dendrite growth interface for alloys with the distribution coefficient k<1, causing a depression of the freezing point. An undercooling zone in front of the interface is established according to the solute distribution in the melt, as shown in figure 1.7. At the beginning of columnar growth, the undercooling zone is confined at the interface. The temperature in the bulk melt remains higher than the liquidus of the bulk melt. The columnar crystals keep growing until the effective nucleation of new equiaxed crystals occurs when the constitutional undercooling zone is sufficiently developed. As a result, the equiaxed zone is produced in the center of castings.

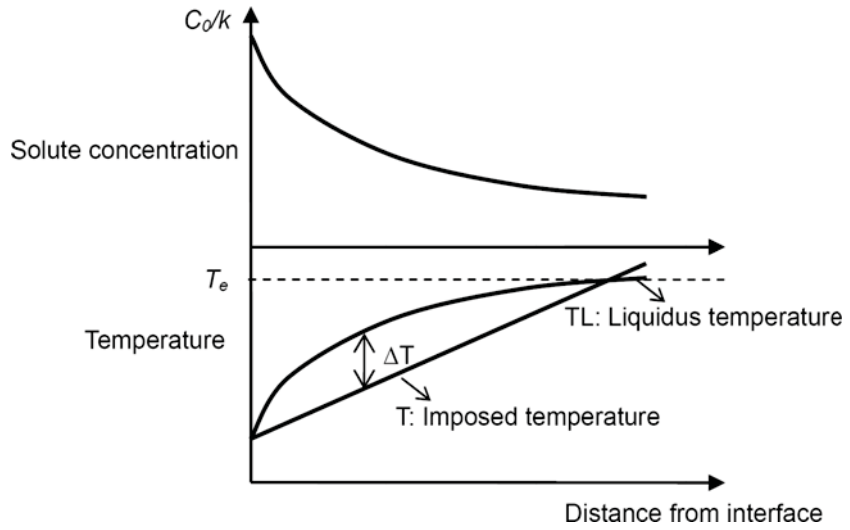

Figure1.7: Solute concentration and resulting change in freezing temperature ahead of a dendrite tip. The actual level of undercooling depends on the thermal and compositional conditions at the tip. T_e: equilibrium liquidus, C_o: mean liquid compostion, k: distribution coefficient (redrawn from reference [113]).

Free chill crystals

The free chill crystal theory was originally proposed by Genders[114]. Subsequently, it was developed by Chalmers [115] considering the effect of pouring temperature on the equiaxed zone in the Al-Cu alloys. It is found that the equiaxed zone is increased with the lower pouring temperature. The following events are proposed to explain this experimental phenomenon: (a)

The thermally undercooled zone is produced in the vicinity of the mould wall when the liquid metal contacts the cold mould. Copious nucleation occurs on the wall and throughout the zone. (b) The solute is rejected on the interface of crystals that are nucleated and grows directly on the wall. The formed constitutional undercooling zone protects some of the nuclei that were nucleated previously in the thermally undercooled zone. The constitutional undercooling zone would extend for lower pouring temperature. Therewith, the number of survived crystals is increased. (c) The survived crystals are carried away from the interface into the center of the castings by the convection of melt. These drifted crystals grow and then contact each other to form a skeleton network as well as an inner equiaxed zone.

Dendrite fragmentation

Jackson et al. proposed the dendrite arm remelting as well as the dendrite fragmentation for understanding the origin of the inner equiaxed zone [116]. The dendrite arm remelting process is shown in figure 1.8 [113]. For alloys of distribution coefficient $k<1$, the solute rejection occurs around the dendrite arms. The solute built up near the root of secondary arms produce the root with the necked shape. Then, secondary arms are detached and grow as the equiaxed grains. It has been proposed that the detachment of dendrite arms can be caused by temperature fluctuations. For example, Flemings [117] proposed that the flow of the hot melt into the mushy zone can cause the detachment of dendrite arms, as shown in figure 1.9. Moreover, solute fluctuations are supposed to induce the detachment of arms. It has been proved by the X-ray in-situ observations technique that the flow of the solute rich melt into the mushy zone due to buoyancy force can induce the detachment of high-order dendrite arms during directional solidification of an aluminum alloy [118]. In addition, Jackson et al. [116] proposed that the surface energy can induce dendrite arms detachment because the melting point is changed at the necked root where the curvature is largest. Ananiev et al. [119] presented similar knowledge based upon theoretically analyzing the effect of surface energy (elastic energy) on the thermodynamical equilibrium at necked root.

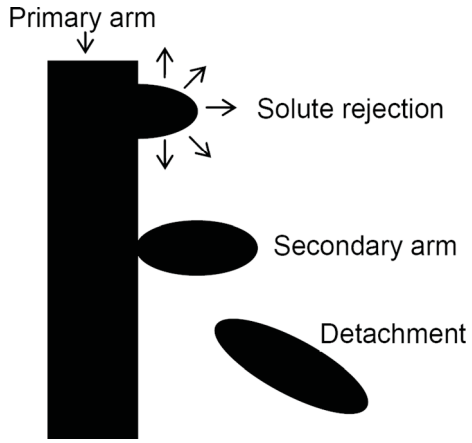

Figure 1.8: Schematic view of secondary dendrite arms detachment from the primary arm (redrawn from reference [113]).

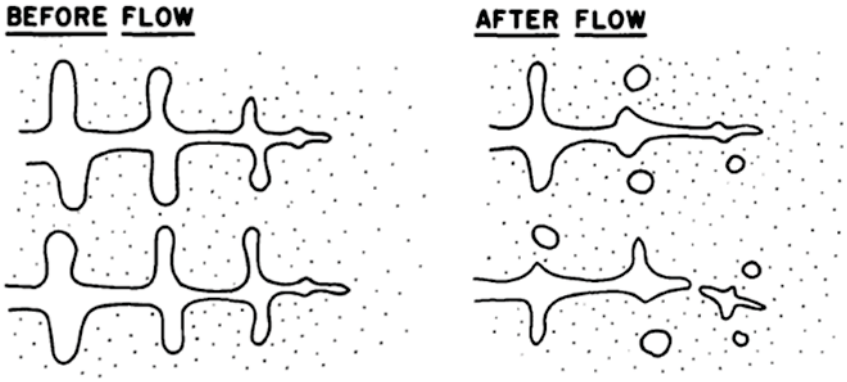

Figure 1.9: Schematic view of the dendrite multiplication resulting from the thermal fluctuations induced by flow [117].

Showering from the surface

In 1967, Southin [120] performed a series of solidification experiments using Al, Al-0.1 and Al-2%Cu. The crystal showering from the surface is proposed by observing the solidified structure that the macrostructure of cast ingots consists of four zones rather than the previously accepted three zones. The fourth zone is a coarse dendrite layer across the top open surface. The equiaxed zone is considered as the result of dendrite showering from the surface dendrite layer (the fourth zone) and then sinking down into the liquid. This mechanism is proved by performing hot-top and mechanical barriers experiments. The hot-top experiments were employed to eliminate the surface dendrite layer using a gas flame over the surface to add a small amount of heat. The results show that the macrostructure is completely columnar. A stainless steel gauze barrier was horizontally located in the mould. The almost completely columnar zone is observed

below the barrier whereas an equiaxed zone with fine grains is obtained above the barrier. The mechanism of dendrite leaving the surface is discussed. It may be that the weight of growing dendrite at the surface is sufficient to overcome the surface tension forces. In addition, the dendrite would fall freely from the surface layer during the formation of shrinkage because the layer would break. The higher temperature of the bulk melt reduces the survival probability of falling crystals. It indicates that this knowledge can also explain the results that the equiaxed zone decreases with the higher pouring temperature.

Crystal separation at the mould wall

This explanation was proposed by Ohno et al. [121, 122]. A novel solidification setup was designed to observe directly the equiaxed grains formation of Sn alloys on the mould wall in the initial stage of air forced cooled horizontal directional solidification. It is observed that numerous crystals are separated from the mould wall at the initial stage of solidification process. The separation process of crystals (see figure 1.10) describes that the nucleation occurs on the mould wall, and then the necked nuclei is formed because of the solute rejection, eventually the nuclei is separated from the wall. These separated crystals are transported to the centre and grow as the equiaxed grains. It is observed that the crystal separation process is stopped when a solid shell is formed at the mould wall in the subsequent stage of solidification process. The separation of crystals from the mould wall at the initial stage of the solidification process is considered to be the source for the formation of the inner equiaxed region.

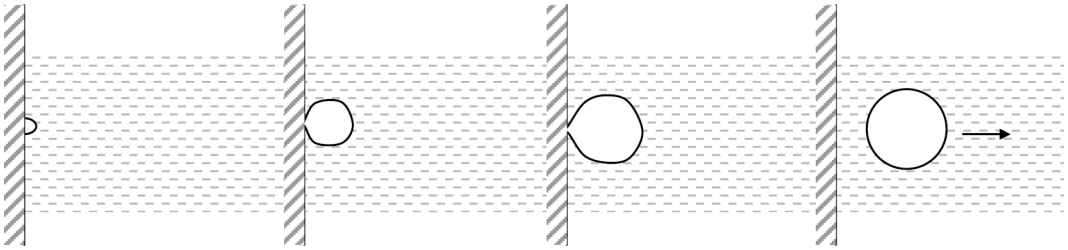

Figure 1.10: Schematic view of the nucleus separation from substrate (redrawn from reference [122]).

The validity of these five proposed explanations have been intensively argued and discussed. However, no one has been accepted as the sole mechanism to understand the origin of equiaxed grain, because each of them is supported by strong experimental evidences. Now, an accepted view is that the five major explanations have their own suitable experimental conditions, and may

control the grain size together in some special cases [113].

1.5.3 Grain refinement mechanism under the application of electric currents

Numerous understandings and explanations about the grain refinement driven by electric currents have been proposed, such as heterogeneous nucleation, dendrite fragmentation and crystal rain mechanism. Details will be discussed in the following sub-sections.

Heterogeneous nucleation

According to the classical nucleation theory [104, 111], the heterogeneous nucleation can be promoted if the deeper undercooling and/or the decreasing of the nucleation energy barrier are achieved. Hence, many scholars proposed that electric currents can enhance the heterogeneous nucleation rate by changing the undercooling and/or nucleation energy barrier [67-71, 73, 80, 93]. Barnak et al. [67] reported that the application of ECP increased the undercooling of solidifying SnPb alloy. As shown in figure 1.11, it can be observed that the undercooling even can be increased to about 10 ^{o}C when a current density 1500 A/cm^2 is applied. Zhao et al. [93] proposed an undercooling mechanism driven by ECP to predict the grain size of alloys. It was suggested that the undercooling was determined by two competitive effects: the electromagnetic force and Joule heating. The electromagnetic force was indicated to increase the undercooling. Inversely, the Joule heating showed a negative effect on the undercooling. They thought that the overheating in the melt could rapidly be lost by the application of the electromagnetic force to increase the undercooling; Joule heating could supply a temperature increment during solidification to decrease the undercooling. However, it is not clear how the electromagnetic force removes the overheating; the value of the temperature increment should be examined. Hence, the undercooling mechanism proposed by Zhao et al. [93] should be verified by more research.

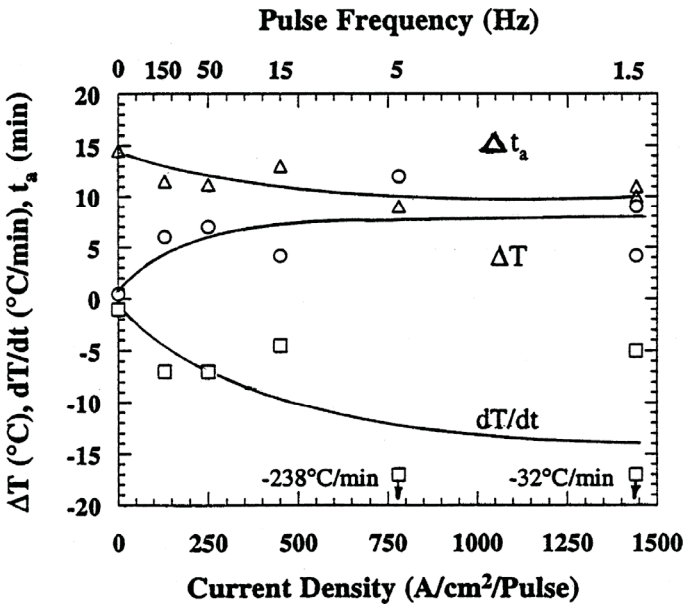

Figure 1.11: Effect of ECP on the characteristics of the cooling curves during solidification of 60Sn40Pb: (a) ΔT, the amount of undercooling, (b) dT/dt, the average rate of temperature rise between the minimum undercooled temperature and the thermal arrest temperature and (c) Δt_a, the duration time of the thermal arrest. From Barnak et al. [67].

Moreover, Barnak et al. [67] proposed that both, the volumetric and interfacial free energy changes between the solid-liquid phase and the nucleation energy barrier may be modified to increase the nucleation rate under the treatment of ECP. Subsequently, Qin et al. and Zhou et al. [68-71] analyzed the effect of electric current on the nucleation energy barrier ΔG^* theoretically. The change of the nucleation energy barrier under the application of electric current $\Delta G_{EC}{}^*$ is given by:

$$\Delta G_{EC}^* = K\mathbf{J}^2 \zeta V_n \tag{1.24}$$

where K is the constant of material, V_n is the volume of nucleus, ζ is calculated by:

$$\zeta = \frac{\sigma_0 - \sigma_n}{\sigma_n + 2\sigma_0} \tag{1.25}$$

where σ_0 is the electric conductivity of melt, and σ_n is the electric conductivity of nucleus.

The final nucleation energy barrier ΔG^* is given by:

$$\Delta G^* = \Delta G_v^* + \Delta G_i^* + \Delta G_{EC}^* \tag{1.26}$$

For most alloys the electric conductivity of melt is less than that of the nuclei (solid phase). It means that the ζ, as well as the $\Delta G_{EC}{}^*$, has a negative value. Hence, the nucleation energy barrier

ΔG^* decreases under the application of electric current. It was concluded by authors that the reduction in the nucleation energy barrier caused the grain refinement in the alloys, even the nano-scale grains. Gao et al. also [73] reported that the effect of electric current on the nucleation energy barrier was one of the reasons for the grain refinement induced by ECP in alloys according to Dolinsky and Elperin's theoretical analysis work [123]. The equation with respect to the change of the nucleation energy barrier by applied electric current is similar to that proposed by Qin et al. and Zhou et al [68-71]. However, it should be noted that the corresponding experimental research should be performed to prove this theoretical analysis.

Dendrite fragmentation

The grain number can be increased when the formed dendrite is fragmented into many small pieces. These pieces can directly become nuclei without undercooling, because the pieces are from the mother phase (melt) and can be well wetted. Hence, dendrite fragmentation promoted by electric currents was widely proposed to explain the grain refinement formation driven by electric currents [65, 73-75, 77, 81, 85, 96].

As reviewed in 1.4.2.3 about the dendrite fragmentation process without the influence of external energy fields, various possibilities were discussed to explain the detachment of necked dendrite arms from the primary trunk, such as temperature fluctuations, solute fluctuations, and surface energy effect. It seems like that Joule heating can cause the temperature fluctuations. Figure 1.12 schematically shows electric current flowing through a dendrite (solid phase). For most alloys the solid phase has a lower electric resistivity than the surrounding melt. It means that the dendrite has a higher electric current density. When the electric current flows from the primary trunk to the dendrite arm, higher temperature has the potential to be generated at the root of the dendrite arm in view of the fact that the root has a smaller sectional area as well as higher electric resistivity. According to equation 1.2 the higher electric current density and electric resistivity can generate the higher quantity of Joule heating. Hence, Gao et al. [73], Yang et al. [77, 85] and Yin et al. [96] proposed that the temperature fluctuations induced by Joule heating in dendrite promoted the detachment of dendrite arms and then produced the grain size reduction in alloys during the solidification process. However, on account of the high thermal conductivity of alloys, the temperature fluctuations induced by Joule heating is possible to be homogenized rapidly.

Hence, more research should be performed to investigate this process in detail.

In addition, Nakada et al. [65] firstly suggested that the dendrite arms can be mechanically broken by electric currents to promote the detachment of dendrite arms. The applied high intensity of ECP can generate the strong electromagnetic force which may induce the dendrite arms fracture. Subsequently, Gao et al. [73], Yang et al. [77, 85], He et al. [74, 75] and Ban et al. [81] proposed the similar explanation to discuss the grain fragmentation promoted by the application of electric currents. However, there is no more research with respect to the mechanically broken physical process of dendrite arms driven by the electromagnetic force.

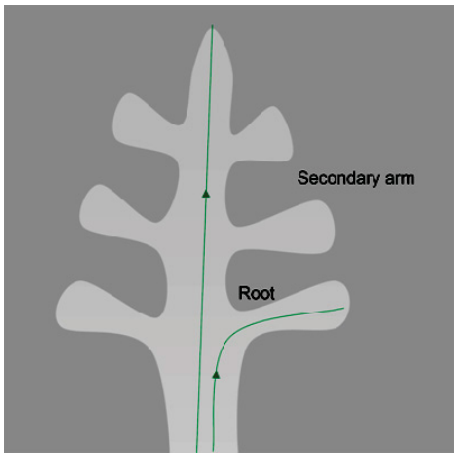

Figure 1.12: Schematic view of electric current (green line) flowing through a dendrite.

Crystal rain

The crystal rain mechanism was proposed by Liao et al. [82] and Li et al. [86] based on a series of solidification experiments. A configuration of upward-downward electrodes was employed by Liao et al. to conduct ECP during the solidification of commercial pure aluminum. A cylindrical wire netting was located in the sample to prohibit the free crystal flowing in or out. As the macrostructure on the longitudinal section shown in figure 1.13a, coarse grains are formed in the inner region of the cylindrical wire netting for both, treated and untreated samples. However, the significant grain size reduction can be observed between the wall of the crucible and the outer wall of the netting in the sample treated by ECP, compared with the reference sample without ECP. Hence, it was concluded that the equiaxed grains originated from the wall of the crucible during the solidification process. Liao et al. thought that the crystal nuclei formed on the mould wall would be broken, detached off and moved into the melt under the action of electromagnetic force generated by electric current through the configuration of upward-downward electrodes.

Then, a large number of nuclei in the melt, as well as the grain refinement, was generated as schematically shown in figure 1.13b.

Subsequently, Li et al. considered the grain refinement of commercial pure aluminum under the configuration of a pair of vertically arranged parallel electrodes. It was found that the significant grain refinement was also achieved. Li et al. proposed that a thin solidified shell may form at the free surface in view of the fact that the free surface directly contacts air. A large number of nuclei can be detached from the surface of melt under the influence of electromagnetic force, as shown in figure 1.14.

Liao et al. and Li et al. termed the two grain refinement processes as the crystal rain or grain rain mechanism. Recently, based on this proposed crystal rain mechanism, Qi et al. [100] developed a mathematic model to investigate the crystal detachment from the wall by analyzing the applied force on the nucleus. They considered the electromagnetic force from electrodes (F_1, F_2), pressure from melt (F_p) and interfacial tension (F_j) (see figure 1.15), then gave a criterion for the nucleus detached from the wall:

$$F_1 \geq F_2 + F_p + F_j \tag{1.27}$$

However, this proposed model is really rough. For example, the adhesive force between the nucleus and the wall should be calculated.

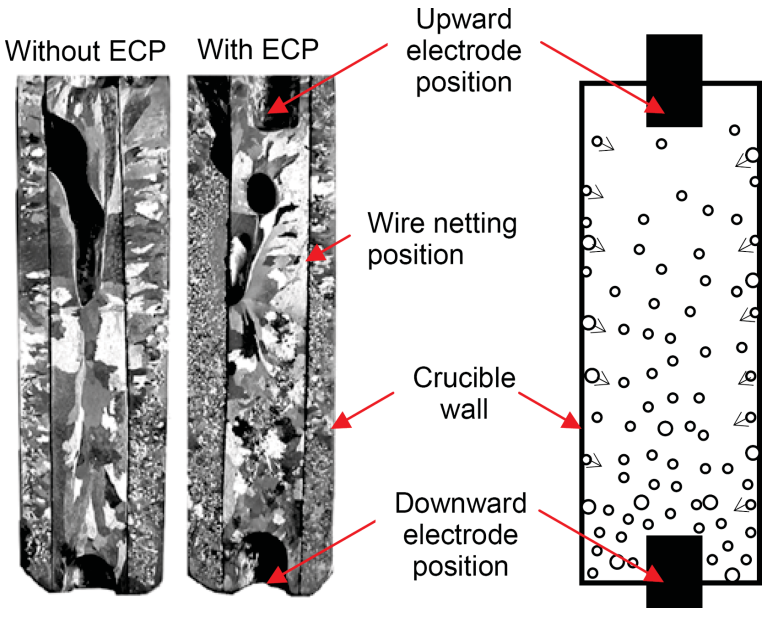

Figure 1.13: Crystal rain mechanism for the configuration of upward and downward electrodes: (a) macrostructure on the longitudinal section [82], (b) schematic view.

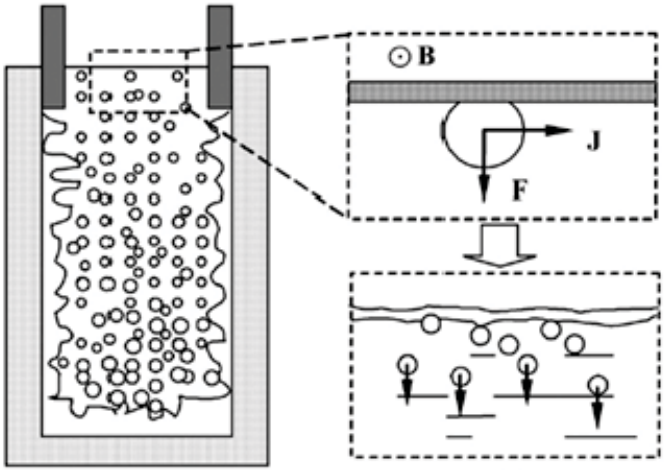

Figure 1.14: Schematic view of crystal rain mechanism for the configuration of two parallel electrodes [86].

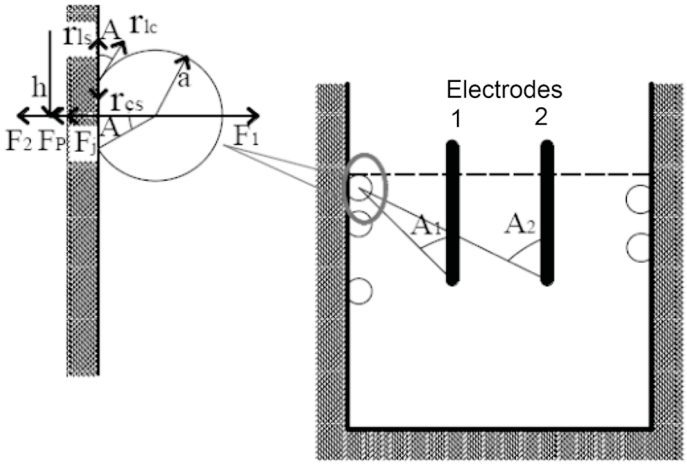

Figure 1.15: Schematic view of the force analysis on a nucleus under the application of electric current [100]. F_1: electromagnetic force from electrode 1, F_2: electromagnetic force from electrode 2, F_p: pressure from melt, F_j: interfacial tension.

In summary, although several grain refinement mechanisms under the application of electric currents have been proposed, the knowledge has not shown a consistent picture with respect to the grain refinement formation process driven by electric currents. Further research should be carried out to investigate this process in detail.

1.5.4 Grain refinement mechanism under the application of magnetic field

Electromagnetic stirring (EMS) has been utilized to control the solidification structure of alloys. It has been recognized for many years that the EMS has the capability to generate the grain refinement of alloys during the solidification process. For the grain refinement of alloys under the application of EMS, there is no doubt that the induced forced flow in the melt drives the grain refinement formation. It is also widely accepted that the dendrite fragmentation driven by forced flow is the grain refinement mechanism of alloys under the application of EMS [124]. However, the detachment process of dendrite arms from the dendrite trunk is still unclear. Several possibilities are proposed to describe how the dendrite arms are detached from the trunk under the influence of forced flow. The temperature fluctuations and solute fluctuations induced by forced flow are frequently suggested to generate the detachment process [44, 124]. Nevertheless, it still can give a reference for the investigation about the grain refinement of alloys under the application of electric currents. We have shown in section 1.4.2 that the forced flow also may be generated in the melt under the application of electric currents. Hence, according to the investigation about the grain refinement driven by EMS, it is possible that the forced flow induced by electric currents can cause the grain refinement of alloys. Here we will not only confirm that the forced flow can be induced by electric currents, but also investigate the contribution of forced flow to the grain refinement of alloys.

2.Research methods

2.1 Introduction

It has been shown that electric currents have potential to generate the forced flow inside the melt (see 1.3). According to the literature review about the grain refinement driven by electromagnetic stirring (see 1.4.4), the forced flow has capability to cause the grain refinement in alloys. Hence, the fluid flow driven by electric currents will be investigated in the present thesis.

This chapter presents the experimental methods of solidification experiments and flow measurements, covering three components: experimental materials, setup and procedure. The numerical simulation method about the fluid flow under the application of electric current is also introduced. The numerical results can show the flow structure in detail that cannot be sufficiently achieved from the flow measurements. In addition, the distribution of electric currents, induced magnetic fields, and the electromagnetic force inside the melt can also be presented. It is beneficial to estimate the influence of electromagnetic force, Joule heating and skin effect in the grain refinement.

2.2 Experimental materials

2.2.1 Solidification

According to the phase diagram shown in figure 2.1, Al-Si binary alloy has a eutectic reaction during the solidification process. Its eutectic composition is at 12.6wt%Si. For the hypoeutectic alloys during the solidification process, the primary aluminum phase firstly nucleates from the melt and grows in dendrite. When the composition of melt increases to the eutectic point, the eutectic Al-Si phase is formed until the end of solidification. As a consequence, the as-solidified hypoeutectic alloys usually consist of the primary aluminum phase and the harder Al-Si eutectic phase. Here in the present study, an Al-7wt%Si hypoeutectic alloy (nominal composition) was used in the solidification experiments. Selected thermo physical properties of the Al-7wt%Si hypoeutectic alloy are shown in table 2.1.

Dendrite fragmentation is one of the most important grain refinement mechanisms (see 1.4.3). The solute or temperature fluctuations are assumed to cause the dendrite fragment. In order to avoid the solute effect in the dendrite fragmentation, two grades of high purity aluminum, 99.99wt%Al and 99.9999wt% (Hydro Aluminum High Purity GmbH), were also employed as an investigated material.

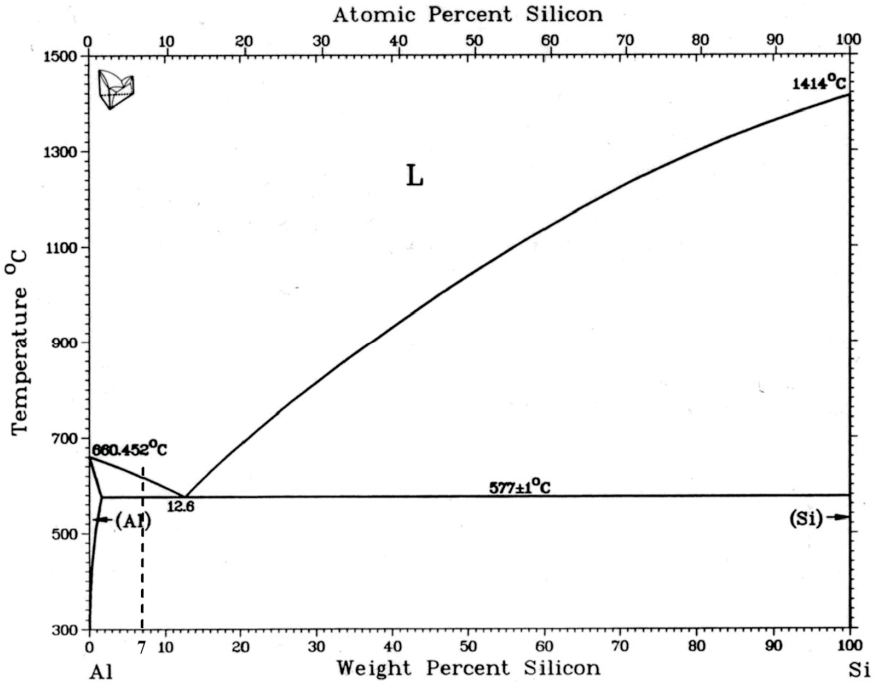

Figure 2.1: Phase diagram of Al-Si binary alloy.

2.2.2 Similarity of GaInSn liquid metal and Al-Si melt

The ultrasound Doppler velocimetry (UDV) technique that can monitor the flow inside the melt of metal was employed to measure the fluid flow velocity. However, the application of this technique in the melt of the Al-7wt%Si alloy has not been well developed because the temperature of melt is too high. In the present study, flow measurements were performed at room temperature in a liquid metal, eutectic alloy Ga-20wt%In-12wt%Sn (T_L=10.5°C). Selected thermo physical properties of Ga-20wt%In-12wt%Sn can be found in the table 2.1. More details can be referred to in literature [125, 126].

It is necessary to assess if the similar flow structure would be generated in both, Ga-20wt%In-12wt%Sn liquid and Al-7wt%Si melt. We follow the paper of Bojarevics et al. [127], who considered a steady electric current *I* passing through a liquid metal hemisphere. They

introduced a dimensionless parameter *S*:

$$S = \mu_0 I^2 / 4\pi^2 \rho v^2 \tag{2.1}$$

where v is the kinematic viscosity, ρ is the density of the liquid metal and μ_0 is the magnetic constant. A comparison between the alloys Al-7wt%Si and Ga-20wt%In-12wt%Sn with respect to the non-dimensional parameter *S* is presented in table 2.1. It becomes obvious that the occurrence of similar flow structures can be assumed for the same electric currents applied, where the intensity of the flow should be even slightly larger in Al-7wt%Si melt as in Ga-20wt%In-12wt%Sn.

Table 2.1: Comparison between Al-7wt%Si and Ga-20wt%In-12wt%Sn with respect to selected material properties

	Al-7wt%Si [128]	Ga-20wt%In-12wt%Sn [126]
Liquidus (T_L), K	888	283,7
Density ρ, kg/m³ (T_L+15K)	2422	6360
Viscosity ν, m/s² (T_L+15K)	$0{,}5 \cdot 10^{-6}$	$0{,}34 \cdot 10^{-6}$
El. conductivity σ, 1/Ωm	$3{,}74 \cdot 10^{6}$	$3{,}27 \cdot 10^{6}$
$S=\mu_0 I^2/4\pi^2\rho\nu^2$	$52{,}6 \cdot I^2$	$43{,}3 \cdot I^2$

2.3 Experimental setup

2.3.1 Solidification

As shown in 1.4.2, both columnar and equiaxed structures are achieved during the solidification process of mould casting. After the columnar zone is formed, the equiaxed grains freely grow as the inner equiaxed zone. Here for simplicity, we will investigate the grain refinement using two different cooling regimes. One type is that the bottom of the mould is put on a water-cooled copper chill which is kept at a constant temperature of about 20°C to achieve directional bottom-up solidification. The other one is that the mould is cooled in air to approach an isothermal solidification.

The two types of cooling conditions were employed to produce different structures. As shown in figure 2.2, a double walled cylindrical stainless steel mould is employed. Beneath the bottom of

the mould, a water cooled copper platform with the temperature of 20 ^{o}C was used to cool the heated mould. Since the side of the mould is double walled, the heat release through the radial direction of cylinder mould can be ignored in comparison with the heat loss through the vertical direction when the bottom of the mould touched the cooling platform. The solidification process can be regarded as the directional solidification. It is well known that the columnar structure can be produced under such kind of cooling condition. In addition, the free growth of equiaxed grains can be achieved when the sample is slowly cooled throughout the mould [20]. Such cooling conditions can be realized when the double walled mould is cooled by air without the bottom forced cooling.

At the top of the mould, thermocouples and a pair of parallel stainless steel cylindrical electrodes (diameter 8mm) were fixed at a stainless steel lid. Thermocouples were vertically located only along the axis of the mould to measure the temperature. The parallel electrodes were vertically and symmetrically arranged in the mould with a distance of 36mm, and immersed into the melt through the upper free surface with a 10mm depth. Electric current was conducted through the electrodes into the melt. The inner wall of the mould was coated by an electric insulation material (BN) to avoid a closure of the current in the wall. Moreover, the lateral surface of the electrodes was also covered by the insulation material to confine the electric current only flowing through the bottom surface of the electrodes (see figure 2.2).

The measurement temperature range for the solidification experiments was between 750^{o}C and 500^{o}C, the NiCr-Ni type thermocouple is suitable and selected to measure the temperature. All the NiCr-Ni thermocouples were embedded in an INCONEL (trademark of INCO Alloys International, Huntington, WV) sheath with an outer diameter of 1.5mm and covered by Al_2O_3 tubes for protection. A multimeter DMM 2700 and a 20-channel differential multiplexer card 7700 (Keithley Instruments Inc., Cleveland) were used to monitor the thermocouple voltages. The monitor frequency, resolution, and the error of the temperature measurement system were 5Hz, 0.01 ^{o}C and ±1 ^{o}C, respectively.

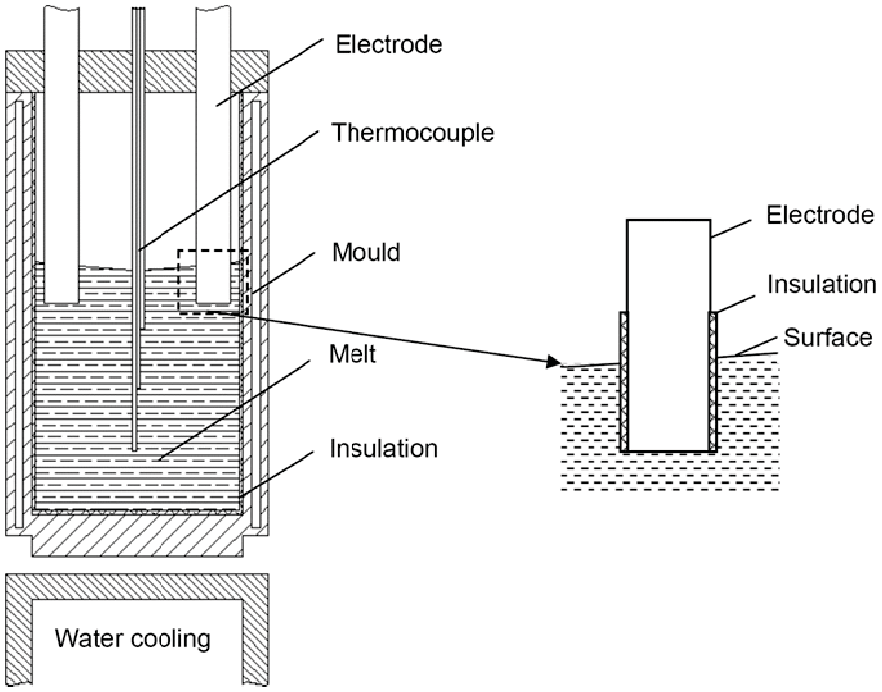

Figure 2.2: Schematic view of solidification experimental setup.

2.3.2 Flow measurements

The schematic view of the flow measurement setup is shown in figure 2.3. The eutectic alloy Ga-20wt%In-12wt%Sn is filled in a cylindrical vessel made of Perspex with the same dimensions as the mould used in the solidification experiments (radius R_0=25mm, height H_0=60mm). A pair of vertically arranged parallel electrodes is inserted through the free surface into the melt with the same dimension in the solidification experiments (insert depth 10mm, electrodes distance r_E=18mm). The electrodes are made of stainless steel with a cylindrical shape of 8mm diameter. For application of DC and pulsed electric current, the power supply is the same as that one used in the solidification experiments.

The ultrasound Doppler velocimetry (UDV) was applied to monitor the fluid flow inside the melt. This method is based on a pulse-echo technique where ultrasonic bursts of a few cycles are emitted from an ultrasonic transducer and propagate along the measuring line perpendicular to the transducer surface. The pulses are scattered by micro particles suspended in the fluid whose echo signals are received by the same transducer. The echo signals enable to determine the velocity profile along the measuring line.

In the present study, both the single transducer and ultrasonic arrays are employed. For the single sensor, an 8MHz transducer (TR0805LS, acoustic active diameter 5mm) of the DOP2000 velocimeter (model 2125, Signal Processing SA, Lausanne) was vertically located at the bottom of the vessel to measure the one-dimensional flow along the vertical direction. The spatial resolution along the vertical direction is about 1.4 mm, and the accuracy of the velocity data can be assessed to 0.15mm/s. The two-dimensional velocity field can be measured by the application of ultrasonic arrays in combination with specific array driving techniques which allow a two-dimensional flow mapping. The linear array, which comprises singular 25 ultrasonic transducers, has a length of about 68mm. It is located radially at the bottom of the cylinder vessel to measure the axial flow component in the plane spanned by height and diameter of the liquid metal column. According to the dimensions of the sensor array and the fluid cylinder, the measuring domain is divided into 20 velocity profile lines. The lid of the vessel fixing the parallel electrodes is pivoted with respect to the cylinder bottom. The rotation of the lid enables flow measurements in different planes with reference to the plane containing the electrodes.

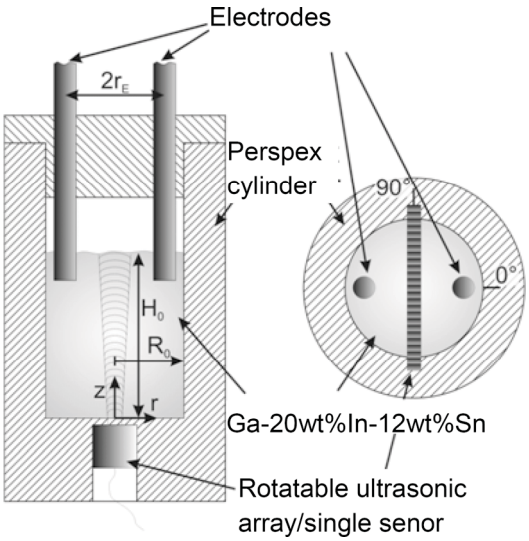

Figure 2.3: Schematic view of the flow measurement setup.

2.3.3 External energy fields

The DC electric current and the current pulses are generated by the water cooled power supply *pe86CWD* (*plating electronic)*. This device gives us the possibility to generate rectangular current pulses of variable pulse length at adjustable frequencies up to 200Hz. Parameter variations in

case of a pulsed electric treatment concern the current amplitude I_0, the frequency f and the pulse length t_p. The scheme of applied ECP is shown in figure 2.4. The chosen electric current parameters can be programmed by a control unit with touch panel (Pe8005).

In addition, the inputting energy in the melt of the Al-Si alloy was estimated. Experiments were conducted using amplitudes of electric current up to 480A corresponding to voltages up to 6V. However, electrodes and power lines have a distinctly higher electrical resistance compared to the liquid metal which leads to the situation that only 1% of the voltage drop occurs in the melt. Therefore, the overall heat input into the melt by Joule heating must be less than 30W.

It has been reviewed that the significant grain refinement can also be generated by the application of a magnetic field (see 1.4.4). Here a traveling magnetic field (TMF) is employed to make comparisons with electric currents. This kind of magnetic fields is supplied by the COMMA (COMbined MAgnetic field) facility, which was constructed at the HZDR. Six horizontal circular induction coils are arranged axially. The wave number k of the TMF is:

$$k = 2\pi / \lambda \tag{2.2}$$

where λ is the wave length. In the present TMF, a wavelength of approximate λ=0,235m is generated in the region of the sampling volume because a phase shift of 60° between adjacent coils is applied. Both upward and downward direction of the TMF can be provided. A low magnetic field frequency of 50Hz was selected in the present study to ignore the influence arising from the skin effect.

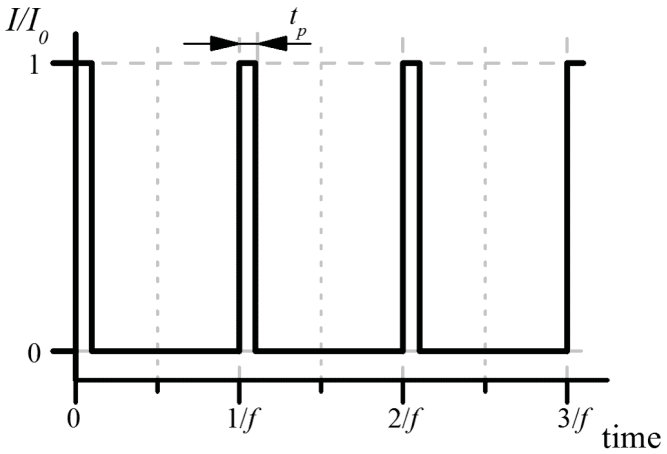

Figure 2.4: Schematic view of the waveform for the pulsed electric current.

2.4 Experimental procedure

2.4.1 Solidification

Al-7wt%Si

An Al-7wt%Si hypoeutectic alloy (nominal composition) was prepared using pure Al (99.99 wt.%) and Si (99.999 wt.%) and modified by Sr at 200ppm in a graphite crucible. The prepared pure aluminum was located in the graphite crucible and heated up to 900^{o}C in a box type electric resistance furnace. After 60mins, the corresponding weighted silicon particles were added into the aluminum melt and kept for another 60mins. Then, the AlSr alloy was put into the melt. Meanwhile, the temperature of the furnace was set at 680^{o}C. Then, the temperature of the molten alloy gradually decreased in the furnace from 900^{o}C to 680^{o}C. After 45mins, the melt was degassed 20mins by argon gas. Finally, the molten alloy at a temperature of 680 ^{o}C was poured into a cylindrical stainless mould of 50mm diameter. Subsequently, each solidified sample was cut to the same weight of 310g (Φ50mm(diameter)×60mm(height)).

The preparatory Al-7wt%Si sample was inserted into the double walled mould and heated up to 750 ^{o}C in a resistance furnace. After a holding time of 45mins the temperature was reduced from 750 ^{o}C to 720^{o}C which has been kept constant for another 30mins. After total melting, the mould with the melt was taken from the furnace and covered with a stainless steel lid. Both, the electrodes and thermocouples were fixed at the lid and immersed through the free surface into the melt. Then, the sample in the mould was cooled and solidified. The temperature measurement of the sample started at the beginning of the cooling of the samples, and stopped until the sample was cooled to 500^{o}C.

Moreover, two experimental details should be mentioned. The thermocouples and the electrodes with the connected power cables were supposed to act as an additional local cooling. To avoid an immediate formation of a solid shell, the thermocouples and electrodes were preheated until achieving the same temperature as the melt before the cooling from the bottom was initiated. The cables between the electrodes and the power supply were fixed at a considerable distance to the mould in order to minimize the interaction between the induced magnet field around the cable and the electric current flowing in the solidifying melt.

High purity of aluminum

As for the high purity aluminum, cylindrical ingots with a geometry parameter Φ50mm×60mm were directly machined from the raw billet to avoid the pollution from the preparation process. The surface of specimens was ground on SiC-paper and cleaned by using an ultrasonic cleaner.

The preparatory high purity aluminum sample was also located into the double walled mould and heated up to 750^{o}C. After a holding time of 75min at 750^{o}C, the double walled mould with melt was moved out and covered with a preheated stainless steel lid, and then cooled on air to achieve an isothermal solidification. Solidification experiments were performed under the influence of both rectangular ECP and TMF. The cooling of the high purity aluminum sample and the treatment by the electric current or TMF were initiated at the same time. When the samples were totally solidified, the application of electric current or magnetic field stirring was powered off.

2.4.2 Flow measurements

The eutectic alloy Ga-20wt%In-12wt%Sn with designed weight was filled into the cylindrical vessel made of Perspex to achieve the volume of Φ50mm×60mm, which is same as the sample for solidification experiment. Then, a lid with a pair of parallel electrodes covered the vessel. The arrangement of electrodes in Ga-20wt%In-12wt%Sn melt is the same as the position of electrodes in Al-7wt%Si alloy. The selected ultrasonic transducer was located at the measurement position. The top of the transducer was connected with the bottom of the vessel by a transparent gel. Finally, the electric current and the flow velocity measurement were initiated at the same time. The measurement was stopped and then the power supply was powered off after several tens of seconds.

2.5 Metallography

Solidified samples were sectioned longitudinally along its mid-plane (perpendicular to the plane containing the electrodes) for metallographic investigations. The metallographic sections were ground on SiC paper. Then, the as-ground sections were etched in an etchant composed of 60mL HCl, 30mL HNO_3, 5mL HF, and 5mL H_2O. Photographs of the macrostructure were taken by a digital camera (Konica MinoltaDimage A2). Selected longitudinal sections were ground and

polished from 6μm to 1μm, electro-etched of 50mm×30mm in Barker etching reagent at 25V, 15Hz for 180s, then examined by using an optical microscope MeF4 (Leica Microsystems, Wetzlar) using the polarized light for the quantitative analysis of the grain size. 540 single pictures (2.88mm×2.16mm) were created firstly and then combined into an entire picture covering the whole sample by using the software (Leica Application Suite V3.6) of Leica Microsystems. The grain size was measured by the linear intercept method in the software package aquinto a4i (Fa. Aquinto AG). As shown in figure 2.5, five horizontal lines and five vertical lines are uniformly distributed on the planar section along the vertical and horizontal direction, respectively. These ten lines are intercepted by grain boundaries, as shown in figure 2.5. The number of interceptions and the length of the ten lines were counted. The mean linear intercept (*MLI*) is given by:

$$MLI = N_t / L_t \tag{2.3}$$

where N_t is the total number of interceptions for the ten lines, and L_t is the total length of the ten lines. The measuring error of ±0.08mm is achieved by performing the measurement in the same sample four times.

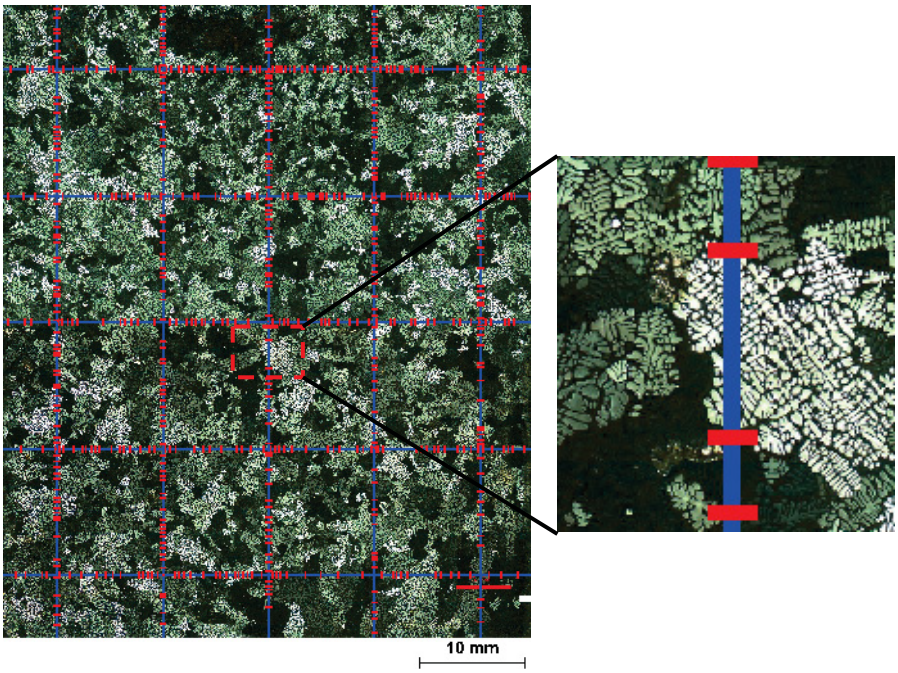

Figure 2.5: Macrostructure of Al-7wt%Si alloy observed under polarized light with intercepted lines for grain size measurement.

2.6 Numerical method

Numerical simulations with respect to the fluid flow inside the liquid metal (eutectic alloy Ga-20wt%In-12wt%Sn) under the application of electric currents were performed by my colleague (Dr. Vladimir Galindo). Here the numerical model and the boundary conditions are introduced, respectively.

2.6.1 Numerical model

For the numerical simulations of the electric current **J** and the magnetic induction **B** in the melt and all electrically conducting parts of the facility, the finite element code OPERA 3d (Cobham plc., [129]) was used. The computational grid was refined near the contact region between the electrodes and the melt and has a total number of 4.3 million of finite elements. In the case of a direct current imposed on the electrodes, we solve the Laplace equation for the electric potential φ taking into account the charge conservation:

$$\nabla^2 \varphi = 0 \tag{2.4}$$

The current density **J** can be calculated from the electric potential φ:

$$\mathbf{J} = \sigma(-\nabla \varphi) \tag{2.5}$$

The continuity of the current density **J** at the interface between two regions with different electric conductivities:

$$J_n = -\sigma_1 \mathbf{n} \cdot \nabla \varphi_1 = -\sigma_2 \mathbf{n} \cdot \nabla \varphi_2 \tag{2.6}$$

The magnetic induction **B** was calculated from the current density **J** using the Biot-Savart's law:

$$\mathbf{B}(\mathbf{r}) = \frac{\mu_0}{4\pi} \int d\mathbf{r}^3 \frac{\mathbf{J}(\mathbf{r}') \times (\mathbf{r} - \mathbf{r}')}{\left|\mathbf{r} - \mathbf{r}'\right|^3} \tag{2.7}$$

where μ_0 is the permeability of a vacuum, **r** is the vector of displacement.

The electromagnetic force per unit volume **F** in a conducting substance, resulting from the interaction between the electric current and the self-induced magnetic field, can be calculated by the following equation:

$$\mathbf{F} = \mathbf{J} \times \mathbf{B} \tag{2.8}$$

The incompressible flow in the volume containing the melt was simulated numerically by means of the open source library Open FOAM [130] solving the Navier-Stokes equation including the continuity equation:

$$\nabla \cdot \mathbf{U} = 0 \tag{2.9}$$

and momentum equations

$$\rho(\frac{\partial \mathbf{U}}{\partial t} + (\mathbf{U} \cdot \nabla)\mathbf{U}) = -\nabla p + \mu \nabla^2 \mathbf{U} + \mathbf{F} \tag{2.10}$$

where **U**, ρ, μ, and p represent the velocity, the density, the molecular dynamic viscosity and the pressure, namely.

2.6.2 Numerical domain and boundary conditions

The geometry for the numerical simulation is shown in figure 2.6. It presents the same dimensions as the configuration used in the melt measurements as well as the solidification experiments. Both, DC and alternating current (AC) are conducted into the melt. Various frequencies of AC are concerned to estimate the effect of the skin effect on the distribution of the magnetic field, Joule heating and electromagnetic force. The boundary conditions for the electric potential are defined by using the amplitude of the imposed electric current I at the end of the electrodes:

$$I = \int_A \mathbf{J} \cdot d\mathbf{s} \tag{2.11}$$

where A is the area of the electrodes cross section.

The boundary conditions for the flow field are the no-slip condition (**U=0**) at the solid container walls. For the melt surface either the no-slip condition or the conditions for a stress-free, non-deformable surface are applied depending on whether the melt flow is evaluated in an open or an enclosed container. A computational grid with 650,000 volume elements was used. We used a second order discretization scheme for the convective term in the equation (2.10).

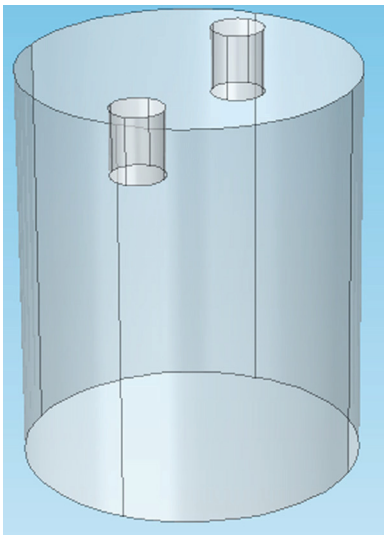

Figure 2.6: Geometry of the simulation domain.

3. Role of electric currents effects in the grain refinement

3.1 Introduction

Understanding the role of various electric currents effects in the resulting grain refinement is of high importance for achieving a beneficial grain refinement mechanism. This chapter is devoted to investigating which effect or effects play a key role in the grain refinement formation of alloys. Firstly, a series of solidification experiments were performed in the Al-7wt%Si hypoeutectic alloy under the influence of ECP and DC with various electric current parameters. Then, the corresponding numerical simulations and forced flow measurement experiments were carried out to investigate the fluid flow inside the melt under the application of electric currents. After that, the temperature distribution was examined in the Al-7wt%Si hypoeutectic alloy under the same electric current parameters used in the solidification experiments. Finally, the role of various electric currents effects was discussed.

3.2 Experimental parameter

Solidification experiments of the Al-7wt%Si alloy were performed under the influence of both, electric currents and the travelling magnetic field (TMF). In the experiments presented here, the cooling of the sample and the treatment by the electric currents or TMF were initiated at the same time. When the temperature of the samples was cooled to the eutectic point, the application of electric currents or the TMF was powered off. In this chapter, all solidified samples were forced cooled by water through the bottom of the mould.

Both, DC and rectangular ECP were applied during the solidification of the samples. In order to compare these two different electric current patterns in the same scale, both DC and ECP were calibrated by the electric energy. The electric energy of DC can be represented by the intensity of electric current. The average inputting electric energy of ECP is reflected by the effective value of the applied current amplitude I_{eff}:

$$I_{eff} = I_p \sqrt{t_p \cdot f} \tag{3.1}$$

where I_p is the current intensity, f is the frequency and t_p is the pulse length. The applied electric current parameters are shown in table 3.1.

Temperature measurements were made within the mould cavity during solidification using 6 type-K thermocouples with an overall sampling rate of 5Hz. Thermocouples were arranged vertically along the axis of the mould and positioned vertically from 5mm to 60mm in a distance of 11mm above the bottom of the mould.

Similarly, the melt flow measurements in the eutectic alloy Ga-20wt%In-12wt%Sn were carried out under the application of DC and ECP. Both, the ultrasonic arrays and single transducer were employed to measure the melt flow.

Table 3.1: Electric current parameters in solidification experiments

	Direct current				Electric current pulse							
Intensity (A)	0	48	120	200	120	120	240	240	120	240	480	480
Frequency (Hz)	-	-	-	-	50	100	50	200	200	100	100	200
Pulse length (ms)	-	-	-	-	0.5	1	1	0.5	2	2	1	0.5
I_{eff} (A)	0	48	120	200	19	38	54	76	76	107	152	152

3.3 Results

3.3.1 Solidified structure

The reference experiment conducted without applied electric current (see figure 3.1) shows a dominance of columnar grains growing parallel to the temperature gradient. A transition to a coarse equiaxed growth occurs only just in the upper third of the sample. The application of DC generates a significant modification of the macrostructure in the samples (see figure 3.2). The grain size in the equiaxed zone is reduced remarkably in comparison with that in the reference sample without electric currents. The area of the equiaxed zone enlarges with increasing current intensity. The totally equiaxed grain zone is obtained when the applied DC intensity reaches values higher than 120A.

The same tendency can be observed for an increasing effective value of the current I_{eff} in the

pulsed regime as shown in the figures 3.3. The growth of columnar grains is gradually suppressed with the increasing intensity of inputting energy. As a result, the area of the equiaxed zone is increased. Several coarse columnar grains grow from the bottom with a direction parallel to the temperature gradient. Then, the coarse equiaxed grains are observed. Subsequently, the finer equiaxed grains appear, especially in the region surrounding the electrodes. The solidified structure becomes more uniform and finer with increasing current intensity. Eventually, the most uniform and finest macrostructure can be observed until the totally equiaxed grain zone is formed in the sample under the applied ECP of I_{eff}=152A.

Respective dot plots in figure 3.4 show variations of the subarea of equiaxed grain growth and the mean grain size as a function of I_{eff}. Remarkable changes of both quantities can already be observed at low electric currents, where the alloy starts to solidify in the form of columnar grains at the bottom before the CET occurs. The columnar growth is completely suppressed if the effective current reaches values being higher than about 120A. The mean grain size approaches a minimum value of about 1mm for high electric currents. The applications of DC or pulsed currents achieve the same results with respect to the grain morphology if the corresponding effective values of the current intensity are identical.

Figure 3.1: Solidified macrostructure of Al-7wt%Si alloy on the longitudinal section of the solidified samples without electric currents.

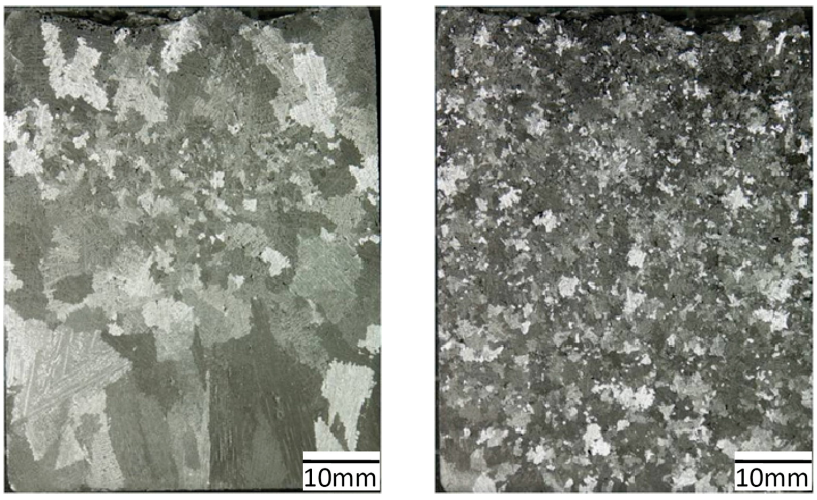

(a): I_{DC}=48A (b): I_{DC}=120A

Figure 3.2: Solidified macrostructure of Al-7wt%Si alloy with direct electric current.

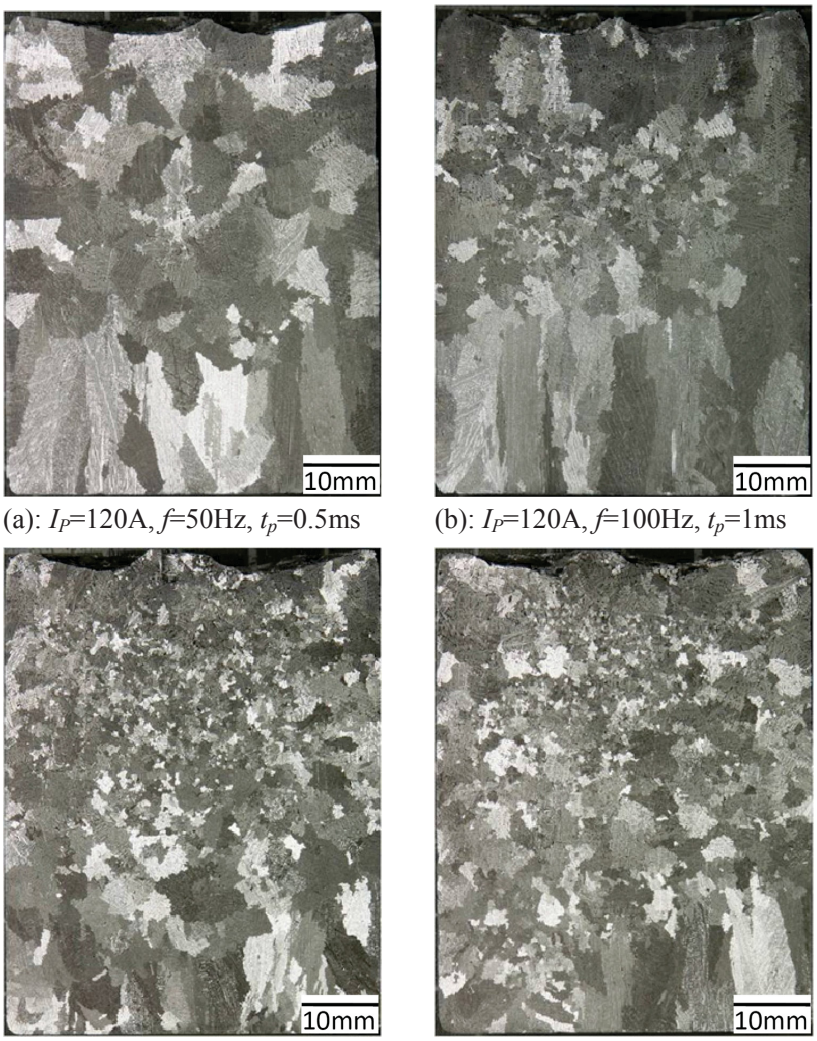

(a): I_P=120A, f=50Hz, t_p=0.5ms (b): I_P=120A, f=100Hz, t_p=1ms

(c): I_P=240A, f=50Hz, t_p=1ms (d): I_P=240A, f=200Hz, t_p=0.5ms

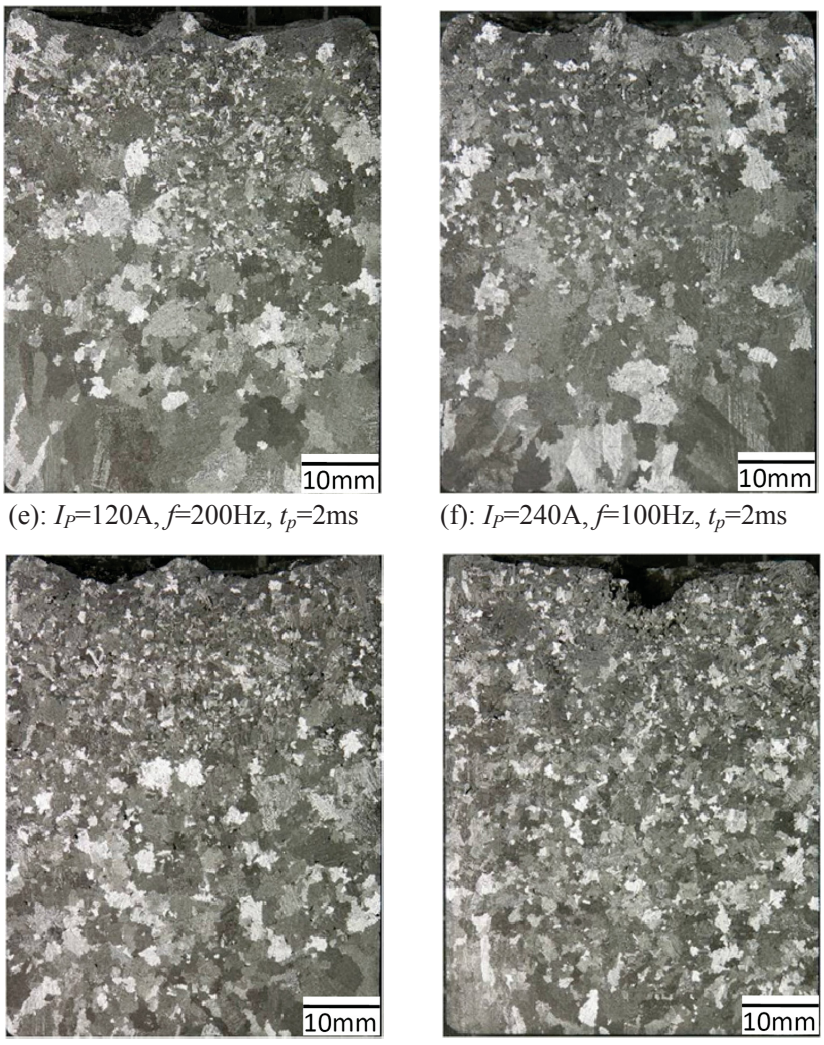

(e): I_P=120A, f=200Hz, t_p=2ms (f): I_P=240A, f=100Hz, t_p=2ms

(g): I_P=480A, f=100Hz, t_p=1ms (h): I_P=480A, f=200Hz, t_p=0.5ms

Figure 3.3: Solidified macrostructure of Al-7wt%Si alloy with pulsed electric current: (a) I_{eff}=19A, (b) I_{eff}=38A, (c) I_{eff}=54A, (d) I_{eff}=76A, (e) I_{eff}=76A, (f) I_{eff}=107A, (g) I_{eff}=152A, (h) I_{eff}=152A.

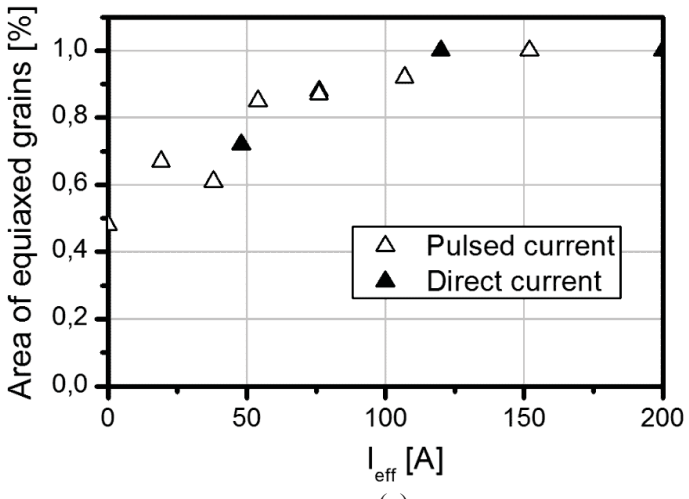

(a)

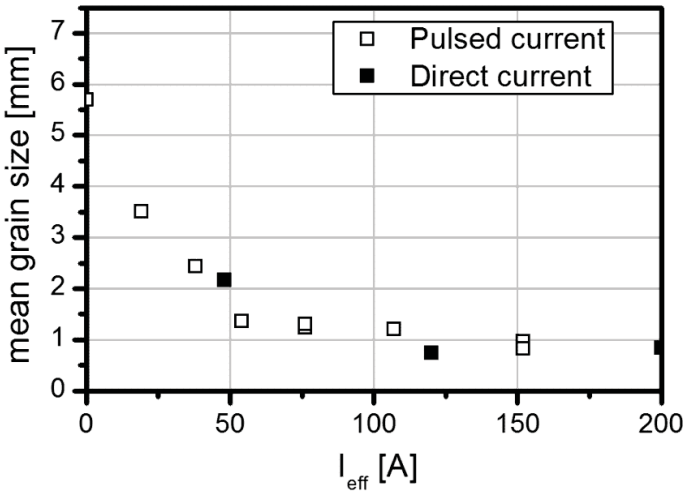

(b)

Figure 3.4: Influence of the applied effective current on the macrostructure of the solidified samples: (a) area of equiaxed grain growth, (b) mean grain size.

3.3.2 Forced melt flow

Flow measurements

The flow measurements are performed within the cylindrical column filled with Ga-20wt%In-12wt%Sn liquid metal. Figure 3.5 shows the two-dimensional distribution of the vertical velocity in the liquid metal for the situation of an applied DC at I_{DC}=48A. The plot in figure 3.5a represents the pattern of the vertical velocity component in the plane containing the electrodes. Obviously, the measurements reveal the downstream jets below the electrodes. The corresponding upward flow along the cylinder side walls, which is less strong as the downward jets, is found in the perpendicular plane (see figure 3.5b). The area around the cylinder axis shows a descending flow in the upper part and an ascending flow in the bottom part. This indicates the occurrence of a vortex pair in the central region between the electrodes. Furthermore, an asymmetry becomes apparent in the velocity distribution in figure 3.5b. The reason for this deviation has not become fully clear yet, however, we assume an influence from the non-symmetric configuration of the power lines around the experimental facility. This assumption is supported by the fact, that the measured flow field shows a deflection in the other direction if the electric current is applied with reversed polarity.

In a next step, we compare the applications of direct (DC) and pulsed currents (ECP). The velocity field shown in figure 3.6 is generated by current pulses with a peak value of the current

I_P=152A, a frequency of f=200Hz and a pulse length of t_P=0.5ms. The resulting effective value of the current I_{eff}=48 A is identical with the direct current amplitude I_{DC} applied in the case of figure 3.5. The comparison of the flow pattern shows only marginal differences, the absolute values of velocities are in the same order of magnitude. The differences between the DC and the ECP regimes are almost negligible.

Further, the flow measurements in the melt are performed under the application of higher I_{eff}. The aim is to examine the evolution of a flow pattern and the intensity with increasing electric currents energy. The single sensor located vertically at the bottom of the cylinder is used to monitor three different positions, as shown in figure 3.7. According to the flow structure observed in figure 3.5 and 3.6, the flow measurements in these three positions can sufficiently reflect the flow pattern and intensity. Figure 3.8 shows the vertical velocity distribution measured at the three positions in cylinder liquid metal under the applied ECP of I_P=480A, f=200Hz, t_p=0.5ms, I_{eff}=152A. The strong downstream is observed under the electrode (see figure 3.8a). The flow measurement at the cylinder axis shows the downward flow in the upper part and upward flow in the bottom part, as shown in figure 3.8b. The upward flow is generated along the sidewalls of the plane which is perpendicular to the plane containing two electrodes (see figure 3.8c). The same flow pattern is formed in the liquid metal for the situation of an applied ECP at I_{eff}=152A according to the flow pattern driven by ECP at I_{eff}=48A shown in figure 3.6. It indicates that the flow pattern is unchanged when the higher I_{eff} is applied. In addition, the flow intensity evolution is considered with an increasing value of effective electric currents. Figure 3.9 presents the measured vertical velocity of forced flow at the cylinder axis under the application of various I_{eff}. The comparison of the measured flow intensity reveals that the forced flow is gradually stronger with increasing intensity of the effective electric currents. Figure 3.10 displays the volume- and time-averaged axial velocity u_z of the melt flow as a function of the effective current I_{eff}. As it was expected, the intensity of the forced melt flow increases with I_{eff}. Moreover, a positive linear relationship between the flow intensity and the I_{eff} can be concluded according to figure 3.10.

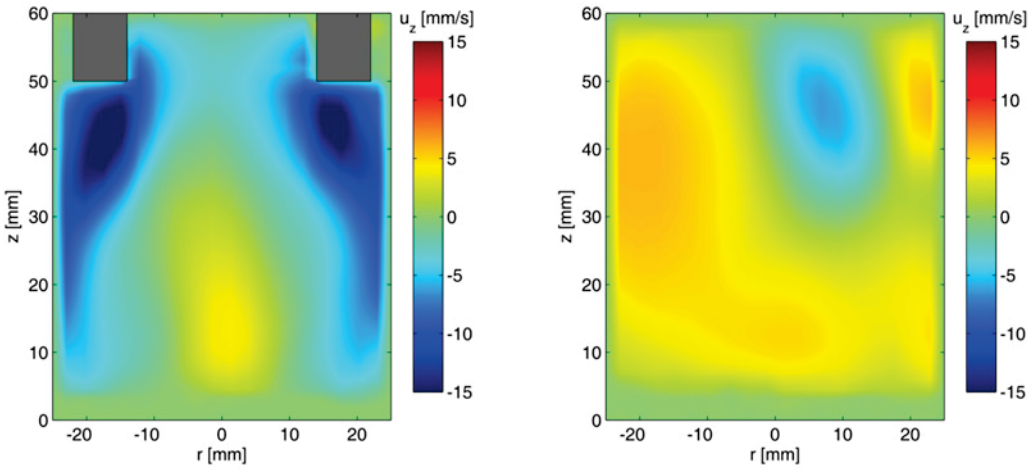

(a) (b)

Figure 3.5: Two-dimensional distribution of the vertical velocity induced by a direct current at I_{DC}=48A: (a) in the plane containing the electrodes, (b) in the plane perpendicular to the electrode plane.

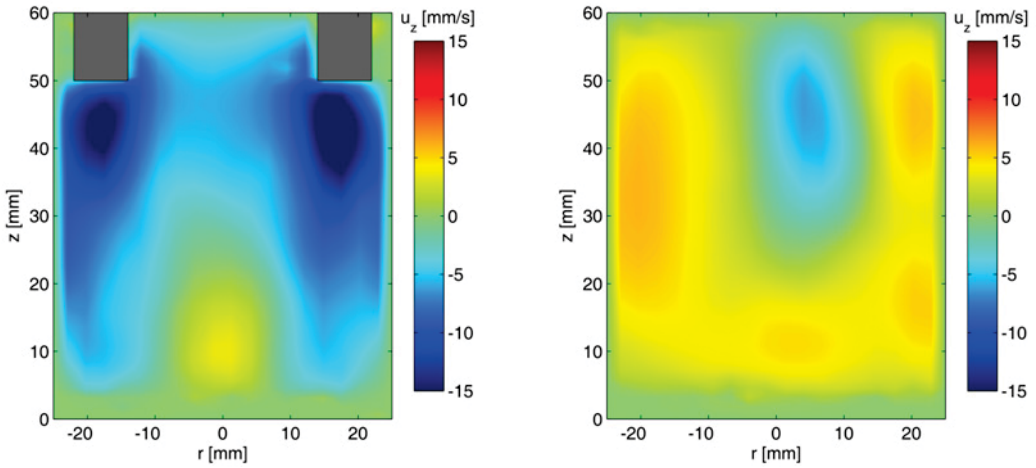

(a) (b)

Figure 3.6: Two-dimensional distribution of the vertical velocity measured at I_P=152A, f=200Hz, t_p=0.5ms, I_{eff}=48A: (a) in the plane containing the electrodes, (b) in the plane perpendicular to the electrode plane.

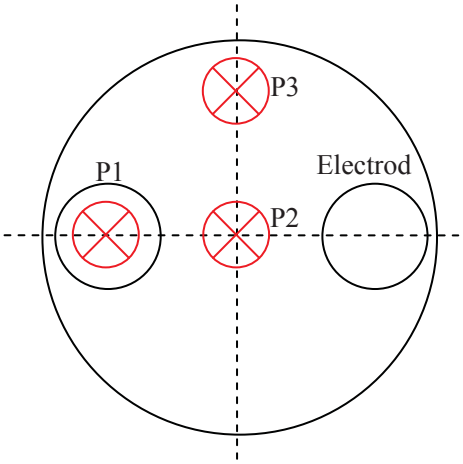

Figure 3.7: Schematic view of single transducer arrangement at the bottom.

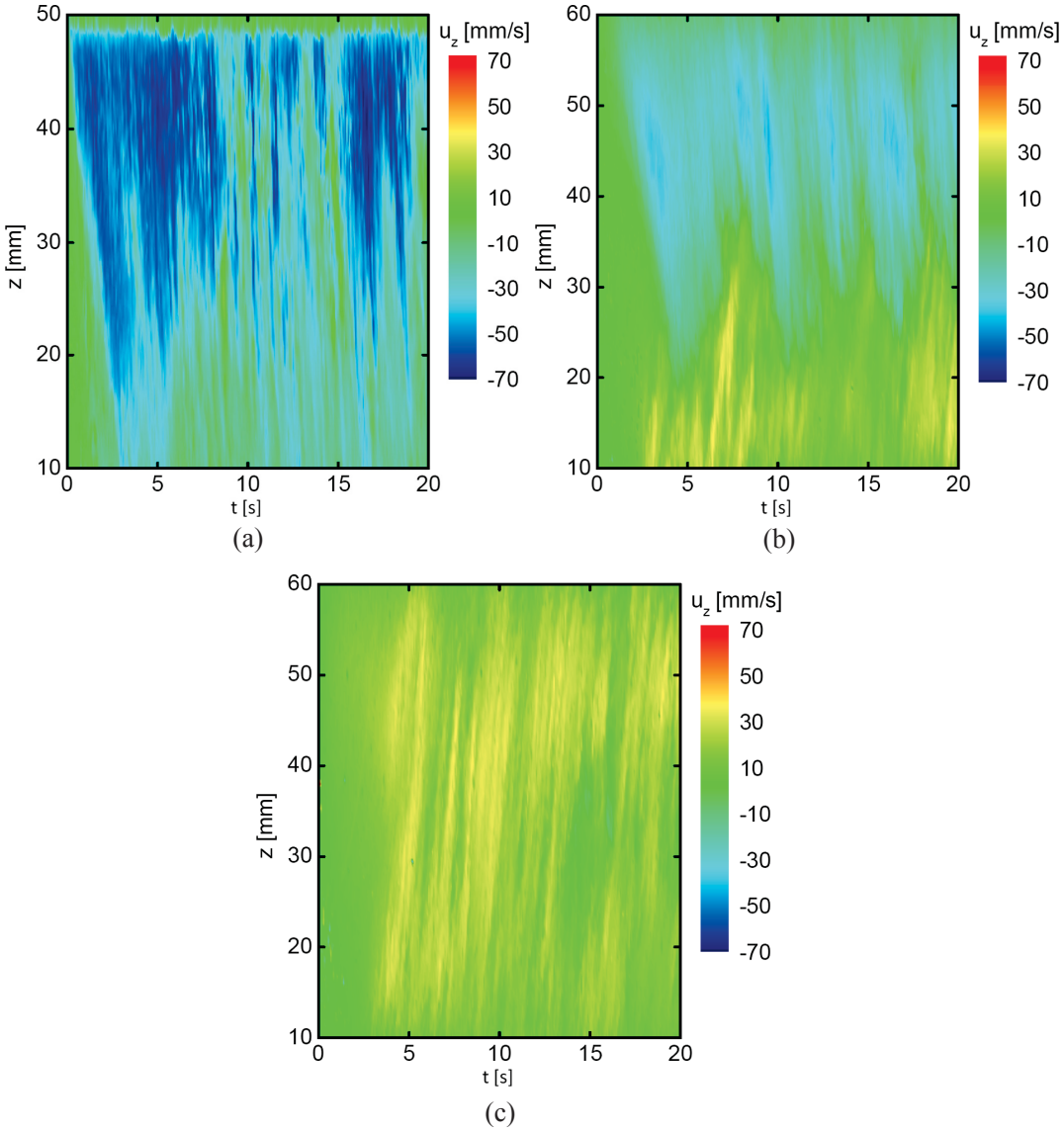

Figure 3.8: Distribution of the vertical velocity measured at three positions under the applied ECP of I_P=480A, f=200Hz, t_p=0.5ms, I_{eff}=152A: (a) P1, (b) P2, (c) P3.

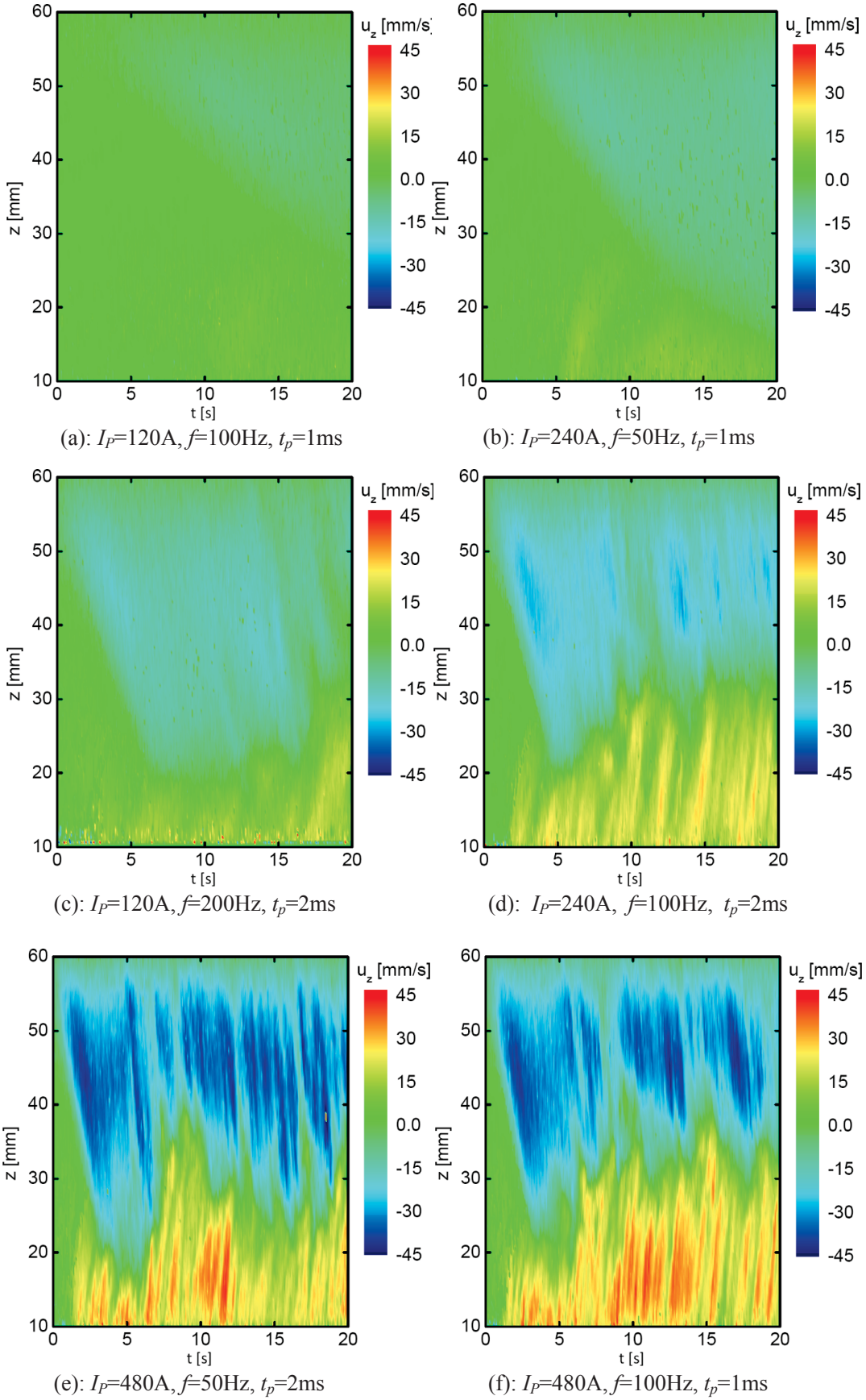

(a): I_P=120A, f=100Hz, t_p=1ms

(b): I_P=240A, f=50Hz, t_p=1ms

(c): I_P=120A, f=200Hz, t_p=2ms

(d): I_P=240A, f=100Hz, t_p=2ms

(e): I_P=480A, f=50Hz, t_p=2ms

(f): I_P=480A, f=100Hz, t_p=1ms

Figure 3.9: Distribution of the vertical velocity measured at central position (P2) under the applied ECP: (a) I_{eff}=38A; (b) I_{eff}=54A; (c) I_{eff}=76A; (d) I_{eff}=107A; (e) I_{eff}=152A; (f) I_{eff}=152A.

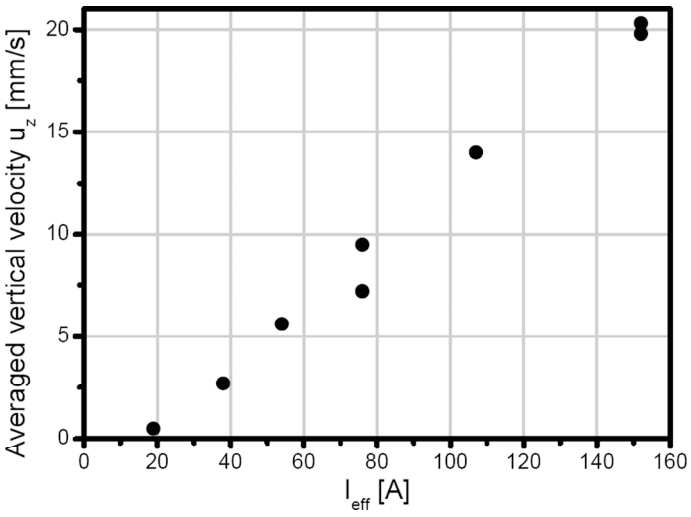

Figure 3.10: Influence of the applied effective current I_{eff} (ECP) on the mean axial velocity of the melt flow.

Numerical simulations

Corresponding numerical simulations were performed to calculate distributions of electric current, the magnetic field, the electromagnetic force and the fluid flow within the cylindrical column filled with Ga-20wt%In-12wt%Sn for the situation of an applied DC at I_{DC}=48A. The numerical results show that a parallel current runs through the electrode and spreads into the liquid metal. The extreme widening of the current streamlines leads to a drastic reduction of the current density from a maximum of about 120A/cm^2 just beneath the electrode by a factor of 5 to values around 20A/cm^2 occurring in the bulk of the melt. The distribution of Joule heating is described by the power density of Joule heating q, given by:

$$q = \mathbf{J}^2 / \sigma \tag{3.2}$$

The distribution of the electromagnetic force is described by the electromagnetic force density **f**, calculated by:

$$\mathbf{f} = \mathbf{J} \times \mathbf{B} / \rho \tag{3.3}$$

where ρ is the density.

Respective distributions of the magnetic field **B**, the power density of Joule heating q, and the electromagnetic force density **f** are displayed in figure 3.11. As shown in figure 3.11a, the magnetic field permeates the upper part of the sample, in particular the domain around and

between the electrodes. It becomes obvious from the figures 3.11b and 3.11c that the impact of both, the Joule heating and the electromagnetic force is limited to a very narrow region in the front of the electrode end faces. The power density of Joule heating reaches a maximum value of about 0.6W/cm^3 at the electrode and falls below a value of about 0.1W/cm^3 in the bulk liquid due to the enormous widening of the current distribution at the electrodes. Also, a significant electromagnetic force only occurs in a small domain just beneath the electrodes. The interaction between the radially diverging electric current and the almost azimuthally induced magnetic field produces a downward electromagnetic force there (see figure 3.12a). As a consequence, forced melt convection is generated in the sample whose global three-dimensional structure becomes apparent in figure 3.12b. The significant rotational part of the electromagnetic force drives a flow in form of two downward jets. A recirculating flow can be observed covering the lateral area close to the cylinder walls on both sides of the electrodes. The stronger electromagnetic force is caused when a higher intensity of effective electric currents is employed. Hence, the averaged axial velocity u_z of the melt flow increases with I_{eff}. However, the distribution of electromagnetic force remains confined just beneath the electrodes. As a result, the melt keeps the same flow pattern under all the applied electric currents.

The flow measurement shows that the forced flow driven both of the DC and the ECP are almost the same when the same effective electric current is applied. This finding can easily be understood by considering the respective distributions of the magnetic field and the related electromagnetic force for ECP. The skin effect occurring at high frequencies expels the AC fields from the bulk of the sample. This effect can be observed for the induced magnetic field in the figures 3.13a and 3.13d. However, any consequences on the distributions of both, the electromagnetic force and the Joule heating are not detectable (see figure 3.13). Hence, regardless of the chosen frequency the electromagnetic force is significant only in close vicinity to the front surface of the electrodes. The electromagnetically-driven flow retains the global structure of the velocity field for all parameters considered here, whereas the intensity of the mean flow depends only on the effective value of the applied current.

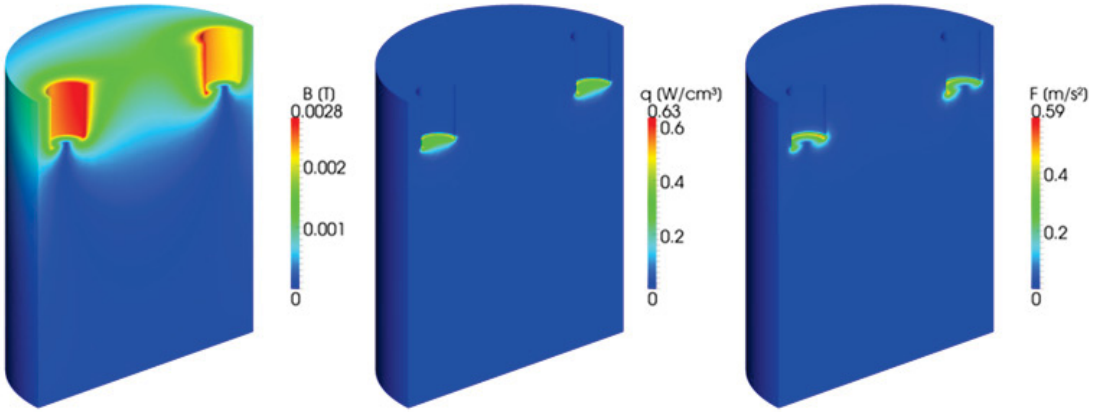

(a) (b) (c)

Figure 3.11: Numerical simulations showing the situation of an applied direct current at I_{DC}=48A: (a) magnetic field strength, (b) Joule heating density, (c) electromagnetic force density.

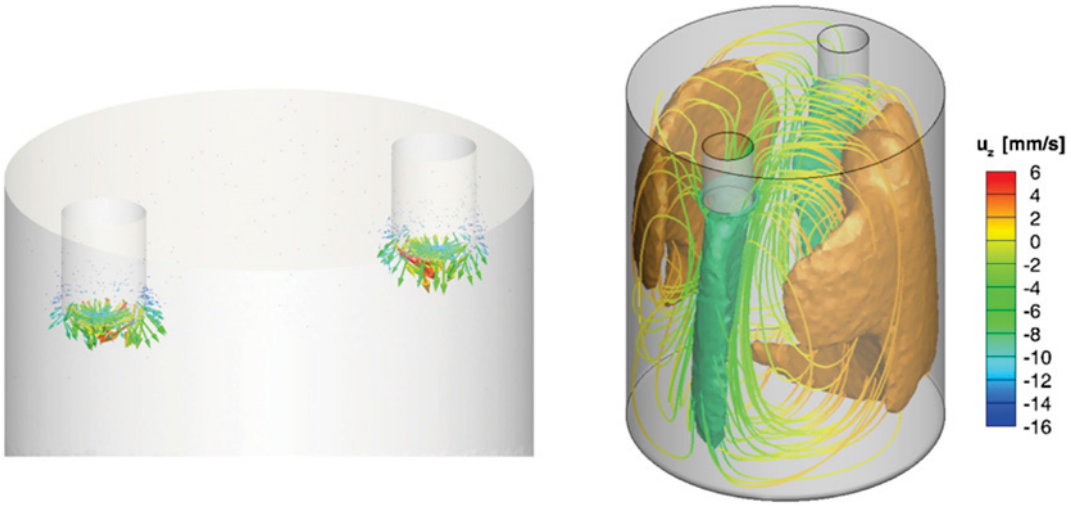

Figure 3.12: Numerical simulations for the situation of an applied direct current at I_{DC}=48A: (a) structure of the electromagnetic force, (b) three-dimensional flow structure.

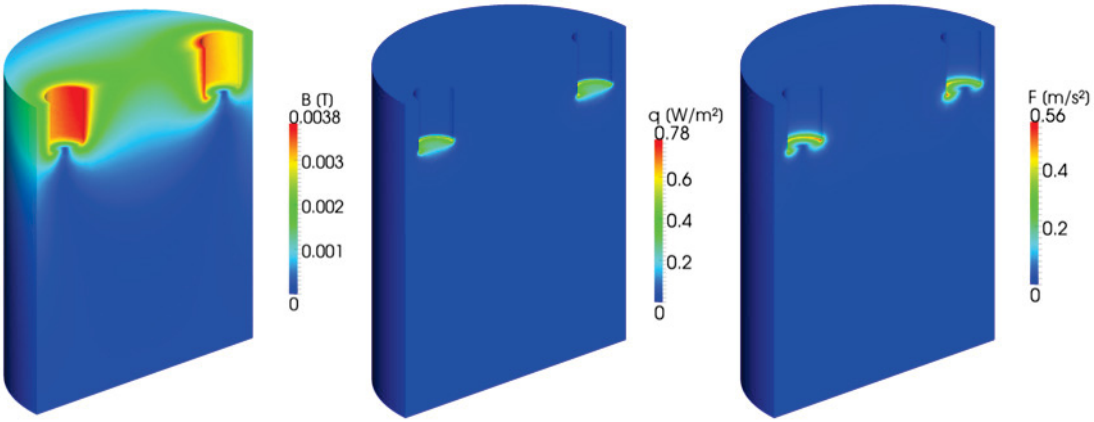

(a) (b) (c)

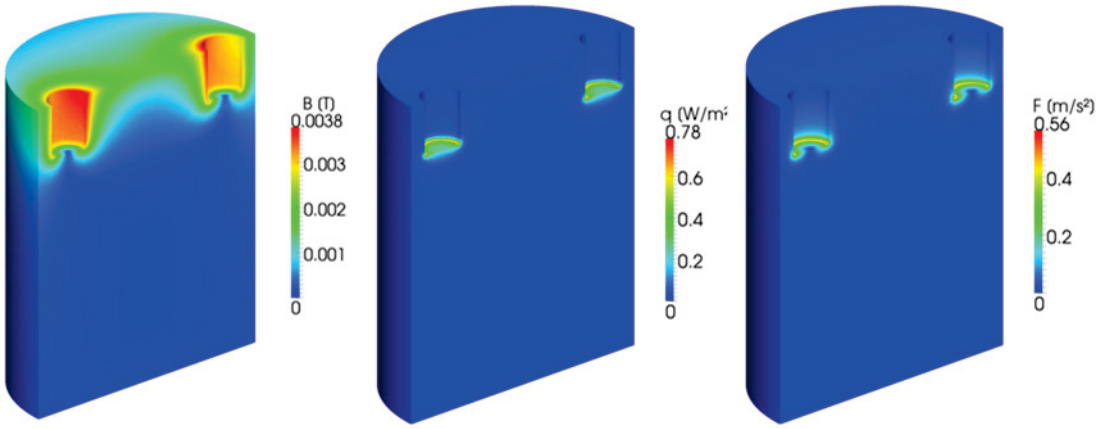

(d) (e) (f)

Figure 3.13: Numerical simulations showing the situation of an alternating current at I_{eff}=48A: (a), (d) magnetic field strength, (b), (e) Joule heating, (c), (f) electromagnetic force density, (a)-(c) f=200Hz, (d)-(f) f=2000Hz.

3.3.3 Temperature distribution

The temperature measurements are carried out within the cylindrical, double-walled mould filled with Al-7wt%Si alloy cooling from melt to solid. Figure 3.14 presents the temperature distribution of samples at the cylinder axis monitored via six vertically arranged thermocouples (z: 5mm, 16mm, 27mm, 38mm, 49mm and 60mm). The reference temperature measurement conducted without electric current shows an apparent positive temperature gradient along the upwards vertical direction (see figure 3.14a). The temperature difference is significantly modified by the application of DC and ECP. The temperature gradient decreases with the increasing intensity of DC as shown in figure 3.14b, c. The same evolution of the temperature field can be found in the increasing value of the effective electric current in the pulsed regime (see figure 3.14 d-k). A temperature gradient G is calculated when the temperature of a thermocouple at 5mm decreases to 620°C:

$$G = \frac{T_{z=49mm} - T_{z=5mm}}{49mm - 5mm} = \frac{T_{z=49mm} - 620K}{4.4cm} \tag{3.4}$$

The corresponding dot plots are figured out to show the variation of the temperature gradient as the function of I_{eff} for the situation of both DC and ECP (see figure 3.15). It can be found that the temperature gradient remarkably changed by both DC and ECP. The reference temperature

gradient of the sample without electric currents is about 11.5K/cm. It significantly decreases with the increasing intensity of I_{eff}. The value reaches about 2K/cm when the effective electric current value is higher than 120A.

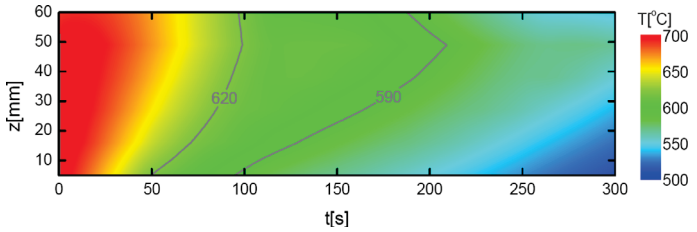

(a): I=0

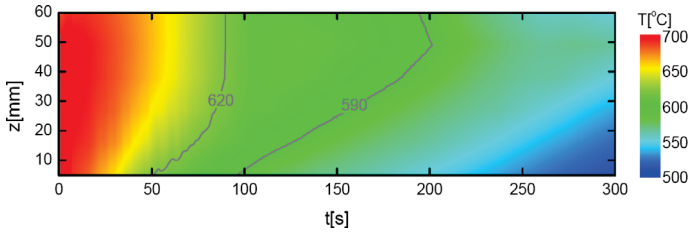

(b): I_{DC}=48A

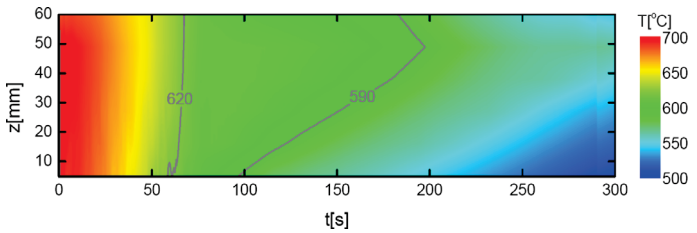

(c): I_{DC}=120A

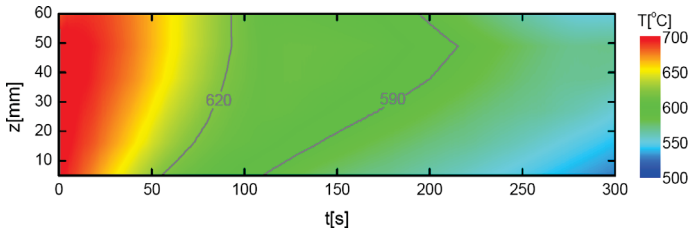

(d): I_P=120A, f=50Hz, t_p=0.5ms, I_{eff}=19A

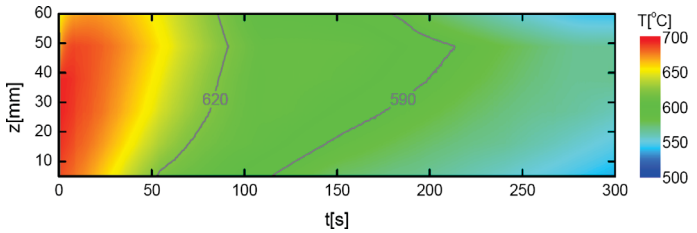

(e): I_P=120A, f=100Hz, t_p=1ms, I_{eff}=38A

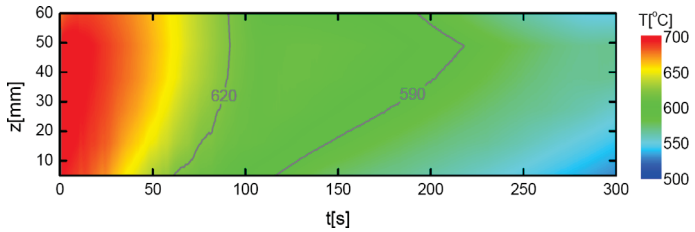

(f): I_P=240A, f=50Hz, t_p=1ms, I_{eff}=54A

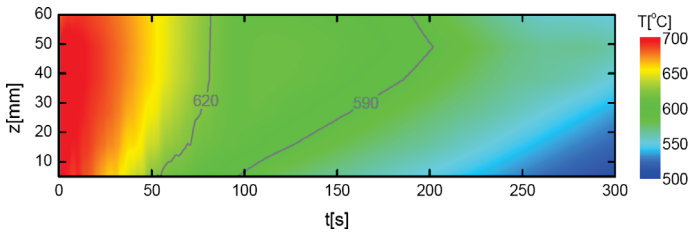

(g): I_P=240A, f=200Hz, t_p=0.5ms, I_{eff}=76A

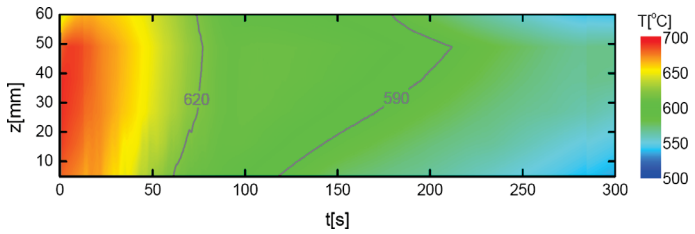

(h): I_P=120A, f=200Hz, t_p=2ms, I_{eff}=76A

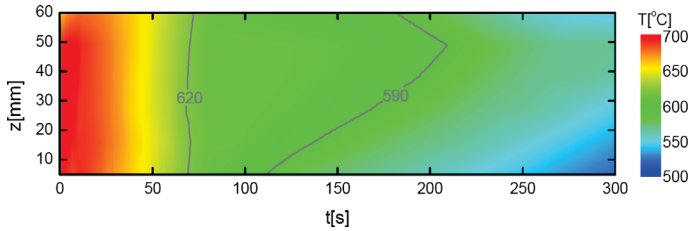

(i): I_P=240A, f=100Hz, t_p=2ms, I_{eff}=107A

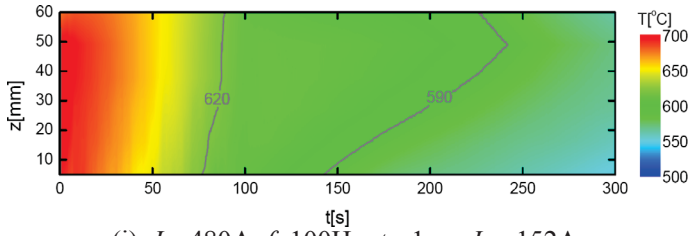

(j): I_P=480A, f=100Hz, t_p=1ms, I_{eff}=152A

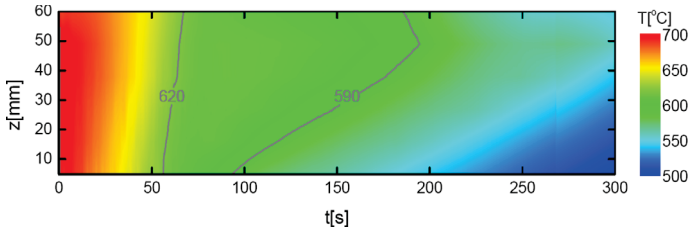

(k): I_P=480A, f=200Hz, t_p=0.5ms, I_{eff}=152A

Figure 3.14: Temperature distribution of Al-7wt%Si alloy under both DC and ECP.

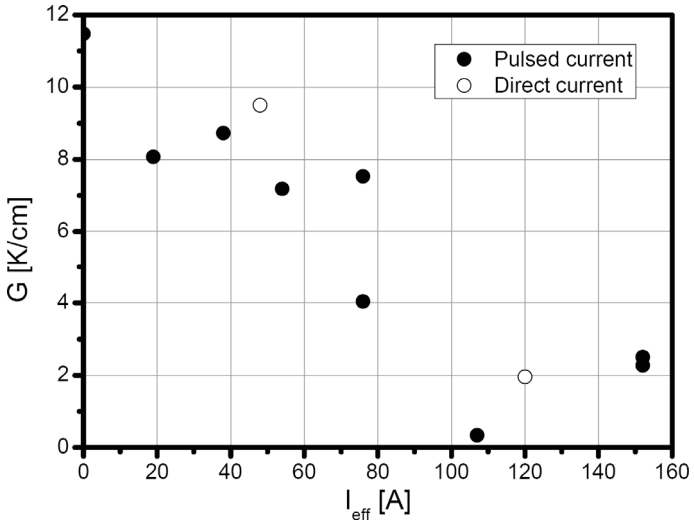

Figure 3.15: Temperature gradient in Al-7wtSi alloy under both DC and ECP.

3.4 Discussion

The present chapter focuses on the question which effect or effects of strong electric currents cause the grain refinement in the solidifying specimens. We consider the situation of a directional, bottom-up solidification in a metal column where two electrodes are installed near the free surface. For this configuration, our numerical and experimental findings reveal the existence of a three-dimensional flow spanning the entire fluid volume. A similar numerical study published by Nikrityuk et al. [103] reports on the formation of distinct electro-vortex flows for the configuration of two central electrodes installed at the bottom and the top of a cylindrical domain. However, we must clarify whether the forced melt convection is the solely driving effect for grain refinement. Further possibilities are discussed in the literature, in particular it is assumed that a strong pinch force (electromagnetic force) is induced at that moment when the electric current pulses discharge. A direct action of this force on the mushy zone is supposed to cause a breaking of the dendrites into small fragments due to high shear stress [65, 66, 74, 75, 81, 86]. Furthermore, it is assumed that the fragmentation process becomes amplified at higher frequencies of pulsed currents when the electromagnetic fields are confined within a thin skin layer [86].

The results of the present chapter do not confirm these assumptions for the configuration studied here. The numerical analysis of the resulting electromagnetic fields presented in section 3.4 demonstrates that any significant effect of both, the electromagnetic force and the Joule heating is

confined to very narrow regions below the electrodes. Directly at the electrodes the local input from Joule heating reaches maximum values of about 0.6…0.8W/cm^3 (see figures 3.10 and 3.12). Estimations with respect to the heat production by the phase change from liquid to solid deliver much larger values of about 8W/cm^3. This difference will be even more pronounced in the bottom area of the sample where higher growth velocities occur and the Joule effect is almost negligible. Hence, for the magnitude of electric currents considered in this study the Joule heating effect does not play any prominent role at all. Any direct impact on the growing dendrites within the mushy zone arising from the electromagnetic force or an electrically induced remelting of the dendritic skeleton can be excluded. Induced liquid flow remains as the most probable reason for the grain refinement observed in the solidified samples. This basically means that the same mechanism of grain refinement can be assumed as it is considered to explain the reduction of grain size due to electromagnetic stirring. For instance, a recent paper by Liotti et al. [131] investigated the effect of a pulsed electromagnetic field by synchrotron X-ray imaging. This work demonstrates that flow-induced local fluctuations of both temperature and concentration profiles within the mushy zone promote dendrite fragmentation by local remelting of side arms. Accruing fragments are transported by the melt flow and grow in undercooled regions [132]. High undercooling and low thermal gradients are favorable for grain refinement because the probability of surviving of dendrite fragments becomes larger with the increasing extent of the undercooled region [133]. The forced flow can promote the heat transfer and homogenize the melt temperature of samples. Figure 3.12 and 3.13 show that a distinct vertical temperature gradient develops in the melt from the beginning of the cooling process for the situation without forced flow. Such a thermal gradient does not exist in the samples under the influence of electric currents, where the melt stirring causes an effective homogenization of the temperature field in the liquid phase.

Melt convection supports the formation of the undercooled regions ahead of the mushy zone by an effective reduction of the temperature gradient across the sample and by a modification of the solute distribution. For instance, a travelling magnetic field (TMF) is known as an efficient tool to achieve grain refinement during solidification [39, 44]. Figure 3.16 displays the grain-refined macrostructure of a sample solidified under the influence of a TMF. The TMF generates a flow pattern in form of a torus, where the melt flows downwards at the axis and upwards along the

side walls of the cylinder [134, 135]. That means that the global flow structures obtained by applying a TMF or an electric current in the experimental configuration considered here are not identical, but rather similar. The parameters of the electric pulses and the TMF (B_{TMF}=12mT) were chosen in such a way that the intensities of the produced melt flows (the downward velocities at the axis or below the electrodes were taken as reference) can be expected to be almost the same as in the ECP experiment shown in figure 3.3h.

Our assumption does not contradict the main findings reported by the previous studies. For example, Li et al. [86] conducted experiments in a similar configuration of parallel electrodes as considered here. Electric current pulses at frequencies between 100 and 1,000Hz were generated by discharging a capacitor. The authors observed an intensification of the grain refinement in pure Al with increasing frequencies. This result can be understood easily, because the increase of the frequency for a constant pulse length is equivalent to an increase of the effective current I_{eff}, which in turn leads to a more intensive melt flow.

Figure 3.16: Macrostructure of Al-7wt%Si alloy treated by TMF of 12mT.

As discussed previously, it could be referred that the forced flow induced by ECP plays a key role in the grain refinement of alloys. It should be noted that any convection can be effectively damped by the high viscosity [136]. During the solidification process, the viscosity in the melt gradually increases on account of the fact that the solid phase is continuously precipitated from the melt. It is evident that the ECP application cannot create a substantial melt flow when the solid fraction in the sample becomes too large. Hence, it is logical to conclude that there may exist an efficient period during which the grain refinement would mainly occur.

According to the schematic view shown in figure 3.17, the solidification process of Al-7wt%Si hypoeutectic alloy can be divided into: the initial solidification period (including nucleation and recalescence), the primary phase growth period and the eutectic structure formation period. As the schematic view shown in figure 3.18a, ECP of I_{eff}=152A was triggered at the initial cooling of samples and then powered off after the initial solidified period and the whole solidified period, respectively. The corresponding macrostructures in the longitudinal section of the solidified samples with forced cooling are presented in figure 3.18b and 3.18c. Significant grain refinement can be observed in both samples. In addition, the mean grain size of these two samples was quantitatively analyzed. Table 3.2 shows that the grain size in both samples approaches a value of about 0.8mm. The achievement of the almost same macrostructure and grain size in these two samples indicates that the grain refinement of a sample treated by ECP is mainly produced during the initial solidification period.

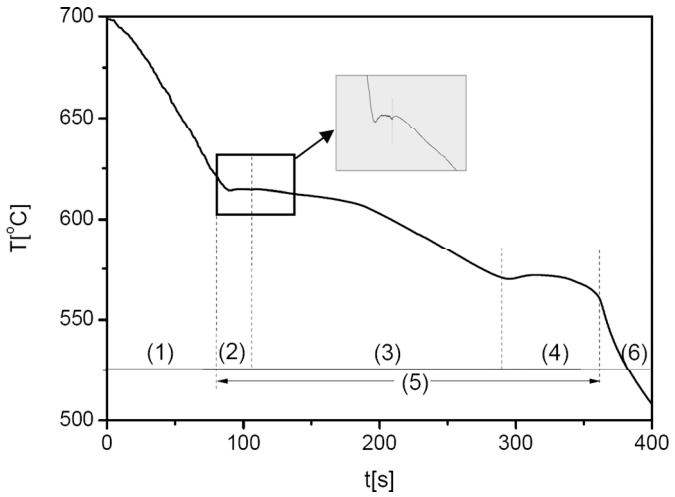

Figure 3.17: Schematic view of divided periods during the cooling of Al-7wt%Si hypoeutectic alloy: (1) melt period, (2) initial solidification period, (3) primary phase growth period, (4) eutectic structure formation period, (5) solidification period, (6) solid period.

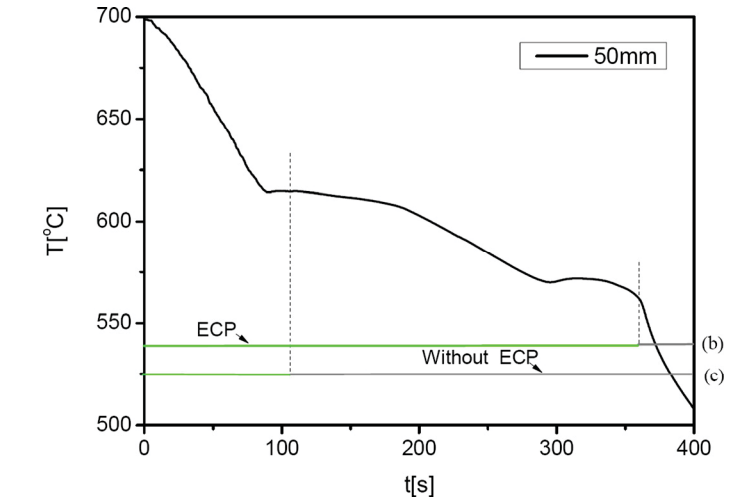

(a)

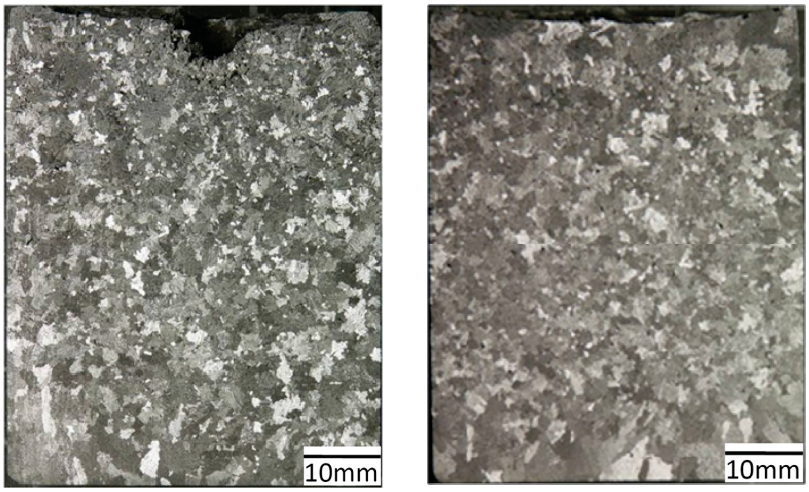

(b) (c)

Figure 3.18: Influence of ECP activated time on the macrostructure in the longitudinal section of the solidified Al-7wt%Si alloy samples: (a) schematic view of ECP activated time (green line: turned on ECP; grey line: turned off ECP), (b) macrostructure for turning off ECP after the whole solidified period, (c) macrostructure for turning off ECP after the initial solidified period.

Moreover, Li et al. [86] have proposed that grain refinement was due to numerous nuclei showering down from the thin solidified shell formed at the free surface under the configuration of two vertically parallel electrodes which is the same with our employed configuration. They thought that the nuclei detachment from the solidified shell was controlled by the electromagnetic force. However, this assumption contradicts with our results that the forced flow induced by electric currents plays the key role in the grain refinement formation. On account of the fact that the forced flow is global, it can predict that the nuclei are not only from the surface, but also from other possible positions, e.g. the lateral and bottom inner-wall of the cylindrical crucible. Hence, in order to confirm this prediction, as shown in figure 3.19, a hot (heating with the mould) or cold

(room temperature) stainless steel block was located above the surface of samples 7mm and cooled with the mould together to suppress or promote the formation of solidified shell. If the formation of solidified shell should have no influence on the grain size, it could be assumed that the nuclei are not only from the surface.

The cooling curves of samples with the hot or cold block are shown in figure 3.20a and 3.20b, respectively. The temperature of the sample with a hot block at cylinder axis height of 60mm (sample height is 63mm) was about 618.6^{o}C at the initial solidification process, which was larger than the liquidus (about 615^{o}C) of Al-7wt%Si samples. It indicates that the alloy is liquid above 60mm of the samples and no crystal nuclei formed on the oxide layer during the initial solidification period. On the other hand, there would be a solid shell at the surface of the samples with the cold block, because the temperature at 60mm was 604.2^{o}C, less than the liquidus.

The corresponding macrostructure in the longitudinal section of the solidified samples with the hot or cold block are presented in figure 3.21a and 3.21b, respectively. A significant equiaxed zone was generated in both of these two samples. The similar macrostructure can be observed as well in the reference sample (without block) in figure 3.18b. In addition, the measured mean grain size of these three samples was in 0.8mm range (see table 3.2). It means that the application of ECP in the solidified samples without the block, with the hot block and with the cold block achieved the same level of grain refinement. It suggests that the formation of the solidified shell has no obvious influence on the grain size and the nuclei may also originate from the substrate including the inner-wall of the crucible, and the surface of the electrodes.

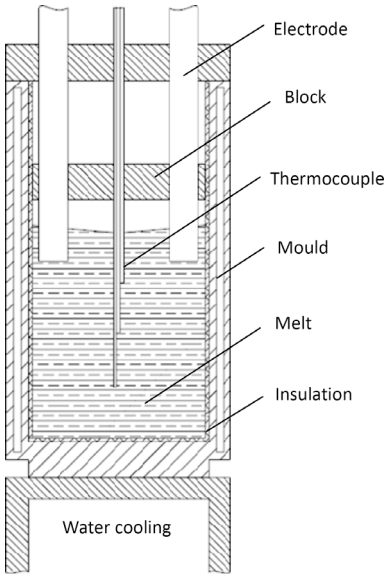

Figure 3.19: Schematic view of solidification experimental setup with block.

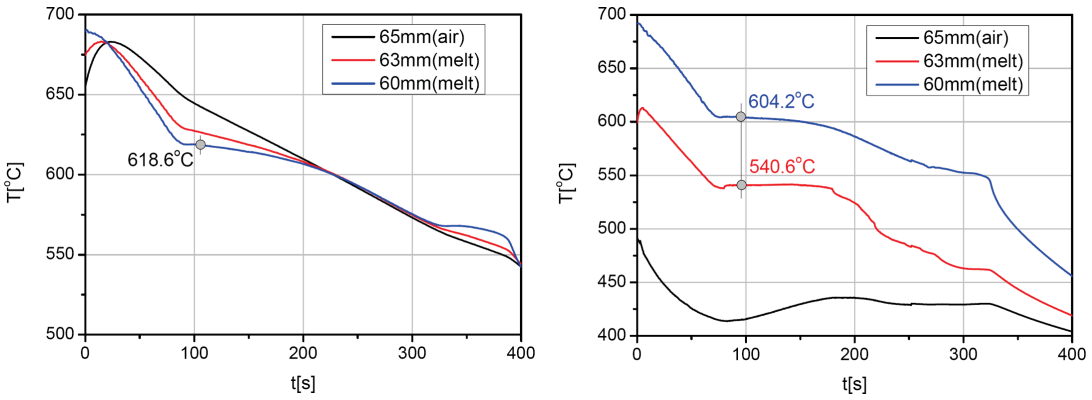

(a) (b)

Figure 3.20: Influence of the block (located above the free surface 7mm) temperature on the cooling curves in the cylinder axis of Al-7wt%Si alloy samples with ECP: (a) hot block, (b) cold block (room temperature).

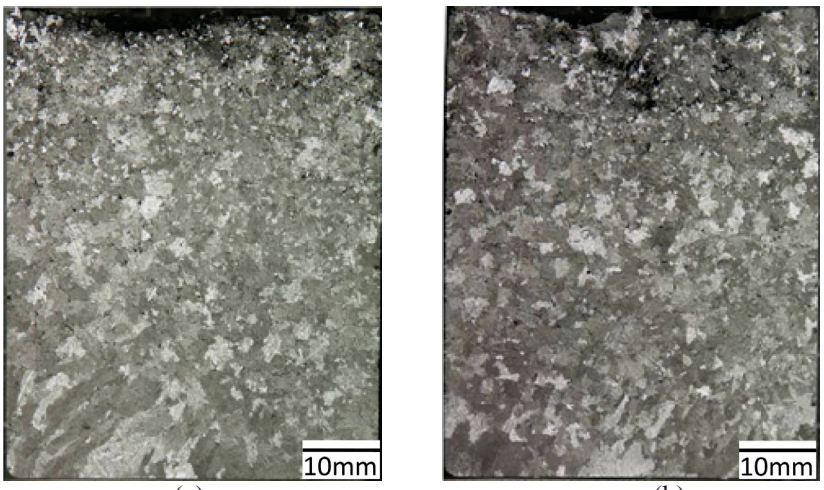

(a) (b)

Figure 3.21: Macrostructure in the longitudinal section of the solidified Al-7wt%Si alloy samples with ECP: (a) hot block, (b) cold block (room temperature).

Table 3.2: Grain size of samples under the application of ECP (I_{eff}=152A)

Figure	3.18b	3.18c	3.21a	3.21b
Mean grain size (mm)	0.82	0.83	0.84	0.81

3.5 Conclusions

The present chapter considers the impact of electric current on the solidification of Al-7wt%Si alloys for the configuration of two parallel electrodes immersed from the free surface into the solidifying alloy. The interaction between the applied current and its own induced magnetic field

causes an electromagnetic force which drives an electro-vortex flow into the melt. Our study focuses on the role of the induced fluid flow in the process of grain refinement.

The application of either direct current (DC) or electric current pulses (ECP) at frequencies up to 200Hz leads to the formation of refined equiaxed grain structures. The consequences on both, the mean grain size and the area of the equiaxed zone in the solidified samples are similar if the effective current of the pulsed regime corresponds to the amplitude of the DC.

The numerical analysis demonstrates that the effect of the electromagnetic force is concentrated on a small domain beneath the electrodes. The interaction between the diverging current at the electrodes and the induced magnetic field causes a very intense driving force in this region which produces a strong downward flow in form of two jets. The predicted flow pattern has been successfully validated by ultrasonic flow measurements in a low temperature Ga-20wt%In-12wt%Sn alloy. Furthermore, the numerical calculations reveal that there does not exist any direct shear force and Joule heating in the mushy zone, regardless whether direct currents or high-frequency alternating currents are applied. The melt flow induced by the electromagnetic force in a restricted area around the electrodes acts as a committer transporting the effect of the applied electric current to the growing dendrites. That means that the same explanatory model as known from grain refinement in metal alloys solidified under the impact of forced convection can be applied for the configuration of electrodes studied here. In our experiments the intensity of the melt flows appears to be sufficient in order to explain the effect of grain refinement in the Al-7wt%Si alloys.

4. Grain refinement mechanism driven by electric currents

4.1 Introduction

We have shown in chapter 3 that the forced melt flow induced by electric currents plays a key role in the grain refinement of solidifying alloy. This chapter concerns the grain refinement formation driven by the forced flow during the solidification process.

Referring to literature [132], the final grain size under the application of the forced flow mainly depends on the origin (where the grain is from) and survival of grains. The formed grains may be remelted and not survive if they were transported to a position with higher temperature. However, in our case, on account of the fact that a thermal homogenization inside the melt was generated under the application of electric current (see section 3.3.3), the survival of grains can be promoted and guaranteed. Hence, the origin of grains has mainly been focused in the present chapter.

Two origins of equiaxed grains under the application of electric currents are frequently proposed: the promoted heterogeneous nucleation and dendrite fragmentation [65, 67-69, 71, 73, 93]. In this chapter, the contribution of the two origins to the grain refinement will be investigated by performing a series of experiments.

4.2 Experimental parameter

As mentioned previously, one of origins of equiaxed grains for grain refinement is the heterogeneous nucleation promoted by electric currents. According to the nucleation theory [20, 111], the heterogeneous nucleation only occurs during the nucleation period and is rapidly reduced during the recalescence period. Hence, it is logical to predict that the grain refinement cannot be generated during the recalescence period if the promoted heterogeneous nucleation is the only origin for grain refinement.

In order to confirm the prediction, the electric current will be applied during the nucleation period and the recalescence period, respectively. As shown in figure 4.1[20, 111], the nucleation

period starts when the temperature is below T_m and ends at T_L; T_m is the liquidus of the sample and T_L is defined as the lowest temperature point before the recalescence phenomenon occurs. The recalescence period is the time in which the temperature of the sample increases from T_L to T_H; T_H is defined as the highest temperature point after the occurrence of the recalescence phenomenon. Here for the purpose of applying electric current during the nucleation period, the pulsed electric current (ECP) was initiated at the temperature of about 700^0C and powered off at a temperature point between T_m and T_L. For the sake of applying electric current during the recalescence period, ECP was initiated just over T_L and powered off near T_H. The electric current parameters were chosen as I_P=480A, f=200Hz, t_p=0.5ms, I_{eff}=152A.

In addition, in order to apply electric current exactly during the nucleation period or the recalescence period, it is necessary to keep the whole sample triggering the nucleation or recalescence at the same time. To achieve it in an attempt, two different cooling conditions were examined. Figure 4.2 presents the cooling curves of Al-7wt%Si alloy solidified in the double-walled mould under the two cooling conditions. It was shown that the nucleation or recalescence phenomenon occurred at various times in different parts of the sample with and without ECP when the forced cooling was conducted from the bottom of the double-walled mould (see figure 4.2a and 4.2b). Figure 4.2c and 4.2d show the cooling curves of Al-7wt%Si alloy with and without ECP solidified in the mould without forced cooling. Although it can be observed that there was a slight difference of the temperature field between the samples with and without ECP, this kind of cooling condition can still guarantee that the nucleation or recalescence phenomenon occurred at the same time in the whole sample. Hence, in the present chapter, the double-walled mould without forced cooling of its bottom was employed.

Another frequently proposed origin for grain refinement under the application of electric currents is the promoted dendrite fragmentation [65, 73]. According to the research about the dendrite fragmentation under the application of forced flow [118, 124], it seems likely that the dendrite arms detachment is caused by the solute fluctuations at the root of the dendrite arm. Here in an attempt to avoid the influence of solute, the high purity aluminum of 99.998% was employed to perform the solidification experiments. To keep the purity of aluminum, the sample was directly cut from the raw high purity aluminum billet and carefully ground on the SiC paper to clean the surface; graphite electrodes were adopted on account of the fact that the diffusion of carbon

atoms into the melt is really slow.

Moreover, it should be noted that it is not easy to form the dendrite during solidification on account of the absence of constitutional undercooling [111]. The research difficulty is also increased in view of the fact that the microstructure morphology cannot be observed in as-solidified pure metal [111]. However, the dendrite can be still formed in pure metal during the solidification process if a homogenized temperature field is achieved [111]. In the present chapter, in order to generate the homogenized temperature field, the solidification of high purity aluminum under the application of electric current was carried out in the double-walled mould and cooled in air. The employed mould cooling in air can significantly decrease the temperature gradient; the forced flow induced by electric current also can homogenize the temperature field. Figure 4.3 shows the corresponding cooling curves under the application of ECP (I_P=480A, f=200Hz, t_p=0.5ms, I_{eff}=152A). It can be found that the homogenized temperature field was well guaranteed at the beginning of the solidification period.

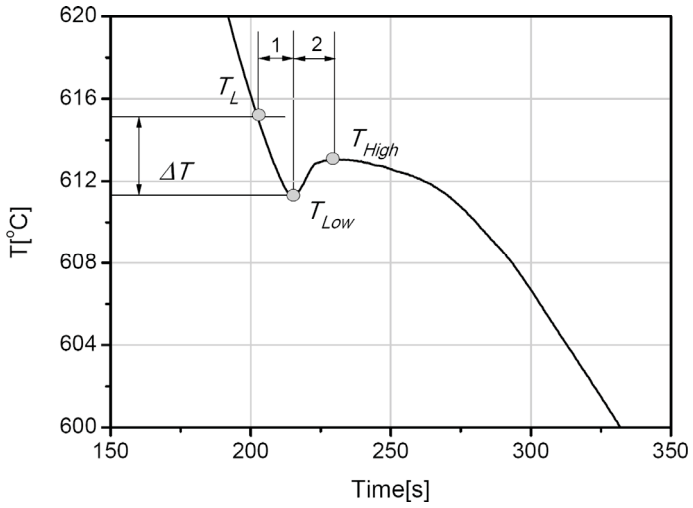

Figure 4.1: Schematic view of a cooling curve during the initial solidification. T_m: liquidus of sample, T_L: lowest point before recalescence, T_H: highest point after recalescence, ΔT: undercooling, 1: nucleation period, 2: recalescence period.

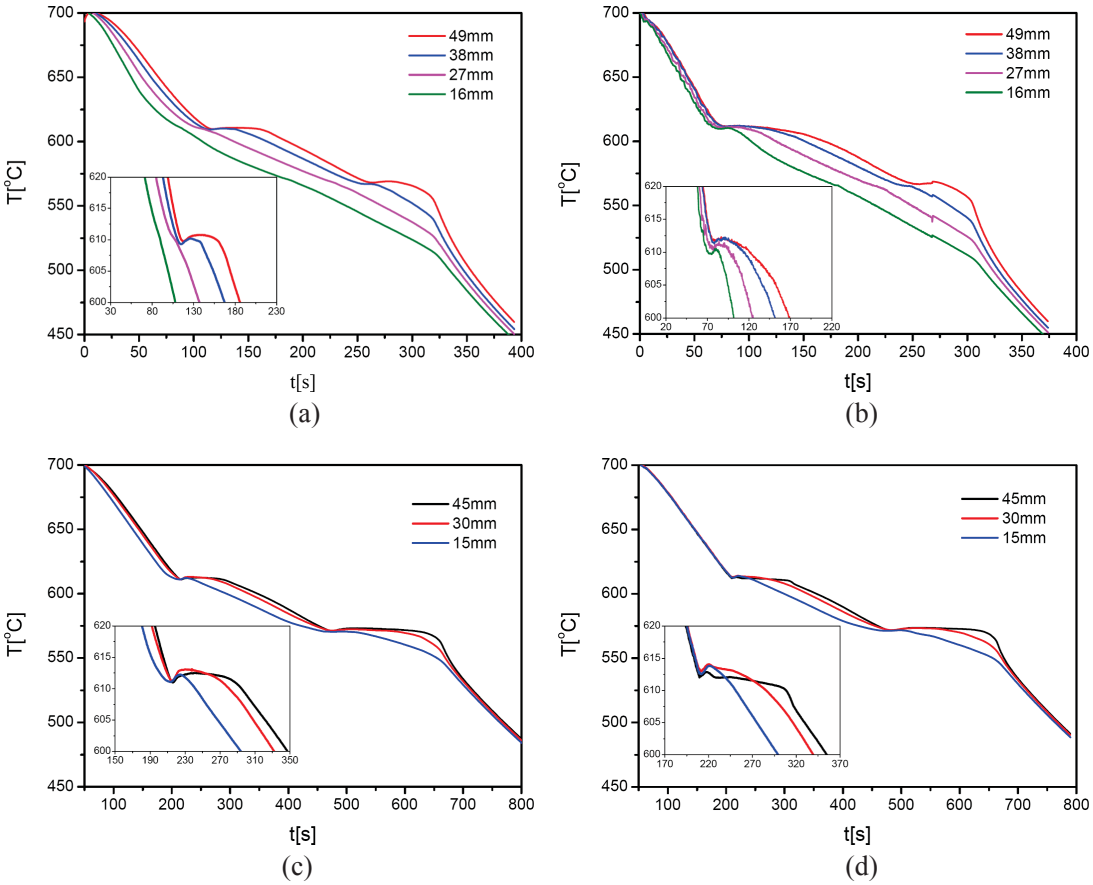

Figure 4.2: Cooling curves of Al-7wt%Si alloy solidified in the double-walled mould: with forced cooling (a) without ECP, (b) with ECP; without forced cooling (c) without ECP, (d) with ECP.

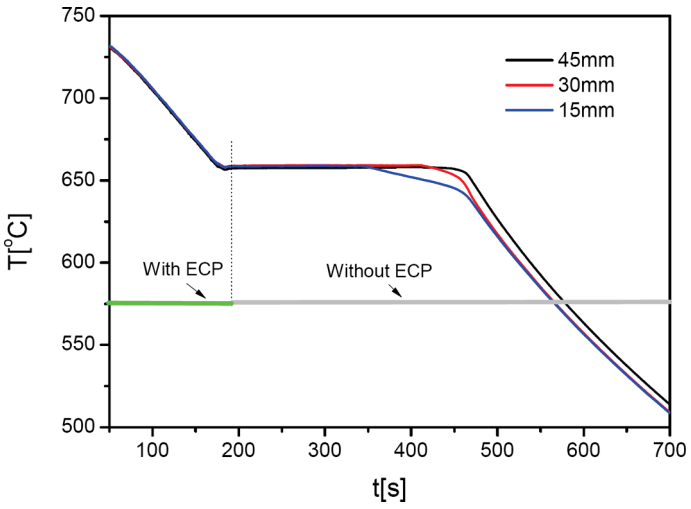

Figure 4.3: Cooling curves of the high purity aluminum solidified in the double-walled mould without forced cooling.

4.3 Results

4.3.1 Solidified structure of Al-Si alloy

The purpose of this section is to investigate the macrostructure formation during the nucleation period and recalescence period under the application of electric current. It is beneficial to understand the origins of grain refinement as mentioned in section 4.2.

Figure 4.4 schematically presents the applying time of ECP during the solidification of Al-7wt%Si alloy. It can be seen that solidification experiments of six samples were carried out. The first sample was solidified without the influence of electric current as a reference. As for the second one, the electric current was applied at a temperature of about 700^0C until the recalescence period almost finished. The electric current was also turned on at a temperature of about 700^0C for the following three ones. The difference is the powered off electric current in the nucleation period. As regards the last one, the electric current was only applied during the recalescence period.

Corresponding macrostructures in the longitudinal section of the solidified samples are shown in figure 4.5 and 4.6. Figure 4.5 shows the macrostructure of the whole sample photographed by a digital camera, while figure 4.6 shows an enlarged view of macrostructure in figure 4.5 photographed by a microscope using the polarized light. In figure 4.5a and 4.6a a few numbers of coarse equiaxed grains with dendrite morphology solidified in the reference sample without the impact of electric current can be seen. Figure 4.5b and 4.6b show the macrostructure when ECP has the influence on the solidification during both the nucleation period and recalescence period. It can be seen that a significant grain refinement was generated. The obtained finer equiaxed grains are really similar to the macrostructures of the sample (see figure 3.18b) in which the same electric current parameter was applied during the whole solidification process. It seems likely that the grain refinement mainly occurs during the nucleation period and recalescence period under the application of electric current. Figures 4.5c-e and 4.6c-e show macrostructures of samples treated by ECP during the nucleation period. It can be observed that the macrostructure of the samples was gradually refined when the ECP stopping time is closer to the T_L. However, it should be noted that although the finer grains were generated, the grains are still coarser than the

grains in figure 4.5b. It indicates that the grain refinement also should be caused during the recalescence period. Figures 4.5f and 4.6f present the macrostructure of the sample treated by ECP only during the recalescence period. It can be seen that the grain refinement occurred in view of many tiny generated grains. The occurrence of so many tiny grains may be due to the influence of the suddenly applied electric current (e.g. the effect of transient flow (spin-up [137])). Nevertheless, the phenomenon still indicates that the grain refinement occurs during the recalescence period under the application of electric current. As mentioned previously in section 4.2, it was proposed that the grain refinement cannot be observed during the recalescence period if the promoted heterogeneous nucleation was the only origin for grain refinement. Our results do not confirm this assumption, which means that there should be another origin (dendrite fragmentation) to supply the refined equiaxed grains for grain refinement.

Respectively, measured mean grain size of samples shown in figure 4.5 is presented in table 4.1. The grain size in the sample without ECP was 2.82mm. When the applied time of ECP during the nucleation period was stopped closer to the T_L, the grain size gradually decreased from 2.12mm to 1.63mm. Finally, the grain size approached at a value of 0.88mm when ECP was applied during both, the nucleation and recalescence period.

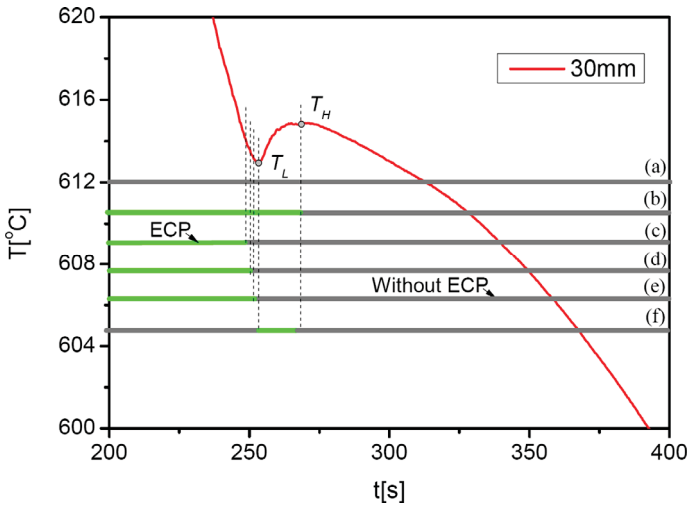

Figure 4.4: Schematic view of ECP applying time (green line: turned on ECP; grey line: turned off ECP; a-f: corresponding the following a-f in figure 4.4 and 4.5).

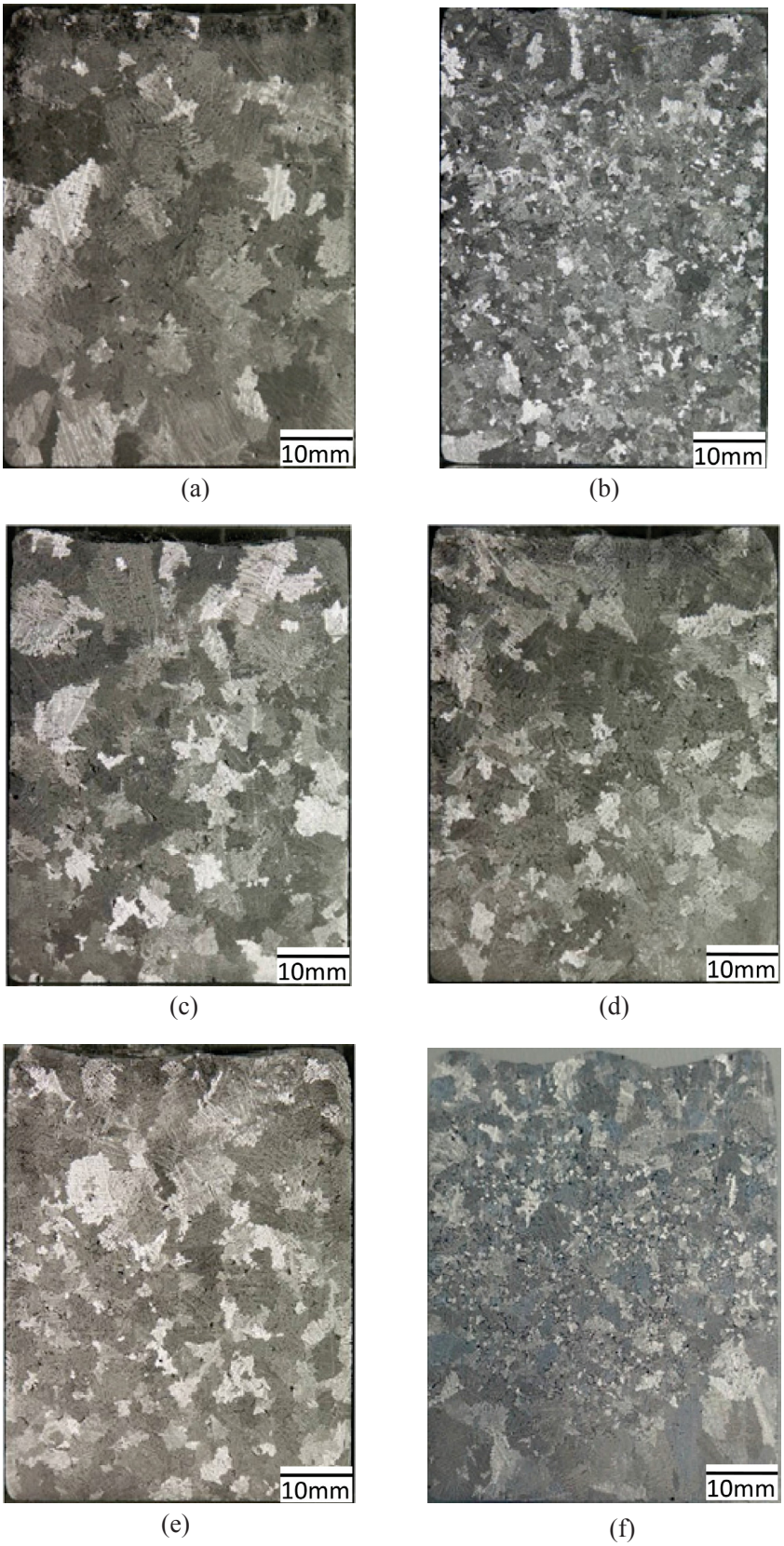

Figure 4.5: Influence of ECP applying time on the longitudinal section macrostructure of the solidified Al-7wt%Si alloy samples: a-f corresponding to the various applying time shown in figure 4.4.

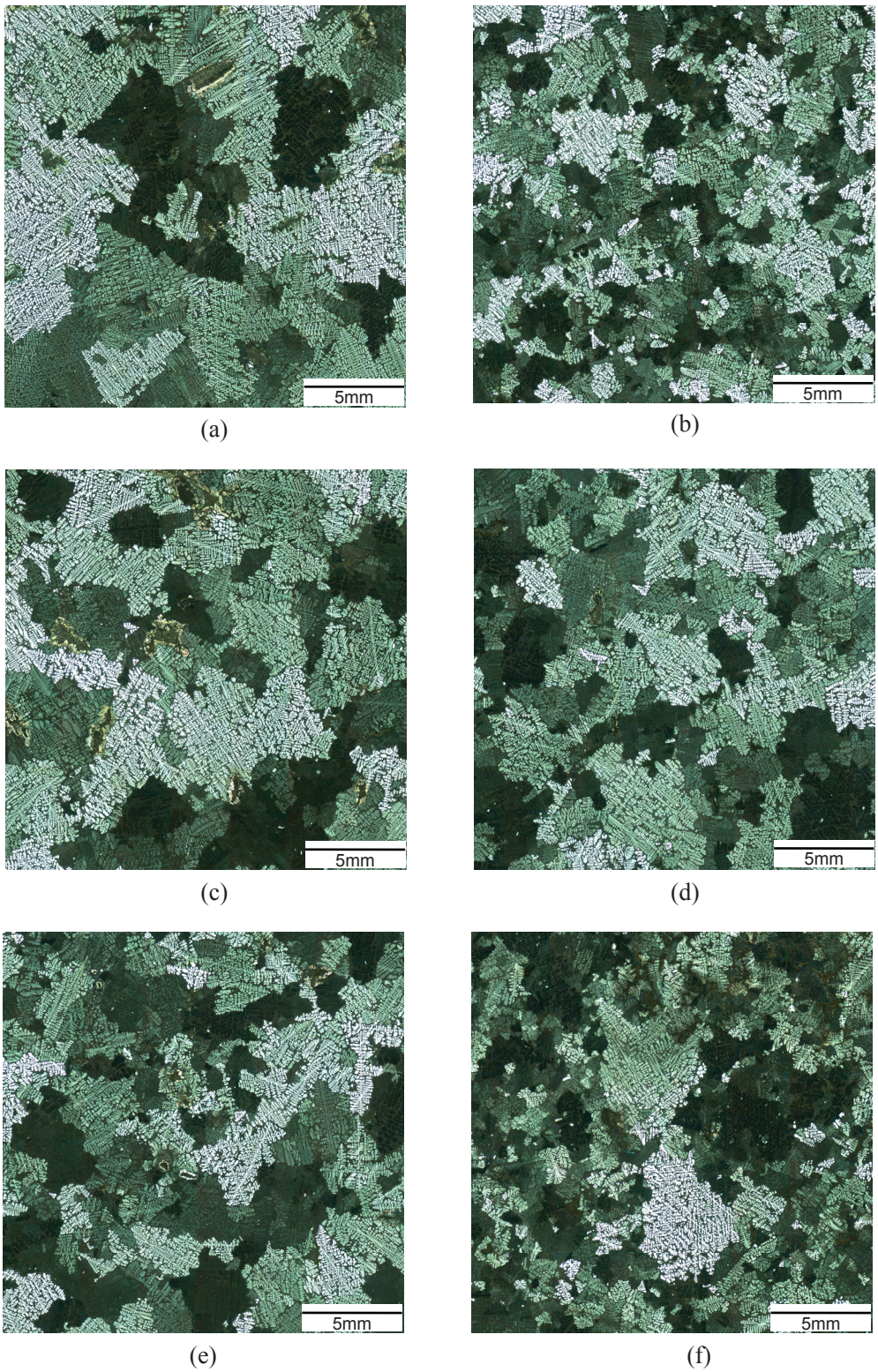

Figure 4.6: Enlarged macrostructures in the longitudinal section observed by microscope with polarized light: a-f corresponding to the various applying periods shown in figure 4.4.

Table 4.1: Influence of the applied ECP (I_{eff}=152A) on the grain size of samples without forced cooling

Figure 4.5	(a)	(b)	(c)	(d)	(e)
Mean grain size (mm)	2.82	0.88	2.12	1.81	1.63

4.3.2 Cooling curves of Al-Si alloy

We have shown in section 4.3.1 that both, the promoted heterogeneous nucleation and the dendrite fragmentation have the potential to be the origin for the grain refinement. Here we will examine the possible contribution of heterogeneous nucleation to the reduction of grain size. According to the classical nucleation theory [104, 111], the heterogeneous nucleation under the application of electric current may be promoted by two possibilities, increasing the undercooling and reducing the nucleation energy barrier ΔG^*. It has been proposed that the undercooling can be increased by electric current to promote the heterogeneous nucleation as well as the grain refinement [67, 93]. However, the cooling curves of the sample under the application of electric current should be carefully examined because the forced flow induced by electric current can modify the temperature field (see section 3.3.3). On account of the change of temperature field by electric current, it is possible that the samples with and without electric currents experienced different cooling rate. It has been reported that the different cooling rate can give rise to different undercooling [138]. Hence, it is necessary to set both of the samples with and without ECP in the same cooling rate to investigate the influence of electric current on the undercooling.

Figure 4.7 displays the measured cooling curves at the cylinder axis height of 30mm for the Al-7wt%Si alloy with and without electric current. Fortunately, it can be seen that the almost same cooling rate and history were achieved in the Al-7wt%Si alloy with and without the application of ECP when the solidification experiments were carried out in the double-walled mould without the forced cooling. Hence, the effect of electric current on the undercooling can be investigated convincingly by carefully comparing the cooling curves with and without ECP. According to the classical heterogeneous nucleation theory [104, 111], the undercooling ΔT is defined as the difference between the liquidus T_m and T_L ($\Delta T = T_m - T_L$). Since T_m should be constant for the alloy with a determined composition, the undercooling only depends on the value of T_L. As shown in figure 4.7, in comparision with the reference sample without electric current,

the T_L was increased in the sample under the influence of electric current. The measured T_L for the sample without applied ECP was 611.3°C; for the sample with applied ECP it was 612.9°C (see table 4.2). It should be noted that although the temperature measurement error of the employed thermocouples is as high as ±1°C, only the repeatability error of the thermocouple was considered here because the same thermocouple was employed in the solidification experiments with and without ECP. The repeatability error of the thermocouple is about ±0.1°C based on four times temperature measurement. Hence, it can fully identify that the T_L was increased under the application of electric current. On account of the relationship between the undercooling ΔT and the T_L, it indicates that the undercooling was decreased when the electric current was applied. It suggests that the heterogeneous nucleation cannot be promoted by electric current through modifying the undercooling.

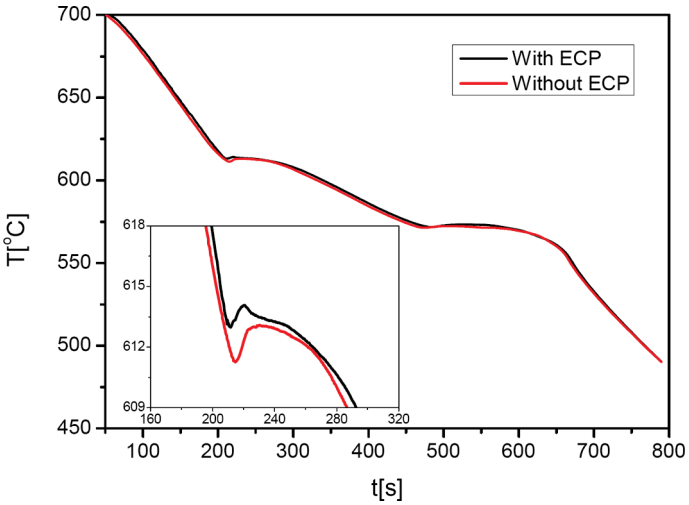

Figure 4.7: Cooling curves of the solidified Al-7wt%Si alloy samples without forced cooling.

Table 4.2: Influence of the applied ECP (I_{eff}=152A) on the T_L of samples without forced cooling

	Without ECP	With ECP
T_L(°C)	611.3	612.9

4.3.3 Solidified structure of high purity aluminum

As mentioned previously, another possibility to promote the heterogeneous nucleation is reducing the nucleation energy barrier ΔG^*. A theoretical analysis has been performed to propose that the heterogeneous nucleation was promoted through reducing the nucleation energy barrier ΔG^* by electric current itself [68-71]. According to this analysis, the reduction of the nucleation energy

barrier ΔG^* by electric current only depends on the fact that the nucleus has a higher electric conductivity than the melt (see equation 1.24). In view of the fact that the electric conductivity of the nucleus (8.0×10^6s/m) is larger than that of the melt (3.5×10^6s/m) in pure aluminum, the reduction in grain size still can be observed in the high purity aluminum under the influence of electric currents. Hence, the solidification experiments were performed in high purity aluminum of 99.998%. Figure 4.8 presents the macrostructure in the longitudinal section of pure aluminum. It can be seen that almost the same macrostructure was generated regardless of the application of ECP. Several coarse grains were observed in both of the samples with and without treatment of ECP. It is evident that the grain refinement was not observed in pure aluminum no matter if the electric current was applied. The experiment results do not confirm the theoretical analysis. It means that the heterogeneous nucleation cannot be promoted by the possibility proposed in the theoretical analysis.

In summary, although it was frequently proposed that the heterogeneous nucleation was promoted by changing the nucleation energy barrier ΔG^* and undercooling ΔT under the application of electric currents [67-71, 73, 80, 93], our experiment results did not support the two possibilities. It could be concluded that the heterogeneous nucleation cannot be promoted by electric current to as the main origin for grain refinement; the main origin for the grain refinement under the application of electric current is more likely to be the dendrite fragmentation promoted by the current-induced forced flow.

In addition, it has been proposed that the dendrite fragmentation, as well as the dendrite arms detachment under the application of forced flow, is caused by the flow-induced solute fluctuations at the root of the dendrite arm [118, 124]. As mentioned previously in section 4.2, in order to confirm if the dendrite fragmentation is promoted by the solute fluctuations induced by the forced flow, the high purity aluminum of 99.998% was employed to avoid the influence of solute. Figure 4.8 presents that no grain refinement is generated regardless of the application of ECP. It means that the grain refinement is not produced when the solute effect is irrelevant. Hence, the achieved experimental results can fully identify that the flow-induced dendrite fragmentation is an important origin for the grain refinement driven by electric current; the detachment of dendrite arms are mainly due to the solute fluctuations induced by the forced flow.

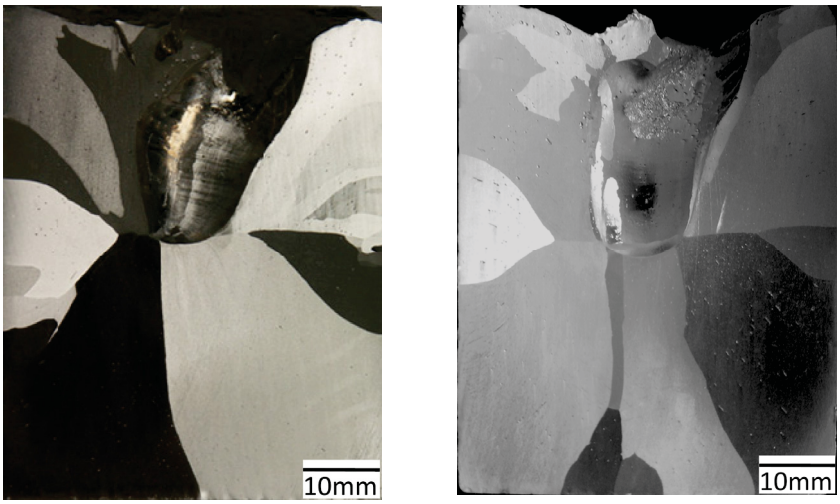

(a) (b)

Figure 4.8: Influence of the ECP on the longitudinal section macrostructure of the solidified pure Al (99.998%) samples without forced cooling: (a) without ECP, (b) with ECP.

4.4 Discussion

The main purpose of this chapter is to investigate the contribution of the two origins (heterogeneous nucleation and dendrite fragmentation) to the grain refinement under the application of electric current. As concluded from the experiment results, the heterogeneous nucleation cannot be promoted under the application of electric current. A reduction of undercooling can be observed in the sample under the impact of electric current; solidification experiments of high purity of aluminum have not shown the possibility to cause the grain refinement by reducing the nucleation energy barrier ΔG^*. The equiaxed grains in the refined alloy under the application of electric current are mainly from the dendrite fragmentation that are promoted by the induced forced flow during both, the nucleation period and the recalescence period. The reduction of grain size cannot be achieved in the sample with electric current when the solute effect is irrelevant. It indicates that the promoted dendrite fragmentation, as well as the dendrite arm detachment in alloys driven by electric current, is mainly due to the flow-induced solute fluctuations.

Actually, the dendrite fragmentation phenomenon was frequently observed in the solidification of various alloys by using the X-ray in-situ observation technique [118, 131, 139-142]. The results have shown that the dendrite fragmentation can be intensively promoted under the application of

external energy fields [131, 140]. As shown in figure 4.9, the dendrite fragmentation of the Sn-Bi alloy was promoted by the ultrasonic vibration [140]. Figure 4.10 shows the dendrite fragmentation of the Al-Cu alloy under the application of a pulsed electromagnetic field [131]. It is evident that the dendrite fragmentation was promoted by the pulsed electromagnetic field. As for the dendrite fragmentation under the application of ultrasonic vibration or pulsed electromagnetic field, both Liotti et al. [131] and Nagira et al. [140] suggested that this phenomenon was promoted by the forced flow in the inter-dendritic liquid that was generated by the applied external energy fields.

It has often been proposed that the forced flow can induce the temperature fluctuations [44, 117, 143] and/or solute fluctuations [44, 143, 144] to promote the dendrite arms remelting as well as the dendrite fragmentation. Recent investigations [131, 140] showed that the dendrite fragmentation was mainly promoted by the solute enrichment induced by the forced flow. In particular, the dendrite arm remelting process caused by the solute enrichment was directly observed using X-ray techniques [118]. Figure 4.11 shows the contour of solute distribution during the fragmentation of a dendrite arm. It is evident that the solute enrichment caused the detachment of dendrite arm. It is consistent with our experiment results. As shown in section 4.3.2, the grain refinement was not observed in the high purity aluminum regardless of the application of electric current.

In addition, Campanella et al. [124] and Kumar et al. [145] formulated a simple criterion for fragmentation induced by fluid flow on the basis of solute remelting of dendrite arms. They concluded that dendrite fragmentation occurs when the component of inter-dendritic fluid velocity $u_{l,z}$ along the thermal gradient becomes larger than the velocity of the isotherms V_T for the alloys of the distribution coefficient k<1.

$$C_R = u_{l,z} / V_T > 1 \tag{4.1}$$

Here we cannot show the real value of the $u_{l,z}$ and V_T in our case. However, the value of the $u_{l,z}$ should be far larger than the V_T to provoke dendrite fragmentation on account of the low cooling rate and the strong forced flow generated by electric current in our experiment. The cooling curves of the Al-Si solidified in the double-walled mould without forced cooling presented that the cooling rate of the melt was only about 0.5^0C/s. As for the applied ECP of I_{eff}=152A (see section 4.2), our flow measurements in Ga-20wt%In-12wt%Sn revealed a value of about 70mm/s

for the vertical velocity arising from the downward jets below the electrode (see figure 3.6), which corresponds to an approximate value of almost 77mm/s in Al-7wt%Si.

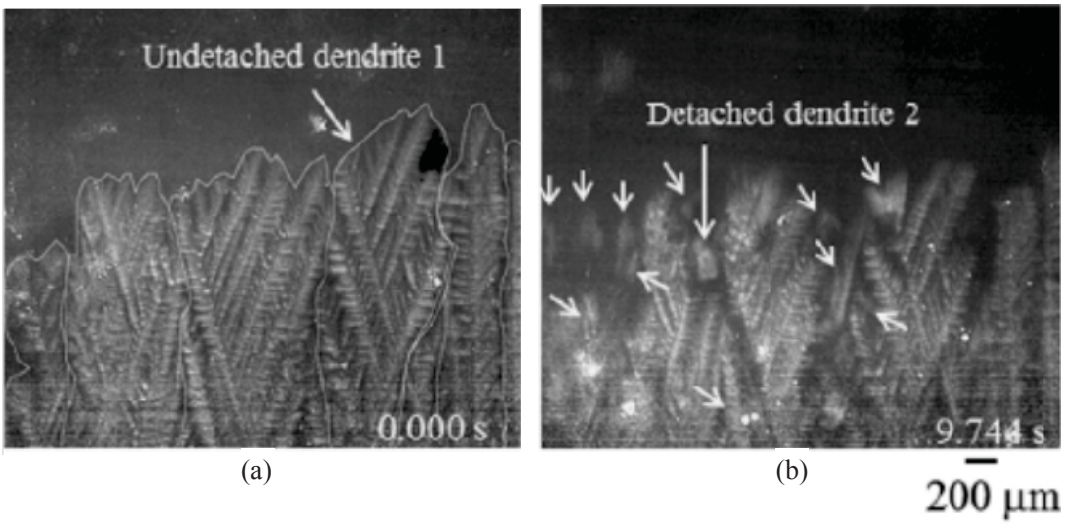

(a) (b)

Figure 4.9: Dendrite fragmentation of Sn-Bi alloy under the application of ultrasonic vibration (UV): (a) without UV, (b) with UV. The fragmentation event is identified by the white arrows [140].

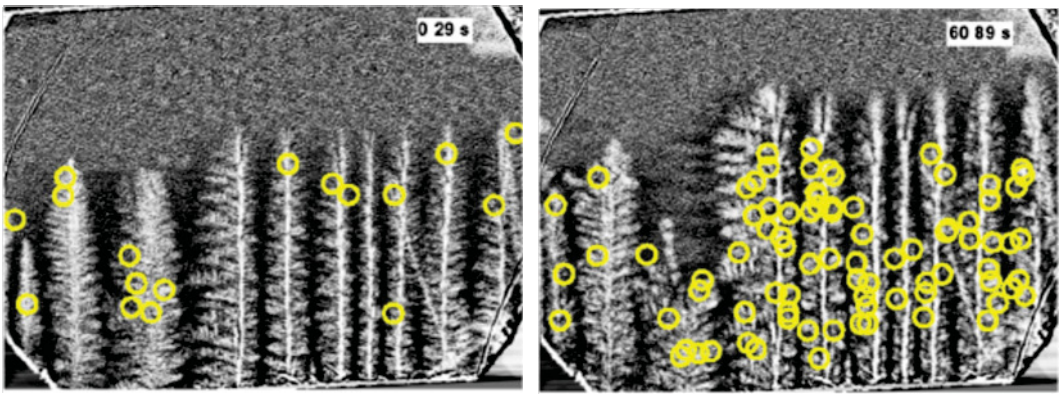

(a) (b)

Figure 4.10: Dendrite fragmentation of Al-Cu alloy under the application of a pulsed electromagnetic field (PEMF): (a) without PEMF, (b) with PEMF. The fragmentation event is identified by the yellow circles [131].

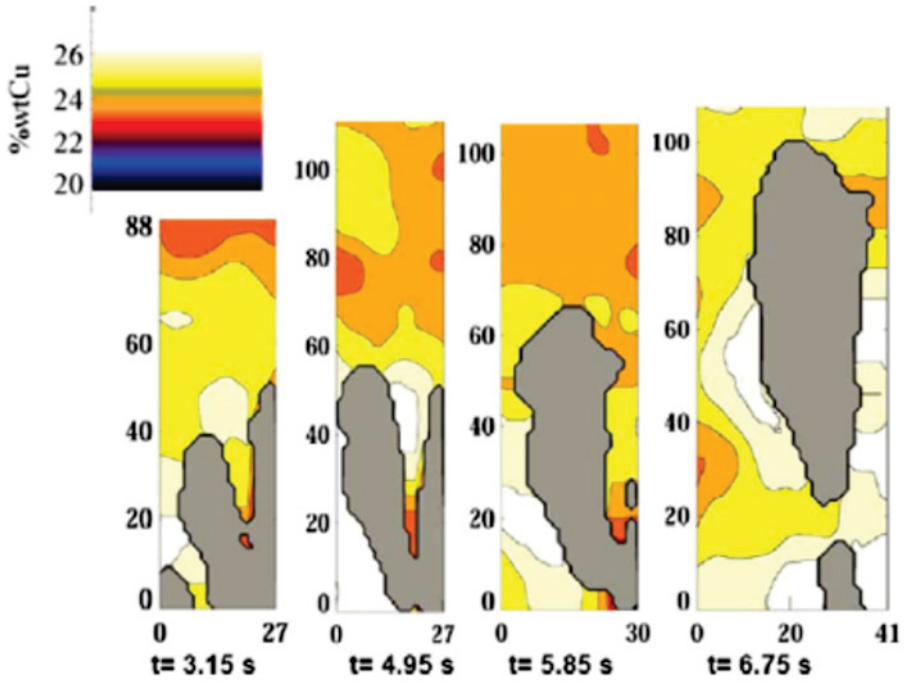

Figure 4.11: Contours showing solute-enrichment during the fragmentation of a dendrite arm (colored in grey) in Al-Cu alloy observed by X-ray [118].

4.5 Conclusions

The present chapter investigated on the origin of equiaxed grain for grain refinement under the application of electric current. The experimental results showed that the grain refinement of Al-7wt%Si alloy under the influence of electric current was generated not only during the nucleation period, but also during the recalescence period. It is also presented that the grain refinement did not occur in the high purity aluminum no matter whether the electric current was applied. Based on the experiment results, it can be concluded that the main origin of equiaxed grain for grain refinement was from the detached dendrite arms. The detachment process, as well as the dendrite fragmentation, was promoted by solute fluctuations induced by the forced flow.

5.Supplemental investigations

There are two highlights that have been presented in chapter 3 and 4: the forced flow induced by electric currents is the leading effect to drive the grain refinement; it is suggested that the dendrite fragmentation promoted by the forced flow was the main origin for the grain refinement. Based on these two points, some further experiments will be performed in this chapter to gain knowledge with respect to the application of the two highlights.

5.1 A potential approach to improve the grain refinement

5.1.1 Introduction

We have experimentally and numerically approved that a strong global forced flow was induced by applied electric currents in the melt under the configuration of two parallel electrodes immersed from the free surface into the electrically conducting melt. Subsequently, the relevance of forced convection to the grain refinement of Al-7wt%Si alloy was demonstrated. Numerical results showed both, the maximum electromagnetic force and Joule heating were confined in a small domain beneath two electrodes. Meanwhile, the experiment results presented that the almost same equiaxed structures were observed under the same flow intensity induced by ECP and TMF. When the higher intensity of the flow was generated, the smaller grain size was observed in the Al-7wt%Si alloy. It was fully convincing to conclude that the forced flow would be the leading effect for the grain refinement of alloys (see chapter 3).

The employed electric current parameter is really important with respect to the intensity of the forced flow. However, is it possible to increase the intensity of the forced flow when the electric current parameter is fixed? According to the magnetohydrodynamic theory [136], the forced flow is controlled by the electromagnetic force which is caused by the interaction between the applied current and its own induced magnetic field. The electric current distribution must be of importance to the generated electromagnetic force and to the forced flow. Hence, it is a potential way to promote the intensity of the forced flow by controlling the electric current distribution.

The present section will investigate the influence of the electric current distribution on the forced

flow as well as the resulted grain refinement under the same inputting electric current parameters. It should be noted that the electric current distribution can be changed by numerous factors, such as electrodes geometry, numbers, conducting position, and so on. Here we just consider the effect of the electric current distribution on the forced flow and grain refinement by arranging the electric current flowing through different part of the electrodes.

5.1.2 Experimental parameter

The geometry of the experimental setup is the same as the one shown in section 2.2. In order to change the electric current distribution, an electric insulation material (BN) covered different parts of the cylindrical electrodes and was used to limit the electric current flowing. As the schematic view shown in figure 5.1a, there is no electric insulation cover on the electrode, which is usually employed by other scholars [73, 86]. Such kind of electrode means that the electric current can flow through the sidewall of the electrode. For the other one, as used in our other solidification experiments (see section 2.3.1) the sidewall was covered with electric insulation to prohibit the electric current flow. Only the bottom surface of the electrode is allowed to conduct the electric current (see figure 5.1b).

Both kinds of electrodes were used to perform solidification experiments by conducting DC of I_{DC}=152A in Al-7wt%Si alloy. The forced cooling of the sample through the mould bottom and the treatment by DC were triggered at the same time. The application of electric currents was powered off when the temperature of the samples was cooled to the eutectic point. The corresponding melt flow measurements were carried out in the eutectic alloy Ga-20wt%In-12wt%Sn to examine if the electric current flow through different parts of the electrodes has an effect on the flow intensity. A single sensor was located at three different positions (see figure 3.5) to measure the melt flow.

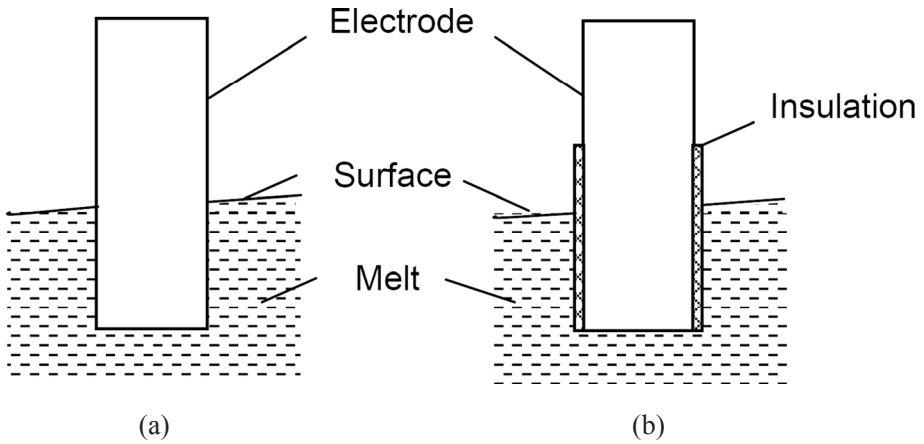

Figure 5.1: Schematic view of the electrode: (a) without electric insulation, (b) sidewall with electric insulation.

5.1.3 Results and discussion

Solidified macrostructure

Figure 5.2 shows the longitudinal macrostructure of solidified Al-Si alloy under the impact of I_{DC}=152A using the two kinds of electrodes. In both of the two solidified samples, it can be found that numerous refined equiaxed grains were produced. The equiaxed grains were almost equally distributed throughout the whole samples. However, it can be still observed that the larger grains occurred in the reference sample treated by DC through two vertically parallel electrodes with an un-insulated lateral surface (see figure 5.2a). In contrast, as shown in figure 5.2b, the finer grains were generated in the sample where the same electric current was only allowed to conduct through the bottom surface of the electrodes into the solidifying sample. The various grain size generated in both samples indicates that the different electrodes conditions, as well as electric currents distributions, have significant impact on the grain refinement of the solidified sample even though the same geometry and electric current parameter were applied.

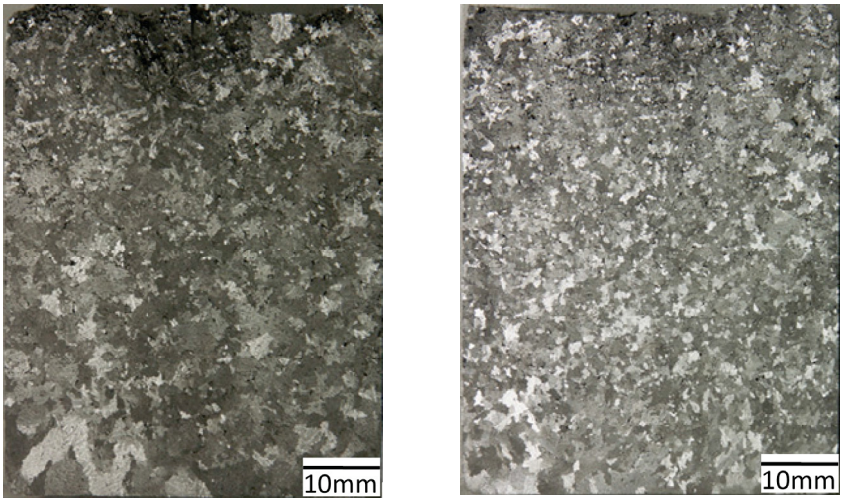

(a) (b)

Figure 5.2: Influence of electric current distribution on the macrostructure of samples ECP: electric current flowing through (a) sidewall of electrode, (b) bottom surface.

Forced flow

Flow measurements were performed in Ga-20wt%In-12wt%Sn melt to investigate the influence of various electric current distributions on the forced flow induced by electric current. Figure 5.3 presents the vertical velocity measured at three positions (see figure 3.5) under the applied ECP of I_{DC}=152A when the electric current flowed through the sidewall and bottom surface of the electrodes, respectively. The same flow pattern can be observed under both of these two different electric current distributions. The flow direction at the cylinder axis was downward in the upper part and upward in the bottom part, as shown in figure 5.3a and 5.3b. For the position underneath the electrodes, a downstream flow was generated (see figure 5.3c and 5.3d). When the measured point was vertically located on the sidewall of the plane perpendicular with the plane containing the two parallel electrodes, an upward flow was observed (see figure 5.3e and 5.3f).

However, although the same flow pattern was generated, the flow intensity inside the melt was obviously stronger at all positions when the sidewall surface of the electrodes was covered by electric insulation material to confine the electric current only flowing through the bottom surface of the electrodes. Particularly, at the measured position beneath the electrodes, the largest vertical velocity was only about 40mm/s for the electrodes without BN (see figure 5.3c) while the value was at least as high as 70mm/s for the electrodes with BN (see figure 5.3d). The presented experimental results can explain why the finer grain size was observed in the solidified sample when the electric current was only allowed to conduct through the bottom surface of the

electrodes (see figure 5.2b). It indicates that the higher flow intensity, as well as finer grain size, can be created by controlling the electric current distribution even if the fixed electric current parameter is applied. Moreover, this potential approach is not only feasible but also flexible. Here we just showed a possible method to control the electric current distribution by means of covering electric insulation materials on electrodes. Various alternative methods can also be developed to improve the electric current distribution. Investigating the effect of the electric current distribution on the grain refinement of alloys should be really attractive for the industry on account of the fact that the finer grain size can be achieved without higher energy input.

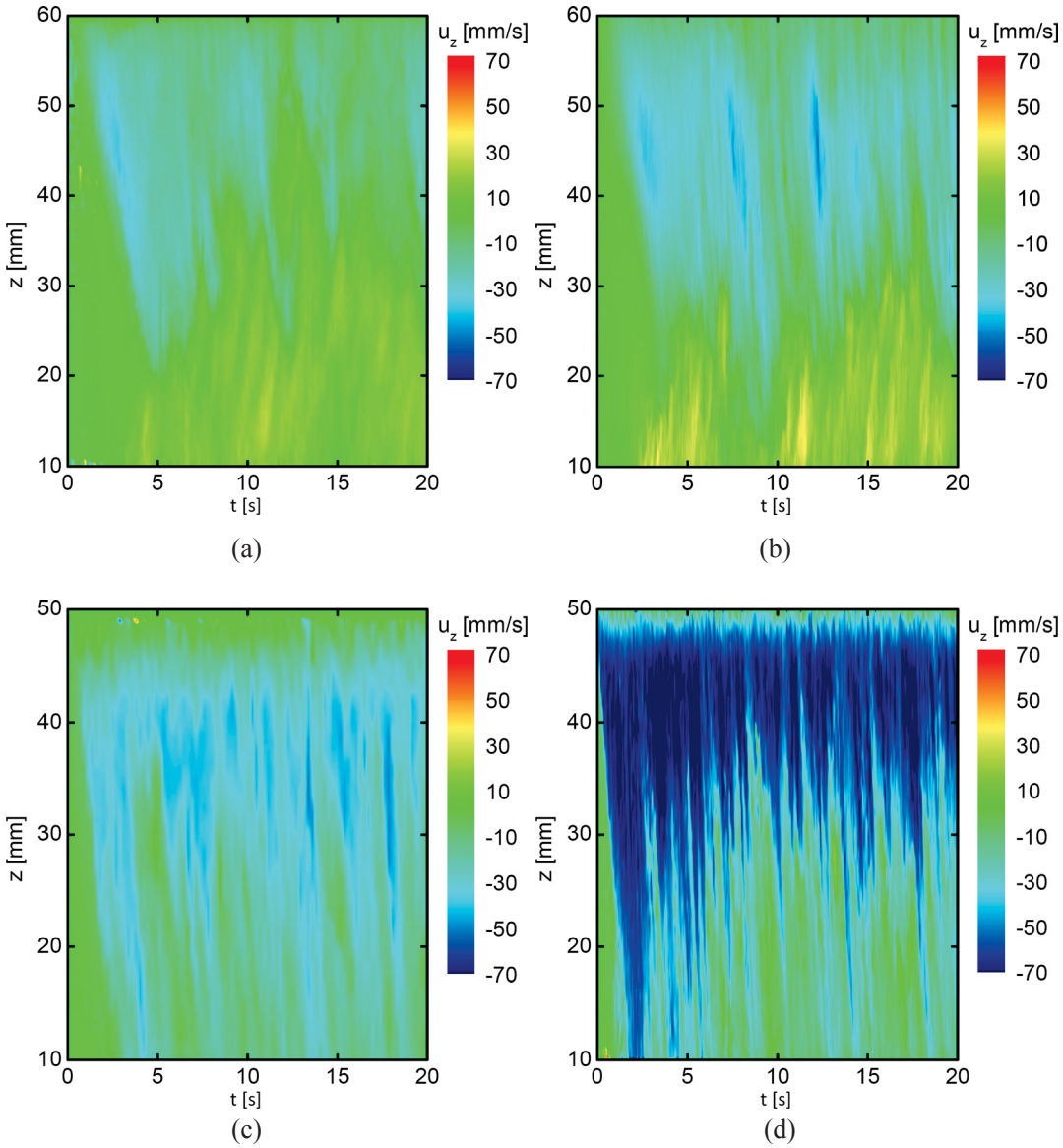

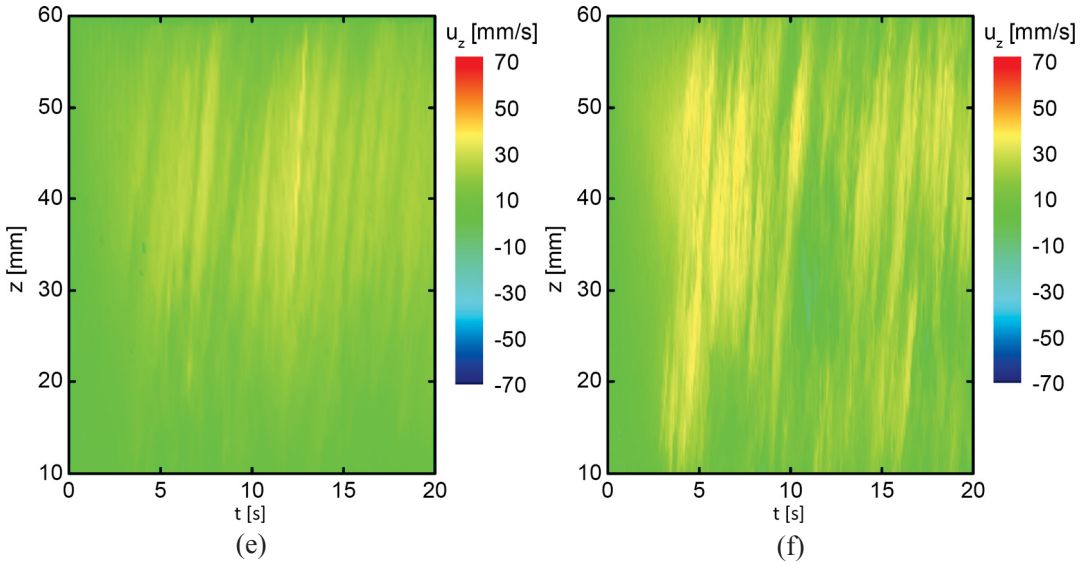

Figure 5.3: Influence of electric current distribution on the vertical velocity measured at three positions under the applied ECP of I_{DC}=152A: electric current flowing through sidewall of electrodes: (a) P1, (c) P2, (e) P3; through bottom surface of electrodes: (b) P1, (d) P2, (f) P3.

5.2 Macrosegregation formation

5.2.1 Introduction

Macrosegregation describes the inhomogeneity of solute distribution in the ingot scale. Investigating the macrosegregation in alloy ingots is of high importance, because a serious macrosegregation can cause inhomogeneous mechanical properties of a product and remarkably deteriorate the quantity of alloy ingots. In order to control the macrosegregation formation in alloys, many studies have been performed and found that the flow plays a key role in the macrosegregation formation [146, 147].

The forced flow can be driven by magnetic fields, such as the rotating magnetic field (RMF) and traveling magnetic field (TMF) [41, 148-151]. Applying RMF in a directionally solidified AlSi7Mg0.6 alloy, Zimmermann et al. found that the forced flow results in an axial macrosegregation (rich silicon) in the centre part of a sample [148]. Meanwhile, Zaïdat et al. reported that a freckled segregation in the directional solidification of Al-3.5wt%Ni alloy was induced under the influence of TMF [149]. Noeppel et al. simulated the macrosegregation formation in directionally solidified alloys under the presence of RMF or TMF and showed that

the macrosegregation pattern was driven by the forced flow structure [150]. Furthermore, a novel approach was invented by Willers et al. to suppress the macrosegregation of solidified Al-Si alloy by controlling the applying time of RMF [41]. Recently, based on a series of Al-Si alloy solidification experiments with RMF, Jie et al. proposed a macrosegregation formation mechanism [151].

However, less attention has been paid to the impact of electric currents on the macrosegregation formation in solidified alloys. We have found out that the electric current can cause a strong forced flow in the melt (see chapter 3). In view of the effect of forced flow on the solute distribution, is it possible to control the macrosegregation by the forced flow solely applying electric currents? The present section is devoted to investigating the solute distribution under the impact of forced flow induced by electric currents.

5.2.2 Experimental parameter

The solidified Al-7wt%Si samples used here to measure the solute distribution in the ingot scale are the samples that have been analyzed on the effect of electric current on the grain size (see figure 3.1). Selected samples were ground and polished from 6μm to 1μm, and then directly photographed under an optical microscope MeF4 (Leica Microsystems, Wetzlar). The 540 single pictures (2.88mm×2.16mm) were created, which fully cover the whole area of a sample.

As the picture of the as-solidified Al-7wt%Si hypoeutectic alloy shows in figure 5.4a, the phases consist of the primary Al phase and the eutectic phase. The primary Al phase is in white color, while the eutectic phase is black under the optical microscope with the grey mode. Hence, the phases can be colored and classified via contrasting the grey values of the phases (see figure 5.4b). Subsequently, the area percentage of the eutectic phase can be calculated. Macrosegregation can be reflected by comparing the area percentage of the eutectic phase in each single picture. The phase analysis was performed using the software package ANALYSIS FIVE (Olympus Europe, Hamburg). In view of the fact that the induced forced flow pattern by electric current is not axially symmetric under our configuration (see figure 3.3), the phase analysis in both, the plane (S1, see figure 5.5) containing the electrodes and the plane (S2) perpendicular to the electrode plane was performed.

Here it should be noted that although 540 single pictures were created to cover the whole area of

the sample, 432 single pictures were used to measure the eutectic phase content because there is an un-measurable region at the top of the sample due to the shrinkage. In order to show the amplitude of macrosegregation in each sample, the variance (*Var*) of the eutectic phase content in the sample was calculated by:

$$Var = \frac{1}{432}\sum_{i=1}^{432}(X_i - \bar{X})^2 \tag{5.1}$$

where X_i is the eutectic phase content in each single picture, $\bar{X}$ is the mean value of the eutectic phase content for 432 single pictures.

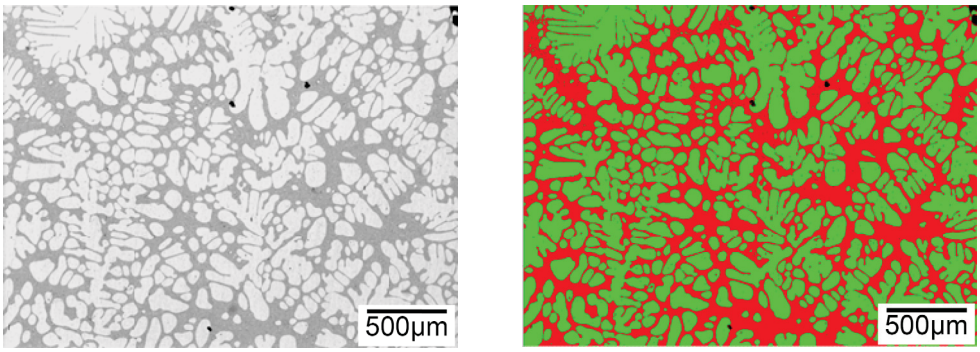

(a) (b)

Figure 5.4: Microstructure of as-solidified Al-7wt%Si hypoeutectic alloy: (a) grey, (b) color.

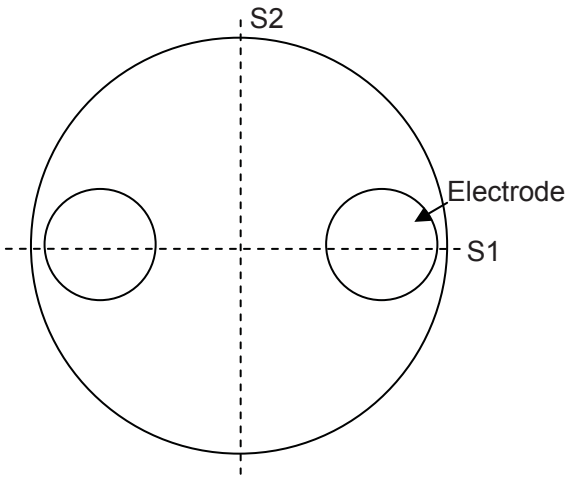

Figure 5.5: Schematic view of the sectioned planes.

5.2.3 Results and discussion

Effect of electric current on solute distribution

Figure 5.6 presents the plotted contour for eutectic phase distribution and the pointed

microstructure of the as-solidified Al-7wt%Si hypoeutectic alloy. The eutectic phase distribution in the S1 of the reference sample without treatment of electric current was not strictly uniform but, the difference is not obvious. The microstructure in the two numbered pictures also showed a non-observable difference for the area percentage of the eutectic phase (see figure 5.6a). A significant difference of the eutectic phase distribution can be observed in the S1 and S2 of the samples treated by ECP of I_P=480A, f=200Hz, t_p=0.5ms, I_{eff}=152A (see figure 5.6b and 5.6c). It means that the macrosegregation of solute was created in the ingot under the influence of electric current. In particular, as shown in figure 5.6b, a really obvious negative macrosegregation was caused at the region (marked with number 1). Two microstructure figures marked in the contour showed an observable difference of eutectic phase content between the region beneath the electrodes and the bottom part.

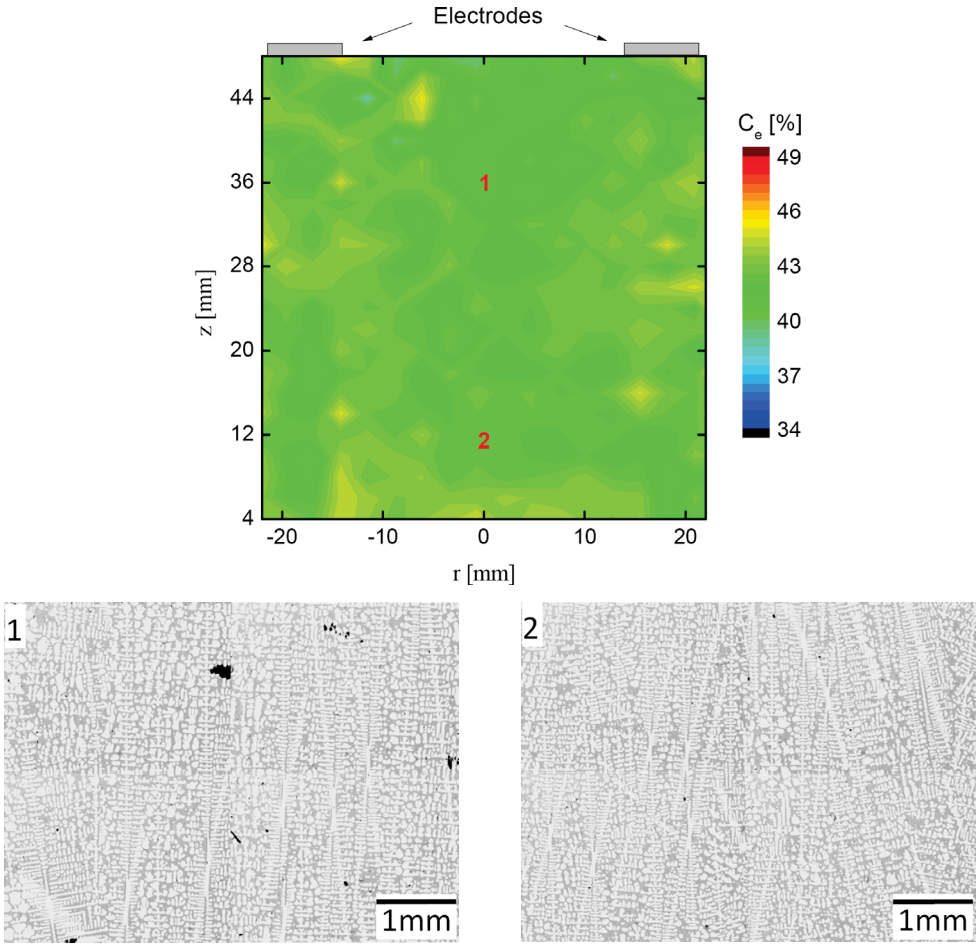

(a)

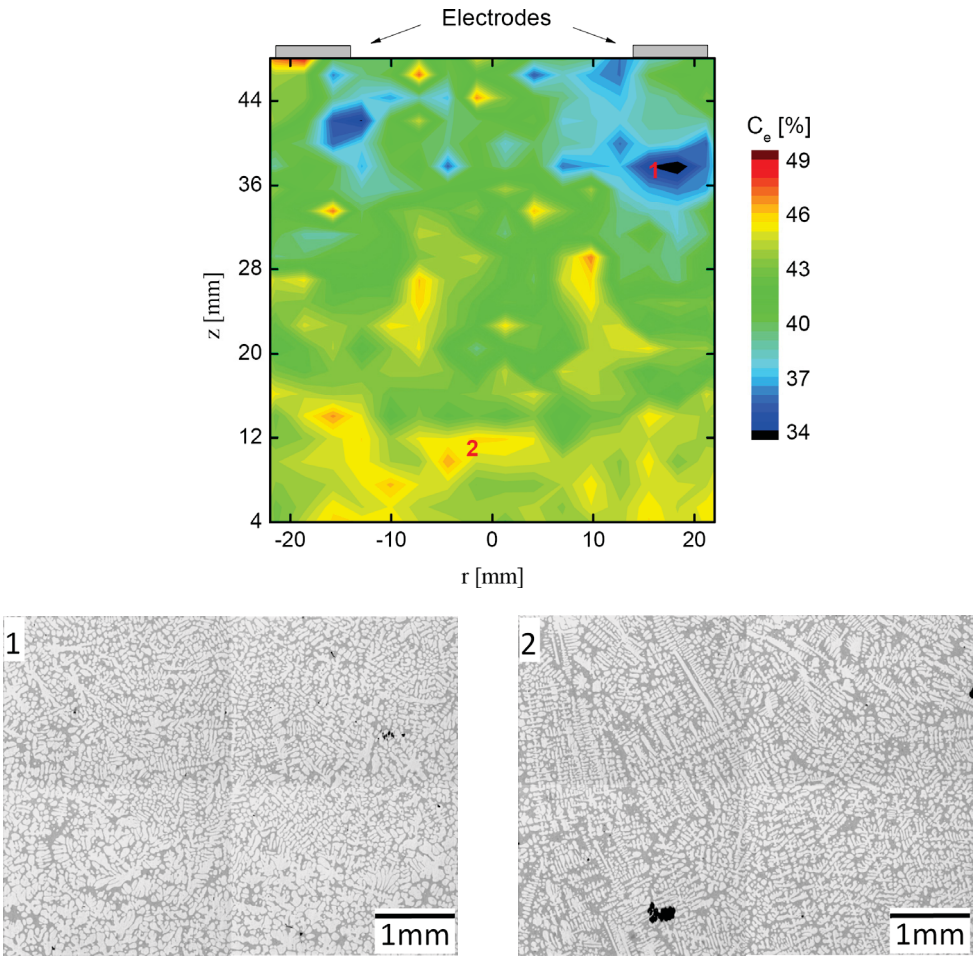
Electrodes
z [mm]
r [mm]
C_e [%]
49
46
43
40
37
34
1
2
44
36
28
20
12
4
-20
-10
0
10
20
1
2
1mm
1mm

(b)

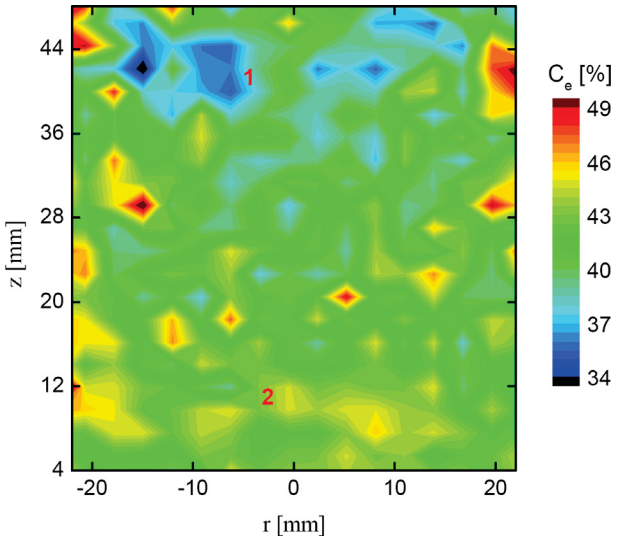
z [mm]
r [mm]
C_e [%]
49
46
43
40
37
34
1
2
44
36
28
20
12
4
-20
-10
0
10
20

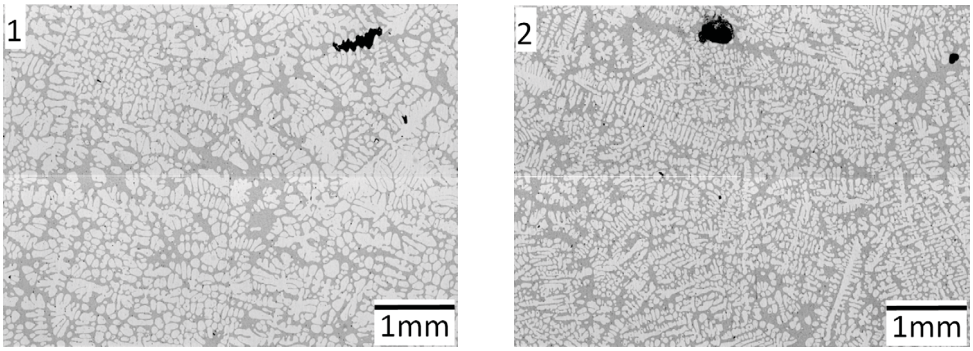

(c)

Figure 5.6: Eutectic phase distribution and microstructures of Al-7wt%Si alloy: S1 (a) without ECP, (b) with ECP; S2 (c) with ECP of I_P=480A, f=200Hz, t_p=0.5ms, I_{eff}=152A.

Effect of I_{eff} on macrosegregation

The influence of the value of effective electric current on the solute distribution is investigated by measuring the eutectic phase distribution in S2 of Al-7wt%Si hypoeutectic alloy samples treated by various parameters (I_{eff}) of electric currents. Figure 5.7 shows the selected contour of the eutectic phase distribution. It can be observed that the difference of the eutectic phase distribution in samples increases with I_{eff}. It means that the macrosegregation turns more obvious with the increase of the effective current intensity (see figure 5.7a-d). In order to display the effect of I_{eff} on the variation of macrosegregation quantitatively, the variance of the eutectic phase content was calculated on the whole longitudinal section for each sample. The corresponding plot is shown in figure 5.8. It can be found that the variance gradually increased with the intensity of the effective current value, which indicates that the macrosegregation increased with I_{eff}.

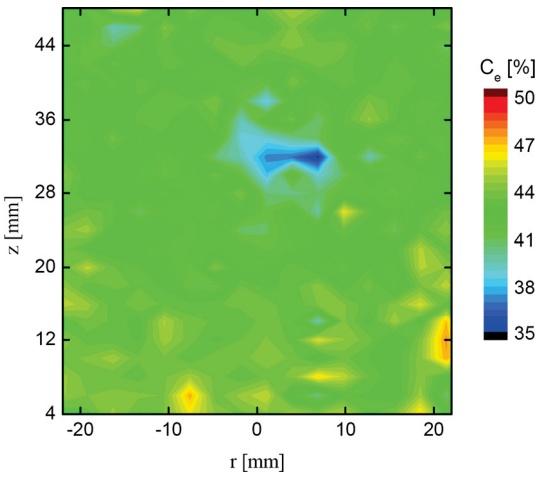

(a) I_P=120A, f=50Hz, t_p=0.5ms

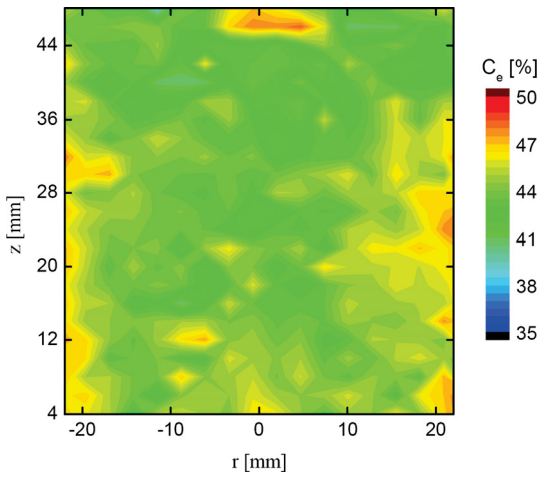

(b) I_P=120A, f=100Hz, t_p=1ms

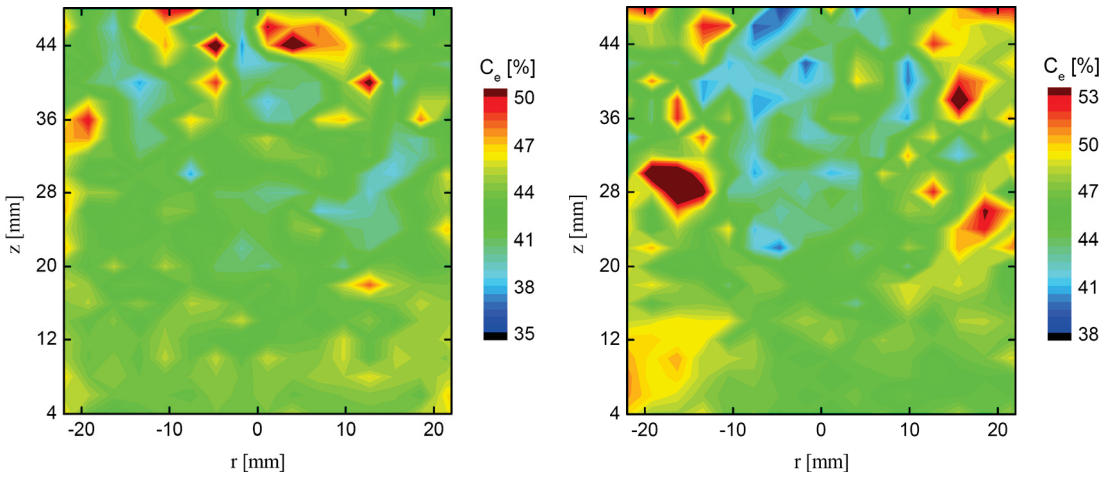

(c) I_P=120A, f=200Hz, t_p=2ms (d) I_P=480A, f=50Hz, t_p=2ms

Figure 5.7: Eutectic phase distribution on the longitudinal section S2 of Al-7wt%Si alloy: (a) I_{eff}=19A; (b) I_{eff}=38A; (c) I_{eff}=76A; (d) I_{eff}=152A.

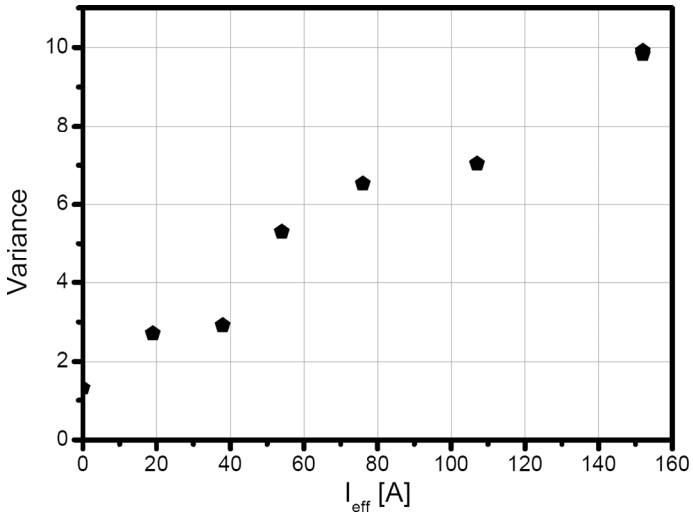

Figure 5.8: Influence of effective electric current on the variance of eutectic phase content.

Discussion

The knowledge with respect to the reasons for the macrosegregation formation during the solidification process has been well developed [146]. It has been recognized that the forced flow is one of reasons to cause the solute segregation [146-151]. As shown in figures 3.4 and 3.6, a forced flow was generated in the conducted $Ga_{68}In_{20}Sn_{12}$ melt under the interaction between the applied electric currents and its self-induced magnetic field. It can be seen that the forced flow was generated in the melt under the impact of electric current. Although the flow measurement was performed in the $Ga_{68}In_{20}Sn_{12}$ liquid melt, the forced flow cannot only occur in the melt of the Al-7wt%Si melt driven by electric current, but the generated flow intensity should be even

slightly higher (see section 2.2.2). Hence, it can explain the macrosegregation formation in Al-7wt%Si alloy under the impact of electric current. Moreover, it was found that the flow velocity was accelerated with the increase of the value of I_{eff} (see figure 3.8). It is consistent with the evolution of macrosegregation with the I_{eff} (see figure 5.8).

5.3 Grain refinement driven by TMF

5.3.1 Introduction

It has been proven that the forced flow induced by electric current was the key effect to cause the grain refinement in alloys (see chapter 3). In addition, our experimental results indicate that the main origin of the equiaxed grains under the application of electric current was due to the dendrite fragmentation rather than the heterogeneous nucleation; the detachment of dendrite arms was driven by the solute remelting (see chapter 4).

As mentioned previously in section 1.4.4, the grain refinement in solidified alloy under the application of EMS was caused by the forced flow inside the melt. Dendrite fragmentation promoted by the forced flow generated by EMS is already widely accepted as the main origin for the grain refinement in alloys. It seems like that the same grain refinement formation process was caused by electric current and EMS.

Nevertheless, it is still necessary to carefully demonstrate this prediction on account of the fact that the electric current and EMS are two totally different patterns of the electromagnetic field. Here TMF as one kind of EMS was applied in the solidification experiments to confirm the prediction.

5.3.2 Experimental parameter

Solidification experiments of Al-7wt%Si alloy and high purity aluminum cooled in air were carried out under the application of TMF (downward, 10mT). In order to compare with the experimental results under the application of electric currents, the same solidification experimental setup, sample geometry, experimental procedure and metallography method (see chapter 2) were employed.

5.3.3 Results and discussion

Solidified structure of Al-Si alloy

As the schematic view shows in figure 5.9, TMF was applied respectively during various solidification periods: the whole solidification period, the initial solidification period, the nucleation period and the recalescence period. The corresponding macrostructure on the longitudinal section of solidified Al-7wt%Si samples are presented in figure 5.10. Comparing the reference sample without the treatment of the energy field shown in figure 4.7a, a significant grain refinement occurred in the sample treated by TMF during the whole solidification period (see 5.10a). It also can be found that the similar macrostructure was generated in the sample of Al-7wt%Si alloy when TMF was applied during the initial solidification period. It indicates the grain refinement formation of the sample with treatment of TMF was also activated in the initial solidification period. Hence, in the following two solidified samples, TMF was applied in the nucleation and recalescence period, respectively. Figure 5.10c presents the macrostructure on the longitudinal section of the solidified Al-7wt%Si sample under the treatment of TMF during the nucleation period. The coarse equiaxed grains can be observed in the sample, but the grain size was still reduced by comparing the macrostructure of the sample without applying TMF (see figure 4.7a). Figure 5.10d shows that the tiny grains were produced and mixed with coarse grains when TMF of 10mT was only applied during the recalescence period. It means that the grain refinement is caused during the recalescence period.

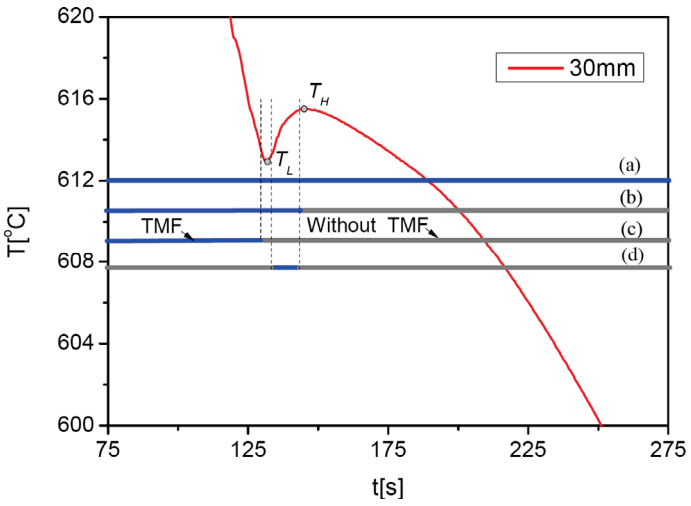

Figure 5.9: Schematic view of TMF (10mT, downward) applying time (blue line: turned on TMF; grey line: turned off TMF; a-d: corresponding the following a-d in figure 5.10).

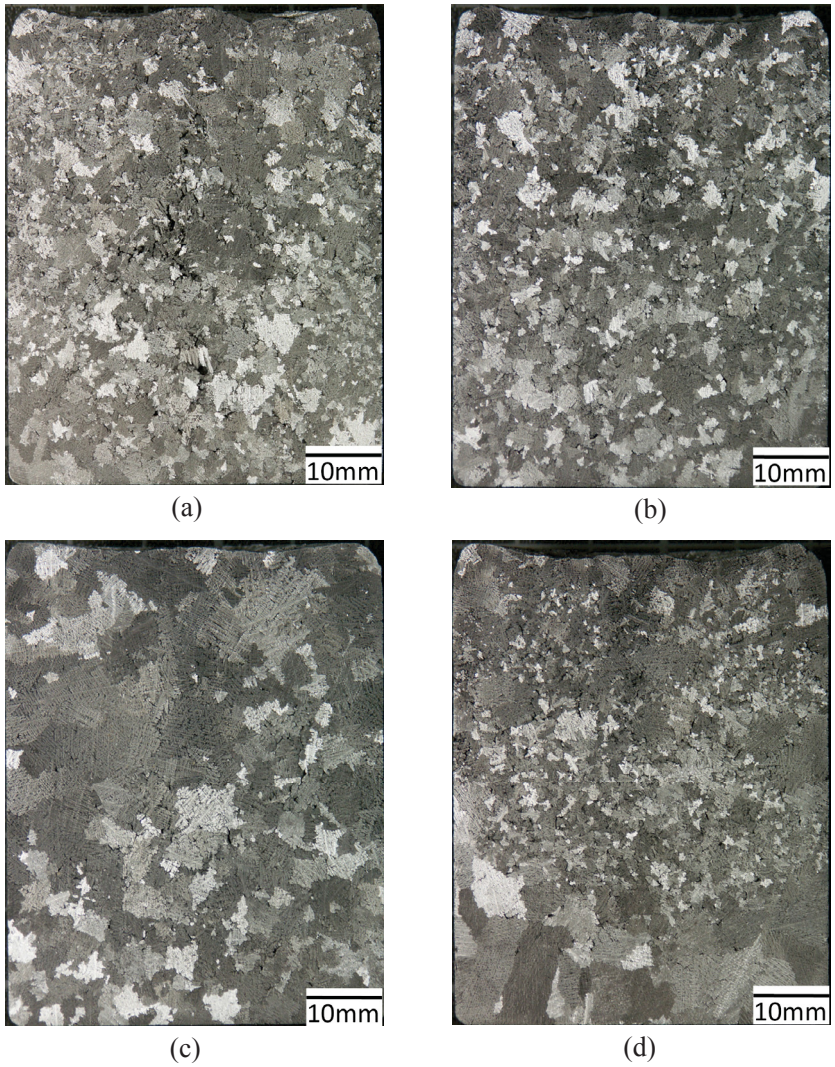

Figure 5.10: Influence of the various TMF (10mT, downward) applying time on the longitudinal section macrostructure of the solidified Al-7wt%Si alloy samples without forced cooling: a-d corresponding to the various applying times shown in figure 5.9.

The corresponding grain size measurements were performed to achieve further insights into the macrostructure evolution driven by applying TMF during different solidification periods (see table 5.1). It can be found that both samples treated during the whole and initial solidification period achieved the grain size level of 1mm. The produced grain of almost the same size can fully approve that the grain refinement occurred during the initial solidification period. Moreover, the grain size of 1.98mm was approached when TMF was applied during the nucleation period. It is less than the grain size of the sample without treatment of TMF (2.82mm). This furthermore indicates that the grain refinement driven by TMF occurred during the nucleation period. In addition, the maximum undercooling is compared between both samples with and without the application of TMF. It can be observed that the maximum undercooling was also decreased when

TMF was applied. As shown in table 5.1, T_L was increased by about 1.8°C from 611.2 °C (without TMF) to 613°C.

Table 5.1: Influence of the various TMF applying time on the grain size and T_L of samples without forced cooling

Figure	4.7a	5.10a	5.10b	5.10c
Mean grain size (mm)	2.82	1.06	1.01	1.98
T_L(°C)	611.25	612.96	612.93	613.08

Solidified structure of high purity aluminum

As mentioned previously (see section 1.4.4), it is widely accepted that the dendrite fragmentation promoted by the forced flow is the main origin for the grain refinement in alloys under the application of EMS. Both, temperature fluctuations and solute fluctuations induced by the forced flow are frequently proposed for the dendrite arms detachment. However, as shown in section 4.3.2, experiment results using high purity aluminum suggested that the dendrite arms remelting process in alloys under the application of electric current was driven by the solute fluctuations rather than the temperature fluctuations. Hence, in the presented section, the solidification experiments of high purity aluminum were also performed under the influence of TMF to confirm if the solute fluctuations drive the remelting process. Two grades of high purity aluminum, 99.998%Al and 99.9999%Al, were employed.

The macrostructure on the longitudinal section of solidified samples is shown in figure 5.11. The several coarse grains were observed in both 99.998%Al and 99.9999%Al samples without treatment of TMF (see figure 5.11a and 5.11c). For the samples treated by TMF, it can be found that a really light grain refinement occurred in the 99.998%Al sample. The finer grains mainly concentrated in the area around the axis of the sample. Several coarse grains still formed in the other area of the sample. In addition, the macrostructure in the sample treated by TMF was almost the same compared to the reference sample (without TMF) when the higher purity of aluminum 99,9999%Al was employed. It means that no grain refinement initiates under the application of TMF if the solute effect (solute fluctuations) is dismissed. The experiment results confirm that the solute fluctuations induced by forced flow play a key role in the grain fragmentation process.

In summary, the macrostructure formation process of samples under the application of TMF is really similar to the samples with ECP (see section 4.3.1). Moreover, the experimental results using high purity aluminum suggest that the grain refinement in alloys under the application of TMF was driven by the solute fluctuations, which is also really similar to the results under the application of electric current. Hence, it can be concluded that the same grain refinement formation process is caused by electric current and EMS.

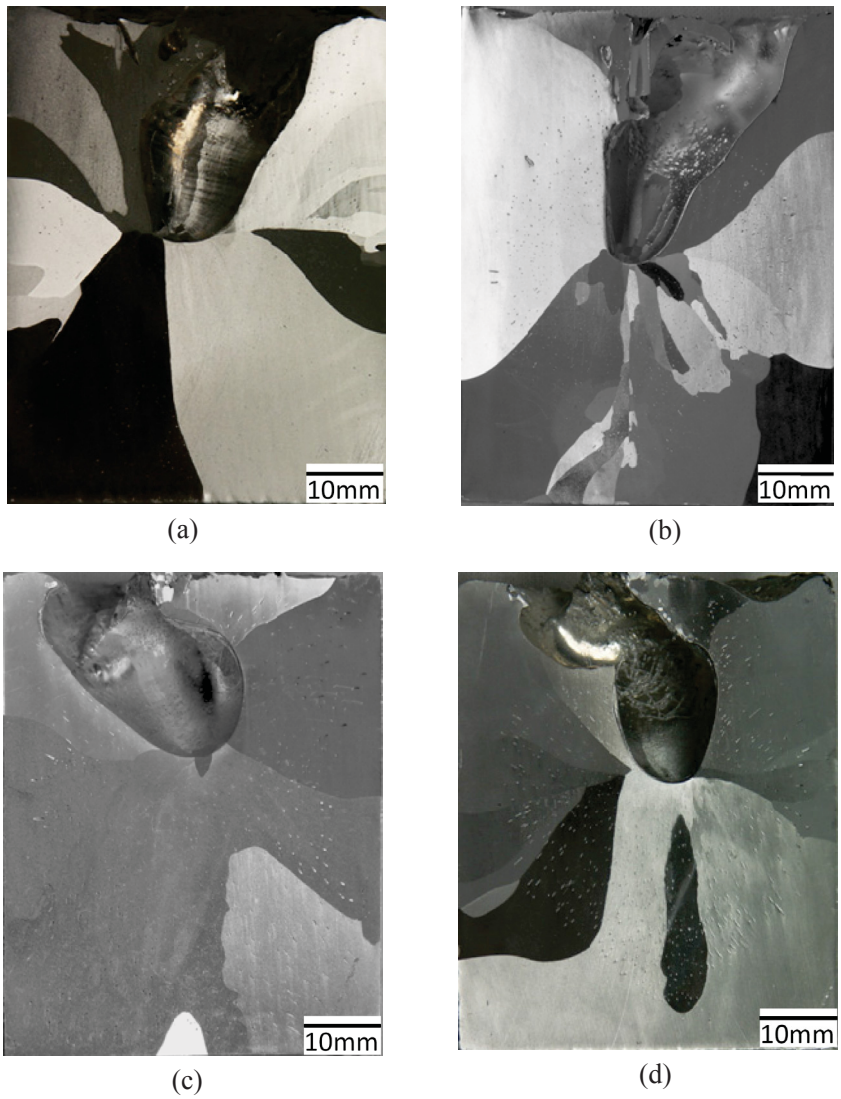

(a) (b)

(c) (d)

Figure 5.11: Influence of the TMF on the longitudinal section macrostructure of the solidified high purity aluminum samples without forced cooling: Al(99.998%) (a) without TMF, (b) with TMF; Al(99.9999%) (c) without TMF, (d) with TMF.

5.4 Conclusions

It has been shown that the forced flow induced by electric currents plays a dominant role in the grain refinement of alloys. Hence, a potential approach to promote the flow intensity was developed to improve the grain refinement in solidified Al-7wt%Si alloys when the electric parameters were fixed. The electric current distribution was controlled by covering the electrodes with electric insulation material. It is found that the higher intensity forced flow and the finer grain size were approached by confining the electric current only flowing through the bottom surface rather than flowing through the sidewall of the electrodes.

The macrosegregation in the solidified Al-7wt%Si alloy under the application of electric current was examined. It can be observed that the macrosegregation was caused in the samples under the application of electric currents. The difference of solute distribution was promoted with the increase of the intensity of the forced flow as well as the value of effective electric currents.

The grain refinement formation driven by TMF was considered. Experimental results showed that the grain refinement under the application of TMF mainly occurred during the nucleation and recalescence period. The solidification experiments using high purity aluminum indicated that the solute fluctuations induced by forced flow drives the dendrite fragmentation. Comparing it with the experimental results under the application of electric current (see chapter 3 and 4), it can be concluded that both, the TMF and electric current caused the almost same grain refinement formation process in solidified alloys.

6. Summary

In the present dissertation, the grain refinement of solidified Al-7wt%Si hypoeutectic alloy driven by electric currents has been focused. Chapter 1 reviews the research motivation, the research history and the already achieved knowledge on the electric currents effects and grain refinement mechanisms. It presents that the application of electric current in the electrically conducted alloys is an efficient approach to reduce the grain size during the solidification process. This subject has been extensively investigated in the recent fifteen years. However, many effects of electric currents were proposed to play a dominant role in the grain refinement, and there is not a widely accepted knowledge on which effect or effects is or are the key to cause the grain size reduction. In addition, the grain refinement mechanism under the application of electric currents still does not show a consistent picture. Hence, this dissertation is devoted to giving a response to these two points. A series of experiments and numerical simulation are designed. Chapter 2 introduces the related experimental and numerical simulation methods, including the experimental materials, setup, procedure, analysis method of solidified samples and numerical model.

In chapter 3, the investigation concerns the relevance of electric currents effects to the grain refinement. Ultrasonic flow measurements in a low temperature Ga-20wt%In-12wt%Sn alloy and the corresponding numerical simulation reveals that a strong electro-vortex flow in the melt can be caused by the electromagnetic force from the interaction between the applied current and its own induced magnetic field. Both, direct current (DC) and electric current pulses (ECP) were applied in the flow measurements. The flow intensity increases with the value of effective electric current regardless of the applied electric current pattern. Similarity, the application of either direct current DC or ECP at frequencies up to 200Hz leads to the formation of refined equiaxed grain structures. The consequences on both, the mean grain size and the area of the equiaxed zone in the solidified samples only depend on the effective current intensity. In addition, the numerical analysis demonstrates that the electric currents and the induced electromagnetic force are concentrated on a small domain beneath the electrodes. Consequently, the shear force and the Joule heating do not directly exist in the mushy zone. It means that the forced flow plays a key role in the grain refinement formation in alloys during the solidification process. A solidification experiments under the application of the travelling magnetic field (TMF) was

performed to make a further validation. A similar macrostructure is resulted when the almost same flow intensity is caused by both, TMF and electric current.

Chapter 4 mainly focuses on the origins of equiaxed grains to understand the grain refinement formation under the application of electric current. A series of solidification experiments were performed in Al-7wt%Si and high purity aluminum to confirm or expel the possible origins of grain refinement. The results indicate that the main origin of equiaxed grain for grain refinement is from the dendrite fragmentation; the dendrite was fragmented by the solute fluctuations that could be caused by the generated forced flow under the application of electric current.

Chapter 5 performs further researches based on the achieved knowledge in chapter 3 and 4. Since the forced flow induced by electric currents play a dominant role in the grain refinement of alloys, an approach to improve the grain refinement in solidified Al-7wt%Si alloy was invented by controlling the electric distribution to promote the flow intensity under inputting the same electric parameters. Moreover, the solute distribution was examined in the solidified Al-7wt%Si alloy treated by electric currents on account of the fact that the macrosegregation can be caused by the forced flow. It is found that a significant macrosegregation was generated in the sample under the application of electric currents. According to the research on the grain refinement formation under the application of electric currents in chapter 4, the grain refinement formation driven by TMF has also been considered. The performed series of solidification experiments show that the same grain refinement formation process is initiated under both, the influence of TMF and electric currents.

Bibliography

[1] Grassel, O.; Kruger, L.; Frommeyer, G.; Meyer, L.W.: High strength Fe-Mn-(Al, Si) TRIP/TWIP steels development-properties-application. In: International Journal of Plasticity. 16 (2000), pp. 1391-1409.

[2] Miller, W.S.; Zhuang, L.; Bottema, J.; Wittebrood, A.J.; De Smet, P.; Haszler, A., et al.: Recent development in aluminium alloys for the automotive industry. In: Materials Science and Engineering: A. 280 (2000), pp. 37-49.

[3] Mordike, B.L.; Ebert, T.: Magnesium: properties-applications-potential. In: Materials Science and Engineering: A. 302 (2001), pp. 37-45.

[4] Williams, J.C.; Starke Jr, E.A.: Progress in structural materials for aerospace systems. In: Acta Materialia. 51 (2003), pp. 5775-5799.

[5] Hall, E.O.: The deformation and ageing of mild steel: III discussion of results. In: Proceedings of the Physical Society Section B. 64 (1951), pp. 747-753.

[6] Petch, N.J.: The cleavage strength of polycrystals. In: J Iron Steel Inst. 174 (1953), pp. 25-28.

[7] Murty, B.S.; Kori, S.A.; Chakraborty, M.: Grain refinement of aluminium and its alloys by heterogeneous nucleation and alloying. In: International Materials Reviews. 47 (2002), pp. 3-29.

[8] Seidman, D.N.; Marquis, E.A.; Dunand, D.C.: Precipitation strengthening at ambient and elevated temperatures of heat-treatable Al (Sc) alloys. In: Acta Materialia. 50 (2002), pp. 4021-4035.

[9] Gong, J.C.; Wilkinson, A.J.: A microcantilever investigation of size effect, solid-solution strengthening and second-phase strengthening for<a> prism slip in alpha-Ti. In: Acta Materialia. 59 (2011), pp. 5970-5981.

[10] Callister, W.D. Fundamentals of materials science and engineering: Wiley, 2001.

[11] Heinz, A.; Haszler, A.; Keidel, C.; Moldenhauer, S.; Benedictus, R.; Miller, W.S.: Recent development in aluminium alloys for aerospace applications. In: Materials Science and Engineering: A. 280 (2000), pp. 102-107.

[12] Dursun, T.; Soutis, C.: Recent developments in advanced aircraft aluminium alloys. In: Materials & Design. 56 (2014), pp. 862-871.

[13] http://www.world-aluminium.org/statistics/#data.

[14] Ye, H.Z.: An overview of the development of Al-Si-alloy based material for engine applications. In: Journal of Materials Engineering and Performance. 12 (2003), pp. 288-297.

[15] Iwahashi, Y.; Horita, Z.; Nemoto, M.; Langdon, T.G.: The process of grain refinement in equal-channel angular pressing. In: Acta Materialia. 46 (1998), pp. 3317-3331.

[16] Zhilyaev, A.P.; Nurislamova, G.V.; Kim, B.K.; Baró, M.D.; Szpunar, J.A.; Langdon, T.G.: Experimental parameters influencing grain refinement and microstructural evolution during high-pressure torsion. In: Acta Materialia. 51 (2003), pp. 753-765.

[17] Maxwell, I.; Hellawell, A.: A simple model for grain refinement during solidification. In: Acta Metallurgica. 23 (1975), pp. 229-237.

[18] Easton, M.A.; StJohn, D.H.: Grain refinement of aluminum alloys: part I. The nucleant and solute paradigms-a review of the literature. In: Metallurgical and Materials Transactions A. 30 (1999), pp. 1613-1623.

[19] Easton, M.A.; StJohn, D.H.: Grain refinement of aluminum alloys: Part II. Confirmation of, and a mechanism for, the solute paradigm. In: Metallurgical and Materials Transactions A. 30 (1999), pp. 1625-1633.

[20] Greer, A.L.; Bunn, A.M.; Tronche, A.; Evans, P.V.; Bristow, D.J.: Modelling of inoculation of metallic melts: application to grain refinement of aluminium by Al-Ti-B. In: Acta Materialia. 48 (2000), pp. 2823-2835.

[21] Easton, M.A.; StJohn, D.H.: A model of grain refinement incorporating alloy constitution and potency of heterogeneous nucleant particles. In: Acta Materialia. 49 (2001), pp. 1867-1878.

[22] Easton, M.A.; StJohn, D.H.: An analysis of the relationship between grain size, solute content, and the potency and number density of nucleant particles. In: Metallurgical and Materials Transactions A. 36 (2005), pp. 1911-1920.

[23] Ma, Q.; Cao, P.; Easton, M.A.; McDonald, S.D.; StJohn, D.H.: An analytical model for constitutional supercooling-driven grain formation and grain size prediction. In: Acta Materialia. 58 (2010), pp. 3262-3270.

[24] StJohn, D.H.; Ma, Q.; Easton, M.A.; Cao, P.: The interdependence theory: the relationship between grain formation and nucleant selection. In: Acta Materialia. 59 (2011), pp. 4907-4921.

[25] Shu, D.; Sun, B.D.; Mi, J.; Grant, P.S.: A quantitative study of solute diffusion field effects on heterogeneous nucleation and the grain size of alloys. In: Acta Materialia. 59 (2011), pp.

2135-2144.

[26] Abramov, V.; Abramov, O.; Bulgakov, V.; Sommer, F.: Solidification of aluminium alloys under ultrasonic irradiation using water-cooled resonator. In: Materials Letters. 37 (1998), pp. 27-34.

[27] Jian, X.; Xu, H.; Meek, T.T.; Han, Q.Y.: Effect of power ultrasound on solidification of aluminum A356 alloy. In: Materials Letters. 59 (2005), pp. 190-193.

[28] Jian, X.G.; Meek, T.T.; Han, Q.Y.: Refinement of eutectic silicon phase of aluminum A356 alloy using high-intensity ultrasonic vibration. In: Scripta Materialia. 54 (2006), pp. 893-896.

[29] Ramirez, A.; Ma, Q.; Davis, B.; Wilks, T.; StJohn, D.H.: Potency of high-intensity ultrasonic treatment for grain refinement of magnesium alloys. In: Scripta Materialia. 59 (2008), pp. 19-22.

[30] Liu, X.B.; Osawa, Y.; Takamori, S.; Mukai, T.: Grain refinement of AZ91 alloy by introducing ultrasonic vibration during solidification. In: Materials Letters. 62 (2008), pp. 2872-2875.

[31] Gao, D.M.; Li, Z.J.; Han, Q.Y.; Zhai, Q.J.: Effect of ultrasonic power on microstructure and mechanical properties of AZ91 alloy. In: Materials Science and Engineering: A. 502 (2009), pp. 2-5.

[32] Shu, D.; Sun, B.D.; Mi, J.W.; Grant, P.S.: A high-speed imaging and modeling study of dendrite fragmentation caused by ultrasonic cavitation. In: Metallurgical and Materials Transactions A. 43 (2012), pp. 3755-3766.

[33] Flemings, M.C.; Riek, R.G.; Young, K.P.: Rheocasting. In: Materials Science and Engineering. 25 (1976), pp. 103-117.

[34] Mehrabian, R.; Flemings, M.C.: Die casting of partially solidified alloys. In: AFS Trans. 80 (1972), pp. 173-182.

[35] Kang, C.G.; Yoon, J.H.; Seo, Y.H.: The upsetting behavior of semi-solid aluminum material fabricated by a mechanical stirring process. In: Journal of Materials Processing Technology. 66 (1997), pp. 30-38.

[36] Sukumaran, K.; Pai, B.C.; Chakraborty, M.: The effect of isothermal mechanical stirring on an Al-Si alloy in the semisolid condition. In: Materials Science and Engineering: A. 369 (2004), pp. 275-283.

[37] Fang, Q.T.; Kinosz, M.J. Fine grain casting by mechanical stirring. Google Patents; 1990.

[38] Flemings, M.C.; Mehrabian, R.; Riek, R.G. Continuous process for forming an alloy containing non-dendritic primary solids. US Patent 3,902,544; 1975.

[39] Griffiths, W.D.; McCartney, D.G.: The effect of electromagnetic stirring during solidification on the structure of Al-Si alloys. In: Materials Science and Engineering: A. 216 (1996), pp. 47-60.

[40] Willers, B.; Eckert, S.; Michel, U.; Haase, I.; Zouhar, G.: The columnar-to-equiaxed transition in Pb–Sn alloys affected by electromagnetically driven convection. In: Materials Science and Engineering: A. 402 (2005), pp. 55-65.

[41] Willers, B.; Eckert, S.; Nikrityuk, P.A.; Räbiger, D.; Dong, J.; Eckert, K., et al.: Efficient melt stirring using pulse sequences of a rotating magnetic field: Part II. Application to solidification of Al-Si alloys. In: Metallurgical and Materials Transactions B. 39 (2008), pp. 304-316.

[42] Eckert, S.; Willers, B.; Nikrityuk, P.A.; Eckert, K.; Michel, U.; Zouhar, G.: Application of a rotating magnetic field during directional solidification of Pb-Sn alloys: Consequences on the CET. In: Materials Science and Engineering: A. 413 (2005), pp. 211-216.

[43] Eckert, S.; Nikrityuk, P.A.; Räbiger, D.; Eckert, K.; Gerbeth, G.: Efficient melt stirring using pulse sequences of a rotating magnetic field: part I. Flow field in a liquid metal column. In: Metallurgical and Materials Transactions B. 38 (2007), pp. 977-988.

[44] Metan, V.; Eigenfeld, K.; Räbiger, D.; Leonhardt, M.; Eckert, S.: Grain size control in Al-Si alloys by grain refinement and electromagnetic stirring. In: Journal of Alloys and Compounds. 487 (2009), pp. 163-172.

[45] Vives, C.: Effects of electromagnetic vibrations on the microstructure of continuously cast aluminium alloys. In: Materials Science and Engineering: A. 173 (1993), pp. 169-172.

[46] Vives, C.: Effects of forced electromagnetic vibrations during the solidification of aluminum alloys: Part I. Solidification in the presence of crossed alternating electric fields and stationary magnetic fields. In: Metallurgical and Materials Transactions B. 27 (1996), pp. 445-455.

[47] Vives, C.: Effects of forced electromagnetic vibrations during the solidification of aluminum alloys: Part II. solidification in the presence of colinear variable and stationary magnetic fields. In: Metallurgical and Materials Transactions B. 27 (1996), pp. 457-464.

[48] Li, M.J.; Tamura, T.; Miwa, K.: Controlling microstructures of AZ31 magnesium alloys by an electromagnetic vibration technique during solidification: From experimental observation to

theoretical understanding. In: Acta Materialia. 55 (2007), pp. 4635-4643.

[49] Li, M.J.; Tamura, T.; Omura, N.; Miwa, K.: Microstructure formation and grain refinement of Mg-based alloys by electromagnetic vibration technique. In: Transactions of Nonferrous Metals Society of China. 20 (2010), pp. 1192-1198.

[50] Yu, J.B.; Jiang, J.M.; Ren, Z.M.; Ren, W.L.; Deng, K.: A new method of continuous casting of copper billets by a combination of AC current and magnetic fields. In: Materials & Design. 30 (2009), pp. 4565-4569.

[51] Wang, B.; Yang, Y.S.; Ma, X.P.; Tong, W.H.: Simulation of electromagnetic-flow fields in Mg melt under pulsed magnetic field. In: Transactions of Nonferrous Metals Society of China. 20 (2010), pp. 283-288.

[52] Zhao, Z.L.; Liu, Y.; Liu, L.: Grain refinement induced by a pulsed magnetic field and synchronous solidification. In: Materials and Manufacturing Processes. 26 (2011), pp. 1202-1206.

[53] Fu, J.W.; Yang, Y.S.: Formation of the solidified microstructure of Mg-Al-Zn alloy under a low-voltage pulsed magnetic field. In: Journal of Materials Research. 26 (2011), pp. 1688-1695.

[54] Li, Y.J.; Tao, W.Z.; Yang, Y.S.: Grain refinement of Al-Cu alloy in low voltage pulsed magnetic field. In: Journal of Materials Processing Technology. 212 (2012), pp. 903-909.

[55] Gong, Y.Y.; Luo, J.; Jing, J.X.; Xia, Z.Q.; Zhai, Q.J.: Structure refinement of pure aluminum by pulse magneto-oscillation. In: Materials Science and Engineering: A. 497 (2008), pp. 147-152.

[56] Pei, N.; Gong, Y.Y.; Li, R.X.; Xia, Z.Q.; Zhai, Q.J.: Mechanism of pulse magneto-oscillation grain refinement on pure Al. In: Research & Development. (2011), pp. 47-50.

[57] Yin, Z.X.; Gong, Y.Y.; Li, B.; Cheng, Y.F.; Liang, D.; Zhai, Q.J.: Refining of pure aluminum cast structure by surface pulsed magneto-oscillation. In: Journal of Materials Processing Technology. 212 (2012), pp. 2629-2634.

[58] Edry, I.; Erukhimovitch, V.; Shoihet, A.; Mordekovitz, Y.; Frage, N.; Hayun, S.: Effect of impurity levels on the structure of solidified aluminum under pulse magneto-oscillation (PMO). In: Journal of Materials Science. 48 (2013), pp. 8438-8442.

[59] Liang, D.; Liang, Z.Y.; Zhai, Q.J.; Wang, G.; StJohn, D.H.: Nucleation and grain formation of pure Al under Pulsed Magneto-Oscillation treatment. In: Materials Letters. 130 (2014), pp. 48-50.

[60] Vashchenko, K.I.; Chernega, D.F.; Vorobev, S.L.; Lysenko, N.I.; Yakovchuk, Y.E.: Effect of electric current on the solidification of cast iron. In: Metal Science and Heat Treatment. 16 (1974), pp. 261-265.

[61] Misra, A.K.: A novel solidification technique of metals and alloys: under the influence of applied potential. In: Metallurgical and Materials Transactions A. 16 (1985), pp. 1354-1355.

[62] Misra, A.K.: Misra technique 1 applied to solidification of cast iron. In: Metallurgical and Materials Transactions A. 17 (1986), pp. 358-360.

[63] Misra, A.K.: Effect of electric potentials on solidification of near eutectic Pb-Sb-Sn alloy. In: Materials Letters. 4 (1986), pp. 176-177.

[64] Smith, R.W.: Electric field freezing. In: Journal of Materials Science Letters. 6 (1987), pp. 643-644.

[65] Nakada, M.; Shiohara, Y.; Flemings, M.C.: Modification of solidification structures by pulse electric discharging. In: ISIJ International. 30 (1990), pp. 27-33.

[66] Li, J.M.; Li, S.L.; Li, J.; Lin, H.T.: Modification of solidification structure by pulse electric discharging. In: Scripta Metallurgica et Materialia. 31 (1994), pp. 1691-1694.

[67] Barnak, J.P.; Sprecher, A.F.; Conrad, H.: Colony (grain) size reduction in eutectic Pb-Sn castings by electroplusing. In: Scripta Metallurgica et Materialia. 32 (1995), pp. 879-884.

[68] Qin, R.S.; Yan, H.C.; He, G.H.; Zhou, B.L.: Exploration on the fabrication of bulk nanocrystalline materials by direct-nanocrystllizing method I. Nucleation in disordered metallic media by electropulsing. In: Chinese Journal of Material Research. 9 (1995), pp. 219-222.

[69] Qin, R.S.; Zhou, B.L.: Exploration on the fabrication of bulk nanocrystalline materials by direct-nanocrystllizing method II. Theoretical calculation of grain size of metals sondified under electropulsing. In: Chinese Journal of Material Research. 11 (1997), pp. 69-72.

[70] Qin, R.S.; Zhou, B.L.: Effect of electric current pulses on grain size in castings. In: International Journal of Non-Equilibrium Processing. 11 (1998), pp. 77-86.

[71] Zhou, B.L.: Some non-equilibrium thermophysical problems to be studied in materials processing. In: Materials Science and Engineering: A. 292 (2000), pp. 133-141.

[72] Conrad, H.: Influence of an electric or magnetic field on the liquid-solid transformation in materials and on the microstructure of the solid. In: Materials Science and Engineering: A. 287 (2000), pp. 205-212.

[73] Gao, M.; He, G.H.; Yang, F.; Guo, J.D.; Yuan, Z.X.; Zhou, B.L.: Effect of electric current pulse on tensile strength and elongation of casting ZA27 alloy. In: Materials Science and Engineering: A. 337 (2002), pp. 110-114.

[74] He, S.X.; Wang, J.; Sun, B.D.; Zhou, Y.H.: Effect of high density pulse current on solidification structure of A356 alloy. In: Chinese Journal of Nonferrous Metals. 12 (2002), pp. 426-429.

[75] He, S.X.; Wang, J.; Jiang, W.; Sun, B.D.; Zhou, Y.H.: Effect of melt pulse electric current and thermal treatment on A356 alloy. In: Transactions of Nonferrous Metals Society of China. 13 (2003), pp. 126-130.

[76] Xu, G.M.; Zheng, J.W.; Liu, Y.; Cui, J.Z.: Effect of electric current on the cast micro-structure of Al-Si alloy. In: China Foundry. 2 (2005), pp. 171-175.

[77] Yang, Y.S.; Zhou, Q.; Hu, Z.Q.: The influence of electric current pulses on the microstructure of magnesium alloy AZ91D. In: Materials Science Forum. 488 (2005), pp. 201-204.

[78] Shi, X.D.; Wang, J.S.; Xue, Q.G.; Cang, D.Q.; Wang, L.P.; Wu, S.P.: Effect of electric pulse treatment on solidification structure of an A1-15% Si alloy. In: Rare Material. 24 (2005), pp. 288-292.

[79] Cui, H.; Cang, D.Q.; Li, L.Z.; Zong, Y.B.; Chen, L.; Zhang, J.: Effects of direct current acting on liquid metal on the solidified structure of commercially pure aluminum. In: Foundry Technology. 27 (2006), pp. 729-731.

[80] Xu, G.J.; Wang, Z.H.; Yin, J.J.; Ding, Y.T.; Kou, S.Z.: Effect of rectangle wave pulse current on solidification structure of ZA27 alloy. In: Journal of Wuhan University of Technology-Mater Sci Ed. 21 (2006), pp. 80-83.

[81] Ban, C.Y.; Han, Y.; Ba, Q.X.; Cui, J.Z.: Influence of pulse electric current on solidification structures of Al-Si alloys. In: Materials Science Forum. 546 (2007), pp. 723-728.

[82] Liao, X.L.; Zhai, Q.J.; Luo, J.; Chen, W.J.; Gong, Y.Y.: Refining mechanism of the electric current pulse on the solidification structure of pure aluminum. In: Acta Materialia. 55 (2007), pp. 3103-3109.

[83] Cui, H.; Zong, Y.B.; Cang, D.Q.; Li, L.Z.; Zhang, J.: Improving the solidification structure of commercially pure aluminium with electropulse acting on liquid metal. In: Journal of

University of Science and Technology Beijing, Mineral, Metallurgy, Material. 14 (2007), pp. 317-320.

[84] Zhang, F.C.; Zhang, M.; Lv, B.; Li, J.H.: Effect of high-energy-density pulse current on solidification microstructure of FeCrNi alloy. In: Materials Science. 13 (2007), pp. 120-122.

[85] Yang, Y.S.; Zhou, Q.; Tong, W.H.; Liang, M.X.; Hu, Z.Q.: Evolution of microstructure of magnesium alloy AZ91D solidified with low-voltage electric current pulses. In: Materials Science Forum. 539 (2007), pp. 1807-1812.

[86] Li, J.; Ma, J.H.; Gao, Y.L.; Zhai, Q.J.: Research on solidification structure refinement of pure aluminum by electric current pulse with parallel electrodes. In: Materials Science and Engineering: A. 490 (2008), pp. 452-456.

[87] Ma, J.H.; Li, J.; Gao, Y.L.; Zhai, Q.J.: Grain refinement of pure Al with different electric current pulse modes. In: Materials Letters. 63 (2009), pp. 142-144.

[88] Ding, H.S.; Zhang, Y.; Jiang, S.Y.; Chen, R.R.; Zhao, Z.L.; Guo, J.J., et al.: Influences of pulse electric current treatment on solidification microstructures and mechanical properties of Al-Si piston alloys. In: China Foundry. 6 (2009), pp. 24-31.

[89] Ma, J.H.; Li, J.; Gao, Y.L.; Jia, L.X.; Li, Z.; Zhai, Q.J.: Effect of peak value and discharge frequency of electric current pulse on solidification structure of Fe-1C-1.5Cr bearing steel. In: Ironmaking & Steelmaking. 36 (2009), pp. 286-290.

[90] Wang, T.M.; Xu, J.J.; Xiao, T.Q.; Xie, H.L.; Li, J.; Li, T.J., et al.: Evolution of dendrite morphology of a binary alloy under an applied electric current: An in situ observation. In: Physical Review E. 81 (2010), pp. 042601.

[91] Ivanov, A.V.; Sinchuk, A.V.; Tsurkin, V.N.: Electric current treatment of liquid and crystallizing alloys in casting technologies. In: Surface Engineering and Applied Electrochemistry. 47 (2011), pp. 456-464.

[92] He, X.Y.; Sun, Q.Z.; Wang, L.; Peng, Q.; Song, C.J.; Zheng, H.X., et al.: Effect of electric current pulse on solidification of silicon steel pertinent to twin roll casting. In: Ironmaking & Steelmaking. 38 (2011), pp. 374-378.

[93] Zhao, Z.L.; Wang, J.L.; Liu, L.: Grain refinement by pulse electric discharging and undercooling mechanism. In: Materials and Manufacturing Processes. 26 (2011), pp. 249-254.

[94] Cao, X.; Yin, Z.X.; Cheng, Y.F.; Li, R.X.; Gong, Y.Y.; Zhai, Q.J.: Solidification structure

refinement of SUS430 ferritic stainless steel by electric current pulse. In: EPD Congress 2012. 2012, p. 135-141th.

[95] Zhu, J.; Wang, T.M.; Cao, F.; Huang, W.X.; Fu, H.W.; Chen, Z.N.: Real time observation of equiaxed growth of Sn-Pb alloy under an applied direct current by synchrotron microradiography. In: Materials Letters. 89 (2012), pp. 137-139.

[96] Yin, Z.X.; Liang, D.; Chen, Y.E.; Cheng, Y.F.; Zhai, Q.J.: Effect of electrodes and thermal insulators on grain refinement by electric current pulse. In: Transactions of Nonferrous Metals Society of China. 23 (2013), pp. 92-97.

[97] Li, X.B.; Lu, F.G.; Cui, H.C.; Tang, X.H.: Effect of electric current pulse on flow behaviour of Al melt in parallel electrode process. In: Materials Science and Technology. 29 (2013), pp. 226-233.

[98] Chen, H.; Zhang, L.; Wang, S.M.: Microstructure refinement of hypereutectic high chromium cast iron with electric current pulse. In: Advanced Materials Research. 690 (2013), pp. 147-152.

[99] Plotkowski, A.; Anyalebechi, P.N.: Refinement of primary and eutectic silicon particles in hypereutectic Al-Si Alloys using an applied electric potential. In: Proceedings of the 2013 International Symposium on Liquid Metal Processing and Casting. 2013, p. 219-227th.

[100] Qi, J.G.; Li, Y.; Tukur, S.A.; Zhao, Z.F.; Wu, D.; Dai, S., et al.: A model study for the electric pulse frequency effects on the solidification behavior of Al-5% Cu alloy. In: International Journal of Scientific & Technology Research. (2014), pp. 267-274.

[101] Li, X.B.; Lu, F.G.; Cui, H.C.; Tang, X.H.: Migration behavior of solidification nuclei in pure Al melt under effect of electric current pulse. In: Transactions of Nonferrous Metals Society of China. 24 (2014), pp. 192-198.

[102] Boi͡arevich, V.V. Electrically induced vortical flows: Springer, 1989.

[103] Nikrityuk, P.A.; Eckert, K.; Grundmann, R.; Yang, Y.S.: An impact of a low voltage steady electrical current on the solidification of a binary metal alloy: A numerical study. In: Steel Research International. 78 (2007), pp. 402-408.

[104] Glicksman, M.E. Principles of solidification: Springer, 2011.

[105] Volmer, M.; Weber, A.: Keimbildung in übersättigten Gebilden. In: Zeitschrift für Physikalische Chemie. 119 (1926), pp. 277-301.

[106] Farkas, L.: Keimbildungsgeschwindigkeit in übersättigten Dämpfen. In: Zeitschrift für Physikalische Chemie. 125 (1927), pp. 236-242.

[107] Volmer, M.: Über Keimbildung und Keimwirkung als Spezialfälle der heterogenen Katalyse. In: Zeitschrift für Elektrochemie und angewandte physikalische Chemie. 35 (1929), pp. 555-561.

[108] Volmer, M.; Flood, H.: Tröpfchenbildung in Dämpfen. In: Zeitschrift fur Physikalische Chemie, Abteilung A. 170 (1934), pp. 273-285.

[109] Becker, R.; Döring, W.: Kinetische behandlung der keimbildung in übersättigten dämpfen. In: Annalen der Physik. 416 (1935), pp. 719-752.

[110] Kelton, K.; Greer, A.L. Nucleation in condensed matter: applications in materials and biology: Elsevier, 2010.

[111] Kurz, W.; Fisher, D.J. Fundamentals of solidification: Trans Tech Publications, 1986.

[112] Winegard, W.C.; Chalmers, B.: Supercooling and dendritic freezing in alloys. In: Transactions of the Metallurgical Society of AIME. 46 (1954), pp. 1214-1223.

[113] Hutt, J.; StJohn, D.H.: The origins of the equiaxed zone-Review of theoretical and experimental work. In: International Journal of Cast Metals Research. 11 (1998), pp. 13-22.

[114] Genders, R. The interpretation of the macrostructure of cast metals: Institute of Metals, 1926.

[115] Chalmers, B.: The structure of ingots. In: Journal of the Australian Institute of Metals. 8 (1963), pp. 255-263.

[116] Jackson, K.A.; Hunt, J.D.; Uhlmann, D.R.; Seward, T.P.: On origin of equiaxed zone in castings. In: Transactions of the Metallurgical Society of AIME. 236 (1966), pp. 149-158.

[117] Flemings, M.C.: Solidification processing. In: Metallurgical Transactions. 5 (1974), pp. 2121-2134.

[118] Ruvalcaba, D.; Mathiesen, R.H.; Eskin, D.G.; Arnberg, L.; Katgerman, L.: In situ observations of dendritic fragmentation due to local solute-enrichment during directional solidification of an aluminum alloy. In: Acta Materialia. 55 (2007), pp. 4287-4292.

[119] Ananiev, S.; Nikrityuk, P.; Eckert, K.: Dendrite fragmentation by catastrophic elastic remelting. In: Acta Materialia. 57 (2009), pp. 657-665.

[120] Southin, R.T.: Nucleation of the equiaxed zone in cast metals. In: Transactions of the

Metallurgical Society of AIME. 239 (1967), pp. 220-225.

[121] Ohno, A. Solidification-the separation theory and its practical applications: Springer, 1987.

[122] Ohno, A.; Motegi, T.; Soda, H.: Origin of the equiaxed crystals in castings. In: Trans Iron Steel Inst Jap. 11 (1971), pp. 18-23.

[123] Dolinsky, Y.; Elperin, T.: Thermodynamics of phase transitions in current-carrying conductors. In: Physical Review B. 47 (1993), pp. 14778-14785.

[124] Campanella, T.; Charbon, C.; Rappaz, M.: Grain refinement induced by electromagnetic stirring: A dendrite fragmentation criterion. In: Metallurgical and Materials Transactions A. 35 (2004), pp. 3201-3210.

[125] Morley, N.B.; Burris, J.; Cadwallader, L.C.; Nornberg, M.D.: GaInSn usage in the research laboratory. In: Review of Scientific Instruments. 79 (2008), pp. 056107.

[126] Plevachuk, Y.; Sklyarchuk, V.; Eckert, S.; Gerbeth, G.; Novakovic, R.: Thermophysical properties of the liquid Ga-In-Sn eutectic alloy. In: Journal of Chemical & Engineering Data. 59 (2014), pp. 757-763.

[127] Bojarevics, V.; Shcherbinin, E.V.: Azimuthal rotation in the axisymmetric meridional flow due to an electric-current source. In: Journal of Fluid Mechanics. 126 (1983), pp. 413-430.

[128] Sklyarchuk, V.; Plevachuk, Y.; Yakymovych, A.; Eckert, S.; Gerbeth, G.; Eigenfeld, K.: Structure sensitive properties of liquid Al-Si alloys. In: International Journal of Thermophysics. 30 (2009), pp. 1400-1410.

[129] http://www.cobham.com/emdesign.

[130] http://www.openfoam.org.

[131] Liotti, E.; Lui, A.; Vincent, R.; Kumar, S.; Guo, Z.; Connolley, T., et al.: A synchrotron X-ray radiography study of dendrite fragmentation induced by a pulsed electromagnetic field in an Al-15Cu alloy. In: Acta Materialia. 70 (2014), pp. 228-239.

[132] Hellawell, A.; Liu, S.; Lu, S.Z.: Dendrite fragmentation and the effects of fluid flow in castings. In: JOM. 49 (1997), pp. 18-20.

[133] Campanella, T.; Charbon, C.; Rappaz, M.: Influence of permeability on the grain refinement induced by forced convection in copper-base alloys. In: Scripta Materialia. 49 (2003), pp. 1029-1034.

[134] Cramer, A.; Zhang, C.J.; Eckert, S.: Local flow structures in liquid metals measured by

ultrasonic Doppler velocimetry. In: Flow Measurement and Instrumentation. 15 (2004), pp. 145-153.

[135] Stiller, J.; Koal, K.: A numerical study of the turbulent flow driven by rotating and travelling magnetic fields in a cylindrical cavity. In: Journal of Turbulence. 10 (2009), pp. 1-16.

[136] Davidson, P.A. An introduction to magnetohydrodynamics: Cambridge university press, 2001.

[137] Räbiger, D.; Eckert, S.; Gerbeth, G.: Measurements of an unsteady liquid metal flow during spin-up driven by a rotating magnetic field. In: Experiments in Fluids. 48 (2010), pp. 233-244.

[138] Gowri, S.; Samuel, F.H.: Effect of cooling rate on the solidification. In: Metallurgical Transactions A. 23 (1992), pp. 3369-3376.

[139] Kang, M.D.; Gao, H.Y.; Shu, D.; Wang, J.; Li, F.G.; Fu, Y.N., et al.: In situ and real-time observation of the solidification process of Al-20 mass% Cu alloy by synchrotron X-ray radiography. In: Materials Transactions. 55 (2014), pp. 774-778.

[140] Nagira, T.; Nakatsuka, N.; Yasuda, H.; Uesugi, K.; Takeuchi, A.; Suzuki, Y.: Impact of melt convection induced by ultrasonic wave on dendrite growth in Sn-Bi alloys. In: Materials Letters. 150 (2015), pp. 135-138.

[141] Mathiesen, R.H.; Arnberg, L.; Bleuet, P.; Somogyi, A.: Crystal fragmentation and columnar-to-equiaxed transitions in Al-Cu studied by synchrotron X-ray video microscopy. In: Metallurgical and Materials Transactions A. 37 (2006), pp. 2515-2524.

[142] Mathiesen, R.H.; Arnberg, L.: Stray crystal formation in Al-20wt.% Cu studied by synchrotron X-ray video microscopy. In: Materials Science and Engineering: A. 413 (2005), pp. 283-287.

[143] Rettenmayr, M.: Melting and remelting phenomena. In: International Materials Reviews. 54 (2009), pp. 1-17.

[144] Liu, S.; Lu, S.Z.; Hellawell, A.: Dendritic array growth in the systems NH4Cl-H2O and [CH2CN](2)-H2O: the detachment of dendrite side arms induced by deceleration. In: Journal of crystal growth. 234 (2002), pp. 740-750.

[145] Kumar, A.; Dutta, P.: A Rayleigh number based dendrite fragmentation criterion for detachment of solid crystals during solidification. In: Journal of Physics D: Applied Physics. 41 (2008), pp. 155501.

[146] Beckermann, C.: Modelling of macrosegregation: applications and future needs. In: International Materials Reviews. 47 (2002), pp. 243-261.

[147] Boden, S.; Eckert, S.; Gerbeth, G.: Visualization of freckle formation induced by forced melt convection in solidifying GaIn alloys. In: Materials Letters. 64 (2010), pp. 1340-1343.

[148] Zimmermann, G.; Weiss, A.; Mbaya, Z.: Effect of forced melt flow on microstructure evolution in AlSi7Mg0. 6 alloy during directional solidification. In: Materials Science and Engineering: A. 413 (2005), pp. 236-242.

[149] Zaidat, K.; Ouled-Khachroum, T.; Vian, G.; Garnier, C.; Mangelinck-Noël, N.; Dupouy, M.D., et al.: Directional solidification of refined Al-3.5 wt% Ni under natural convection and under a forced flow driven by a travelling magnetic field. In: Journal of crystal growth. 275 (2005), pp. 1501-1505.

[150] Noeppel, A.; Ciobanas, A.; Wang, X.D.; Zaidat, K.; Mangelinck, N.; Budenkova, O., et al.: Influence of forced/natural convection on segregation during the directional solidification of Al-based binary alloys. In: Metallurgical and Materials Transactions B. 41 (2010), pp. 193-208.

[151] Jie, J.C.; Zou, Q.C.; Sun, J.L.; Lu, Y.P.; Wang, T.M.; Li, T.J.: Separation mechanism of the primary Si phase from the hypereutectic Al-Si alloy using a rotating magnetic field during solidification. In: Acta Materialia. 72 (2014), pp. 57-66.